Antigen-specific immune modulation using an injectable biomaterial

Antigen-specific immune modulation using an injectable biomaterial

A dissertation presented

by

Catia Stéphanie Verbeke

to

The School of Engineering and Applied Sciences

in partial fulfillment of the requirements

for the degree of

Doctor of Philosophy

in the subject of

Engineering Sciences

Harvard University

Cambridge, Massachusetts

April, 2014

Dr. David J. Mooney Catia Stéphanie Verbeke

Antigen-specific immune modulation using an injectable biomaterial

Abstract

The field of immunology has advanced tremendously over the last 40 years, with seminal findings that have guided the development of powerful new therapies. However, the ability to induce safe and long-lasting antigen-specific tolerance has remained elusive. A therapy that could prevent the immune system from aberrantly destroying self-tissues, without impairing its capacity to eliminate dangerous pathogens, would be transformative for the treatment of autoimmune diseases. In addition, such a therapy could also greatly advance the field of organ transplantation by inducing antigen-specific tolerance to prevent graft rejection.

In this thesis, the overarching goal was to develop a biomaterial delivery system that could recruit and program antigen presenting cells, specifically dendritic cells (DCs), in a non-inflammatory environment, allowing them to orchestrate downstream immune responses that are both antigen-specific and tolerogenic. Gold nanoparticles (AuNPs) were used to deliver a DC recruitment factor, GM-CSF, from an injectable alginate based hydrogel. Both the release of GM-CSF and the physical porous structure of the gel were tuned to achieve effective recruitment of a highly enriched population of DCs. The ability of this system to generate downstream antigen-specific responses in T cells was demonstrated in a mouse model of type 1 diabetes (T1D). Additionally, the DCs

recruited in this system were characterized and found to exhibit features that would make them competent to induce tolerance. Finally, a new method was developed for localized delivery and cell-triggered release of a peptide antigen from the material. Over time, antigen-specific T cells expressing FoxP3, a marker of regulatory T cells, which are key mediators of immune tolerance, accumulated in the gels. Together, these findings demonstrate that it is possible to recruit and program DCs in a non-inflammatory context, and that these DCs can induce downstream antigen-specific responses. These promising results suggest that this system may be able to promote tolerance in the setting of autoimmune disease.

This thesis advances the field of immunomodulatory biomaterials by introducing new methodologies for precisely recruiting and manipulating DCs in a non-inflammatory context. This work may provide the basis for further development of a highly effective and therapeutic antigen-specific tolerogenic vaccine.

Table of Contents

Acknowledgements

During the years that I spent pursuing a Ph.D., I met and interacted with many brilliant, hard-working, and inspiring individuals. I am very grateful for everything that I have learned from them, both on scientific and personal levels.

First and foremost, I would like to express my gratitude to Professor David Mooney, my thesis advisor, for his patience, support, and encouragement. Dave is an exceptional mentor who not only does great science, but also truly cares about the development of each individual in his lab. His inspiring example and guidance have helped me grow into a better scientist and a wiser person. I could not have wished for a better thesis advisor, and I am thankful for the opportunity I had to work with and learn from him.

In addition, I would like to sincerely thank my committee members, Professor Kai Wucherpfennig and Professor Neel Joshi, for their guidance and support. Beyond serving as one of my committee members, Kai was also a close collaborator who contributed his advice and expertise in immunology to the design of many experiments. I would like to thank two former Wucherpfennig lab members, Susana Gordo and David Schubert, with whom I worked as part of this fruitful collaboration. I learned a great deal in the 1.5 years that I worked with Susana, and I also gained a good friend. Thank you as well to Jessica Dobbins (Wucherpfennig lab) and Hye-Jung Kim (Cantor lab) for their help with experiments in the weeks leading up to my thesis defense.

The Mooney lab is a wonderful environment for research and learning, and I feel lucky to have been a part of it. I would like to express my appreciation to Dr. Omar Ali, Dr. Warren Sands, Dr. Gail Chan, Aileen Li, and Sandeep Koshy for insightful discussions related to immunotherapy, as well as for sharing techniques and reagents. I would also like to thank Dr. Nathaniel Huebsch, Dr. Luo Guo, Dr. Cathal Kearney, Dr. Ovi Chaudhuri, Dr. Jaeyun Kim, Rajiv Desai, and Max Darnell for all kinds of advice and help on the materials side. Thank you as well to all the other Mooney lab members, past and present, that I interacted with: Dr. Erin Anderson, Dr. Praveen Arany, Dr. Sidi Bencherif, Yaron Blinder, Dr. Thomas Braschler, Dr. Yevgeny Brudno, Dr. Lan Cao, Christine Cezar, Alex Cheung, Cristiana Cunha, Dr. Steve Kennedy, Darinka Klumpers, Anu Kod, Brian Kwee, Dr. Kangwon Lee, Dr. Evi Lippens, Dr. Beverly Lu, Angelo Mao, Dr. Manav Mehta, Theresa Raimondo, Ting-Yu Shih, Dr. Jae-Won Shin, Dr. Dima Shvartsman, Dr. Eduardo Silva, Dr. Hadas Skaat, Dr. Prakriti Tayalia, Dr. Will Yuen, and Dr. Xuanhe Zhao. Many of you have become great friends, and I will remember fondly all the good laughs, tea time discussions, lunches at the law school, lab retreat memories, and fun adventures outside of lab.

Katie Parodi and Kurt Schellenburg deserve special thanks for the great job that they to do to keep the lab running. Katie is one of the most organized and efficient people that I know, and she assumes her role as the lab administrator with a great deal of patience and grace. Kurt has transformed many aspects of the lab since becoming the lab manager, and I sincerely appreciate all the work that he has done. I would also like to thank former lab administrators Nora McDonald, Jill Larson, and Arlene Stevens.

Many staff members at Harvard and at the Wyss Institute have assisted my research over the years. In particular, I would like to show my appreciation to Sarah Lewin from the Wyss Institute for her invaluable help with animal studies. Thank you to Patricia Rogers and Mandy Tam from the Bauer Core for their assistance with flow cytometry, as well as to Greg Brady, Jose Munguia, and Ken Walker from EH&S for their help with radiation safety. I would like to recognize the lab assistants who have worked in the Mooney lab over the years, as well as staff from SEAS and the BRI animal facility, whose work makes it possible for research to continue on a daily basis. I would also like to acknowledge the funding sources that supported the work in this thesis: NIH, JDRF, Harvard Institute of Translational Immunology (HITI), and the Helmsley Charitable Trust.

Last but not least, I would like to thank my family and friends, who were always there to offer their support and encouragement throughout my time in grad school. A million thanks to my parents, whose love and belief in me is unending.

Catia Stéphanie Verbeke

April 2014

To my parents, who always believe in me.

Savoir s'étonner à propos est le premier pas fait sur la route de la découverte.

(Knowing how to be astonished is the first step taken on the road of discovery.)

–Louis Pasteur

Chapter 1. Introduction

1.1 Background and Motivation

The human immune system defends the body from a constant barrage of pathogens in the environment. Immune cells traffic systemically and are found in almost every tissue in the body, forming an incredibly complex and evolving network. A large number of diseases and disorders are caused by dysfunctional immune responses. Infectious diseases take hold when the immune system fails to be adequately or rapidly activated. Recently, cancer has increasingly been viewed through the lens of immunology, in terms of a tumor's ability to evade elimination by the immune system[1–3]. On the other end of the spectrum, excessive or misdirected immune responses are the cause of chronic inflammation, autoimmune diseases, and allergies. The rejection of organ transplants, though not technically a disease, is another area in which immune activation is undesirable[4]. In addition, new research is revealing that many other diseases, such as Alzheimer's[5], narcolepsy[6], and epilepsy[7], have an important immunological component. There is also a growing appreciation for the capacity of immune cells to alter or direct a variety of processes in development, homeostasis, and repair, such as angiogenesis[8,9], wound healing[10,11], and bone remodeling[12–14].

Vaccination can be considered as one of the most impactful medical advances in history. It has led to the eradication of smallpox, as well as the elimination of polio, measles, and tetanus in much of the world, greatly extending the average life expectancy[15]. However, until recently, vaccine development has been largely

empirical, and there remain are a number of critical areas in which effective vaccination is not possible[15,16]. Pathogens that mutate rapidly, such as retroviruses, are inherently elusive targets[17,18], and tumors develop mechanisms for evading immune surveillance[2]. Of particular interest here, tolerogenic vaccination to treat immune diseases or prevent transplant rejection has not been possible yet[19,20]. Over the last 40 years, the field of immunology has flourished with seminal findings such as the elucidation of the molecular structure and function of major histocompatibility complex (MHC) molecules[21], the discovery of Toll-like receptor (TLR) ligands, and the identification of different cell types such as dendritic cells (DCs)[22] and regulatory T cells (Tregs)[23,24]. With these advances comes an increased ability to manipulate the immune system by developing and designing new therapies in a rational way.

This thesis explores the possibility of developing a materials-based vaccine that can control immune responses towards defined antigens in a non-inflammatory environment, with the goal of inducing tolerance.

DCs and T cells in autoimmunity

Autoimmune diseases represent a significant burden on society. It was estimated that autoimmune diseases affect ~5-8% of the population in the United States, with treatments costing around $100 billion each year in the US, as estimated recently by the NIH[25]. Aside from the economic impact, autoimmune diseases take a serious toll on patients as well as on affected families. Autoimmune diseases arise when the breakdown of multiple barriers results in a loss of tolerance towards self-antigens.

Autoimmune diseases are complex and multifactorial, involving a combination of genetic predispositions and largely uncharacterized environmental factors.

The adaptive branch of the immune system comprises highly specialized cells, known as B and T cells, which mount antigen-specific immune responses and acquire long term immunological memory. The B cell receptors (BCRs) and T cell receptors (TCRs) that mediate the recognition of antigen are generated through an elegant combinatorial mechanism, known as VDJ recombination. The number of unique TCRs represented in one individual is estimated to be approximately $10^7 – 10^8$, which is a fraction of the ~10^{16} possible T cell receptors that can theoretically be generated[26]. This staggering diversity of receptors endows the immune system with the ability to effectively protect its host from a huge range of unknown pathogens, some of which may have never previously been encountered in the history of evolution. Stochastically, some of the receptors generated will recognize self-antigens, and cells cannot intrinsically distinguish self-antigens from foreign antigens. Consequently, there are several mechanisms in place to prevent aberrant destruction of self-tissues. In central tolerance, B and T cells with a high affinity for self-antigens are eliminated by deletion in the thymus. However, some weakly or moderately self-reactive cells escape, even in healthy individuals[27].

Several tightly regulated mechanisms of peripheral tolerance keep these auto-reactive cells in check and maintain tolerance to self-tissues. The most basic mechanism of peripheral tolerance is termed immunological ignorance, which reflects the fact that the immune system has limited access to many self-antigens because they are located either in intracellular compartments or in immunologically privileged tissues, such as the

eyes or brain. The next level of peripheral tolerance encompasses the cell intrinsic signaling networks that control T cell activation, proliferation, and effector functions. To be effectively activated, T cells need to receive "signal 1" from TCR binding to its cognate antigen presented by MHC, together with "signal 2" from costimulatory molecule signaling through CD28. "Signal 3", which is provided by soluble cytokines, controls the polarization of T cells[28]. In the absence of inflammation, self-reactive T cells that encounter their cognate antigen will receive signal 1 from antigen presenting cells (APCs) in the absence of signal 2, leading to unresponsiveness, or anergy[28,29]. Inhibitory molecules such as cytotoxic T-lymphocyte antigen-4 (CTLA-4) and programmed death-1 (PD-1) are also integrated into this signaling network and mediate negative costimulatory signals that are critical for maintaining peripheral tolerance and for resolving inflammation after the clearance of a pathogen[30,31]. The highest level of regulation in peripheral tolerance is sometimes called "dominant suppression", since it is mediated by specialized regulatory cells that can suppress the responses of other effector cells, including ones that recognize a different antigen. In particular, regulatory T cells (Tregs) are critical for maintaining peripheral tolerance[32,33]. $CD4^+$ $FoxP3^+$ natural Tregs (nTregs) are generated during thymic selection[34]. A deficiency in Tregs arising from defects in the *foxp3* gene results in multi-organ autoimmunity in mice ("scurfy") and humans (IPEX)[33]. Tregs exert their suppressive functions both on DCs and on effector T cells through a combination of contact-mediated signals and secreted cytokines[33]. More recently, other $CD4^+$ T cells with regulatory capacity have been described, such as adaptive Tregs[34] or IL-10 producing Tr1 cells, which can be identified based on co-expression of the surface markers LAG-3 and CD49b[35]. In addition, there is

a growing body of research about $CD8^+$ Tregs[36,37], regulatory B cells[38,39], and other suppressive innate cells[40].

For autoimmune disease to arise, several of these barriers need to become disrupted or deregulated. The initial events triggering autoimmunity are still not well understood. It is generally thought that disease processes are initiated following tissue damage or infection, and multiple insults to the tissue may occur before tolerance is broken and autoimmunity develops[41]. Naturally occurring waves of cell death or remodeling that occur during development could be implicated[42] because of the release of damage associated molecular patents (DAMPs) and intracellular antigens that are normally not accessible to immune cells. Infection of a tissue also leads to the release of intracellular antigens, as well as epitope spreading to self-antigens. The theory of molecular mimicry, which holds that self-tolerance is broken following infection by a pathogen expressing antigens that closely mimic self-antigens, has not been definitively proven in the context of human disease[43]. Finally, even though there is strong evidence that environmental factors other than pathogens have a strong impact on the development of autoimmunity, these factors are still largely uncharacterized. One promising area of research investigates the role of the microbiome in shaping the immune system in ways that may promote or suppress autoimmunity[44,45].

Dendritic cells (DCs) play a central role in establishing and maintaining peripheral tolerance. DCs bridge the innate and adaptive branches of the immune system, and orchestrate the downstream responses of the adaptive immune response (Fig. 1.1). DCs constantly patrol almost every tissue in the body to monitor them for invasion by

pathogens. In steady-state conditions, cell debris from normal cell turnover constitutes the main source of antigens[46]. In the absence of inflammatory signals, DCs induce anergy and deletion of autoreactive T cells[28,29,46]. Since DCs direct the differentiation or polarization of effector T cells, they can also induce phenotypic skewing away from Th1 or Th17 subsets, which mediate autoimmunity. DCs also interact with different regulatory cell types[47], triggering the activation or expansion of natural Tregs, or the induction of Tr1 cells.

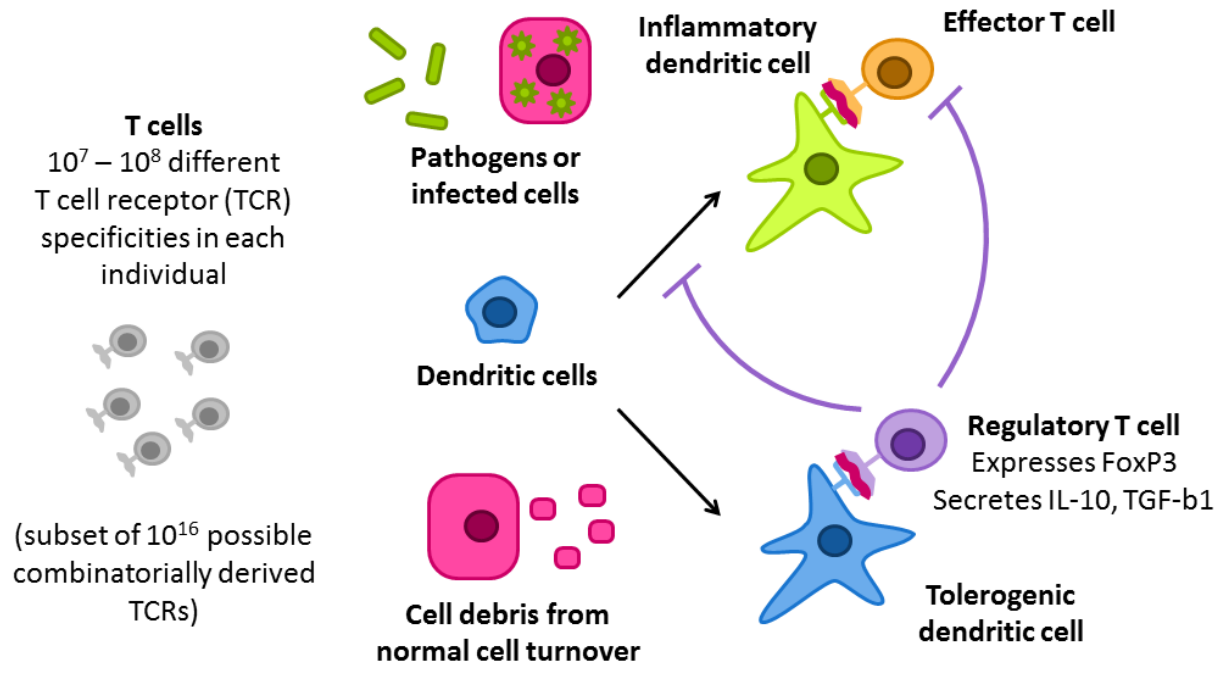

Figure 1.1. The interplay of dendritic cells and T cells in tolerance and immunity. DCs integrate signals from the environment and direct downstream T cell responses. Regulatory T cells have the capacity to suppress both inflammatory DCs and effector T cells, which is critical for the resolution of inflammation after a pathogen is cleared as well as for maintaining tolerance towards self-tissues in steady state conditions.

DCs are very heterogeneous and can be subdivided into conventional DCs (cDCs), Langerhans cells, plasmacytoid DCs (pDCs), and monocyte-derived DCs[48] (Fig. 1.2). cDCs, which predominate in steady-state conditions, arise from a bone marrow

precursor cell. cDCs can be further subdivided into migratory DCs that reside in peripheral tissues and migrate to lymph nodes (LNs), and lymphoid-resident DCs that differentiate and remain in lymphoid organs, i.e. the lymph nodes, spleen, and thymus. Langerhans cells are tissue-resident DCs found in the skin, and, while they exert similar functions as migratory DCs, they are derived from a specialized precursor cell population that resides in the skin. pDCs are characterized by their ability to secrete large amounts of type I interferons (IFNs), making them particularly effective at eliminating viral infections. Finally, monocyte-derived DCs are believed to be a reservoir of APCs that arise in settings of inflammation from circulating blood monocytes that differentiate to acquire prototypical DC features similar to cDCs, including CD11c and MHCII expression, as well as potent antigen-presenting capacity. Within each of these four main DC subsets, there are many further subdivisions based on the expression of different cell surface markers. Adding to this staggering complexity, DCs are plastic, and the surface marker expression of DCs can vary depending on their tissue localization and their level of differentiation or maturation. It has been proposed that certain types of DCs, such as mucosal DCs[49,50] or Langerhans cells[51], may be specialized for inducing regulatory responses, but there is no consensus in the field[52]. Reports in the literature show that many different DC subsets, including conventional (or myeloid) and plasmacytoid DCs, play a role in inducing or maintaining tolerance[28,52].

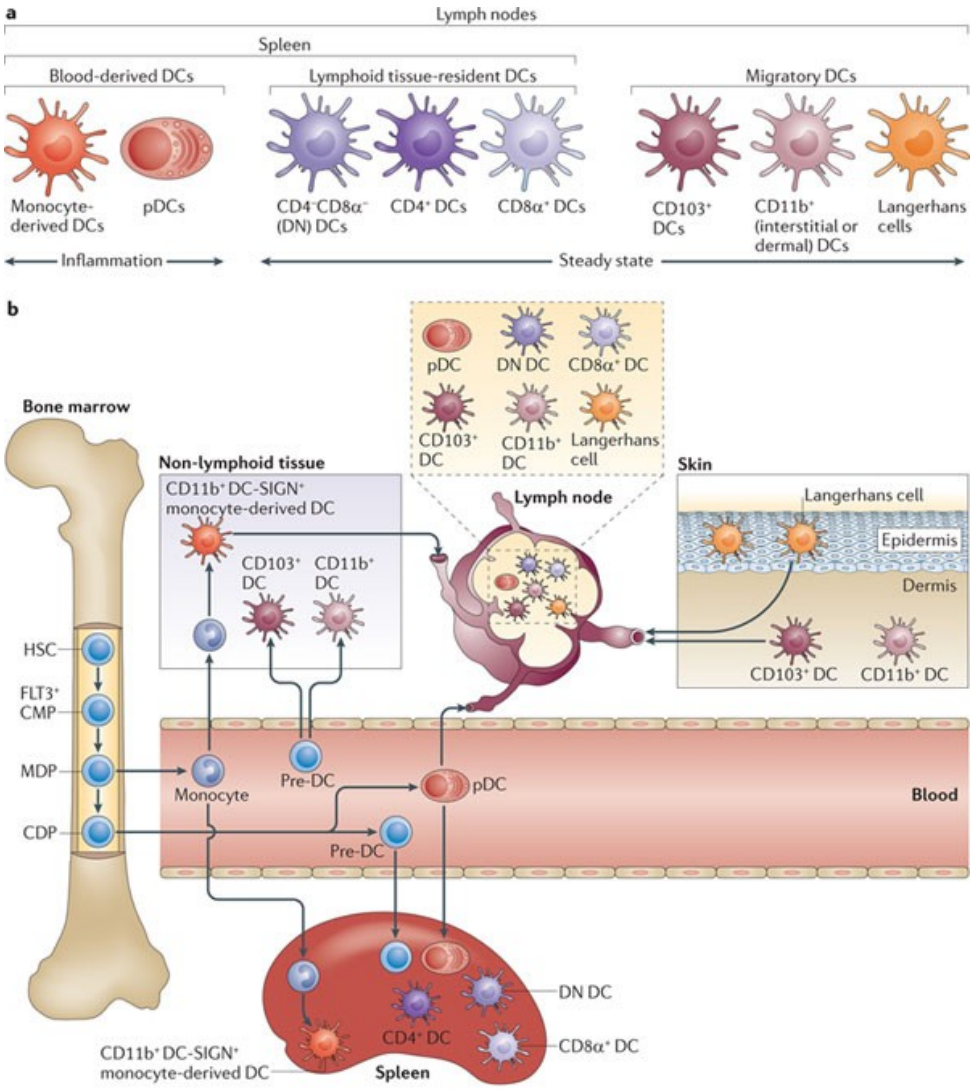

Figure 1.2. Differentiation and tissue localization of different DC subsets. Adapted from Belz and Nutt[48].

Current strategies for treating autoimmune diseases

Immunosuppressive drugs can dampen immune responses and alleviate the destruction of self-tissues by autoreactive immune cells. However, broad immunosuppression has serious consequences on the long-term health of patients,

making them prone to deadly infections. In the setting of type 1 diabetes, cyclosporin A was shown to preserve beta cell function, allowing many patients to live insulin-independent for prolonged periods; however, the treatment caused accelerated renal dysfunction, and the protective effect did not last after cessation of the treatment[53]. This ratio of risk to benefit is not acceptable, particularly for a disease like type 1 diabetes that occurs in young patients. By the same token, autologous HSC transplantation, while it was found to be effective in resetting the immune system and achieving long-term benefits in patients with severe autoimmunity, is currently not a sufficiently safe treatment to be suitable for widespread use[19].

Immunomodulatory therapies targeting immune receptors or cytokines represent a slightly more targeted approach to treating autoimmune diseases, and, as a result, they should be associated with fewer risks than generalized immunosuppression. Therapies such as CTLA4-Ig (abatacept), anti-CD20 (rituximab), and anti-CD3 (teplizumab/otelixizumab) generated great interest and have been tested in clinical trials recently[53]. These treatments are not necessarily viable as long-term treatments, since chronic depletion of B or T cells with anti-CD20 or anti-CD3, respectively, carries serious risks, and chronic costimulatory blockade with CTLA4-Ig may increase the risk of infections and cancer. Instead, the hope is that a short course of treatment could confer longer-term tolerance by interrupting destructive signaling pathways or by enhancing the regulatory capacity of Tregs. Since B cells play an important role as APCs, in addition to producing pathogenic autoantibodies, B cell depletion can be effective even in autoimmune disease that are primarily T cell driven. Depleting B cells reduced disease in preclinical models of T1D and MS, and promising initial results are

emerging from in clinical trials for RA, MS, and T1D[19]. On the other hand, anti-CD3 therapy, which garnered high hopes based on preclinical studies showing reversal of diabetes in several T1D models[53] and amelioration of EAE[19], has seen disappointing results in clinical trials. Second-generation, non FcR binding anti-CD3 is thought to function by preferentially inducing deletion and anergy of effector T cells, shifting the ratio of Teffs : Tregs. Unfortunately, two large phase 3 trials recently failed to meet their primary endpoints[19,53], even though one of the studies in newly-diagnosed T1D patients did initially show some beneficial effects that lasted well beyond the short course of treatment, but were not maintained. A number of trials are still ongoing to continue testing anti-CD3 in a number of different diseases, including T1D. Low dose IL-2 therapy is another example of an immunomodulatory therapy that has not performed up to expectations in clinical trials. This treatment was designed to preferentially expand Tregs, which express the high-affinity IL-2 receptor, as well as correct defects in IL-2 signaling in Tregs that are seen in some T1D patients[19]. This approach did not work well in new-onset diabetic patients because NK cells were dramatically expanded[19]. These recent disappointments highlight the some of the challenges in translating preclinical findings, which are due in part to inter-species differences between the mouse and human immune systems.

An entirely different strategy for treating autoimmune diseases involves cell-based therapies. Dendritic cell based therapies were pioneered in the setting of cancer vaccination, with the first clinical study of a dendritic cell (DC) vaccine reported in 1996[54] and the first therapeutic cancer vaccine, Provenge, approved by the FDA in 2010[55]. Today, DC-based cancer vaccines are an increasingly active area of

investigation, with many current efforts targeting melanoma. In the context of autoimmune diseases, a number of pre-clinical models have shown that administration of Tregs or tolerogenic DCs has the potential to delay or prevent disease, and, in some cases, reverse new-onset disease[56]. There are currently several clinical trials investigating the safety of Tregs[57] and tolerogenic DCs[58,59] in humans. Mesenchymal stromal cells (MSCs) have also been found to exhibit immunomodulatory properties and could have therapeutic effects in autoimmune diseases[19].

Despite a promising outlook in terms of therapeutic potential, the significant cost and complexity associated with cell-based therapies makes them challenging to take into the clinic. Tolerogenic cell therapies face a particularly large hurdle since the cells of interest, i.e. tolerogenic DCs, Tregs, and particularly antigen-specific Tregs, are rare, requiring autologous cells to be expanded *ex vivo* before they can be clinically useful[60]. Contamination with undesired cell populations, such as effector T cells, poses a serious safety concern that may need to be addressed by including additional sorting or purification steps before the cells can be re-administered to patients[60]. Each of these additional manipulations complicates the regulatory path and adds to the high personnel and facility costs for manufacturing such therapies. Only adding to these issues, it has been found that the majority of cells die upon administration or fail to home to the target tissue. For instance, a study in melanoma patients showed that <2% of intradermally injected, mature DCs migrated to the draining lymph nodes, and that the homing efficiency was even lower, only <0.5%, for immature DCs[61]. The stability of the cell phenotype after transplantation is also a concern, particularly for therapies that involve in vitro conditioning using bioactive factors or drugs.

Materials based vaccines for immune modulation

An ever-increasing understanding of the mechanisms controlling immunity and tolerance is laying the ground for the design of novel therapeutic strategies. An exciting and rapidly growing area of research at the intersection of immunology and bioengineering involves the use of materials to exert specific and powerful control over immune responses. Several efforts aim to increase the efficacy of vaccines by using materials to coordinate antigen and danger signal delivery, either by controlling their spatio-temporal presentation or by physically coupling them[16,62]. Further, the material carriers themselves can be designed to act as adjuvants or present adjuvants in a manner that makes them more effective[16]. There are several biomaterials-based particle vaccines currently under commercial development, most of which target infectious diseases[16].

In the area of cancer immunotherapy, Hori et al. have shown that hydrogels made of alginate, a naturally occurring polysaccharide, can be used to deliver DCs or immunostimulatory cytokines to the immediate vicinity of melanoma tumors in the skin. The delivery of either DCs or appropriate bioactive factors both showed promising results, including enhanced leukocyte infiltration into the tumors, control of tumor growth, and increased survival[63]. In a different approach, Ali et al. devised an elegant strategy to address limitations of cell-based therapies by using a porous polymeric scaffold to recruit and program DCs directly *in vivo*. The scaffold mimics a setting of infection by presenting tumor antigens along with danger signals in a coordinated

manner, thus eliciting anti-tumor responses mediated by DCs and cytotoxic T cells. This materials-based cancer vaccine was shown to be effective in mouse models of melanoma[62,64] and glioblastoma[65,66], and it is currently being investigated in a phase I safety study in melanoma patients[67].

In the area of immune tolerance, several noteworthy studies have been published in recent years. Iron oxide nanoparticles presenting self-peptide MHC (pMHC) complexes were discovered to have the unexpected property of expanding a subset of memory CD8+ T cells with regulatory capacity. These regulatory $CD8^+$ T cells were found to suppress other T cells and mediate killing of autoantigen-presenting DCs, leading to therapeutic effects in a mouse model of T1D[68]. Another interesting approach involved the use of gold nanoparticles to co-deliver a peptide antigen together with ITE, a small molecule aryl hydrocarbon receptor (AHR) ligand that was shown to act on both DCs and T cells[69]. Co-delivery of a disease-related antigen with ITE on the gold nanoparticles was found to ameliorate disease in EAE, a mouse model of MS, by inducing tolerogenic DCs and increasing the numbers of $CD4^+$ Tregs[70]. Also in the setting of EAE, peptide-coupled polystyrene or PLGA particles were successfully used to induce tolerance in prophylactic and therapeutic settings[71]. This work built on previous findings showing that EDCI-fixed, peptide-coupled apoptotic splenocytes could induce tolerance[72]. The polymeric particles were used as mimics of apoptotic cells, making the strategy more appealing for potential use as a therapy both from both regulatory and manufacturing standpoints. The size and delivery route leads these particles to be taken up by a specialized population of splenic macrophages, and therapeutic effects were attributed to both Treg activation, as well as T cell anergy[71].

Overall, the application of biomaterials to the field of immunotherapy has great potential to yield vaccines with increased specificity, efficacy, and potency. In addition, it opens up new possibilities for developing a tolerogenic vaccine, which has not been possible to date using more traditional vaccination strategies. This thesis attempted to address some of the challenges associated with cell-based tolerogenic therapies by using a material to program DCs for tolerance in a spatio-temporally controlled manner (Fig. 1.3).

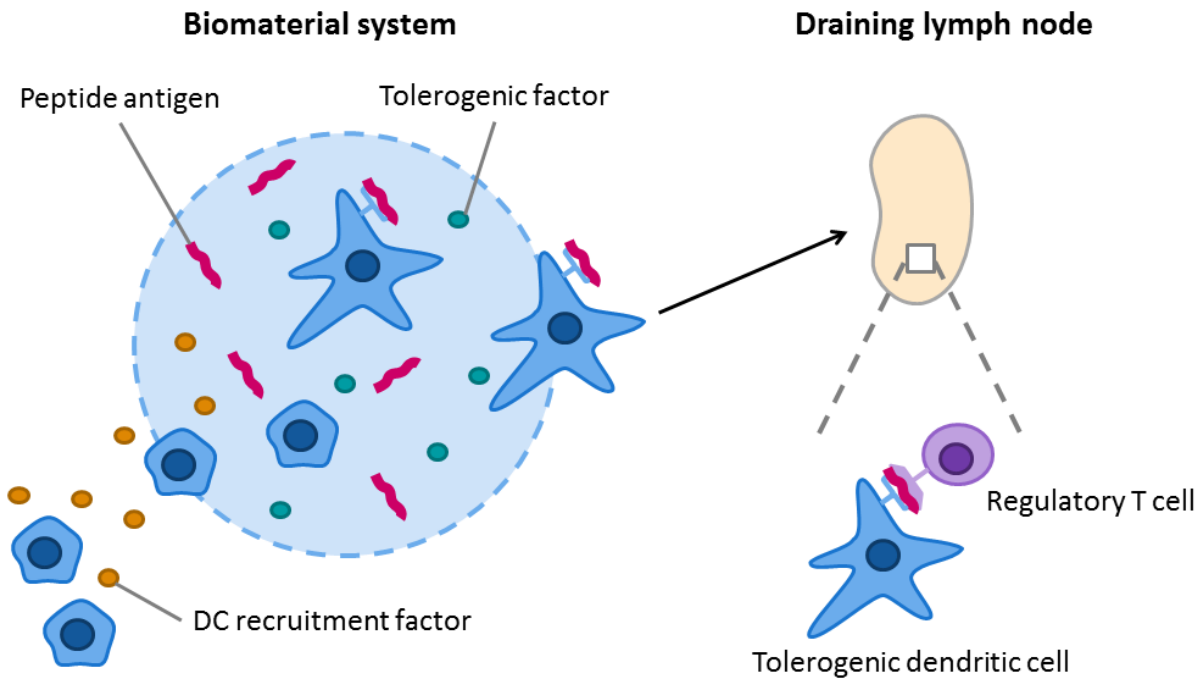

Figure 1.3. A biomaterial can be designed to modulate the immune system in an antigen-specific manner. A delivery system releasing bioactive factors in a spatio-temporally controlled manner could be used to recruit DCs into the material and program them for tolerance. After exposure to a defined peptide antigen in a non-inflammatory environment, the DCs would be redeployed to the draining lymph nodes, where they could induce, expand, and/or activate antigen-specific regulatory T cells, which have the capacity to traffic systemically and control autoimmunity.

1.2 Hypothesis

A non-inflammatory material system releasing defined recruitment and programming factors can orchestrate the recruitment of DCs and induce antigen-specific T cell responses towards immune tolerance

1.3 Specific Aims

Three specific aims tested the above hypothesis:

Aim 1: Develop a non-inflammatory alginate-based material system to effectively recruit DCs

Aim 2: Characterize the recruited DCs and demonstrate that they can orchestrate antigen-specific T cell responses

Aim 3: Conjugate a peptide antigen to alginate as a delivery strategy for generating antigen-specific tolerogenic responses *in vivo*

1.4 Significance

This work will expand the possible applications of biomaterials for immunomodulation and take steps towards the development of an effective materials-based, antigen-specific tolerogenic vaccine. The material delivery system described here builds on previous work to create a hydrogel that is non-inflammatory, can be administered in a minimally invasive manner, and effectively recruits DCs. In addition, strategies are explored for presenting defined peptide antigens to DCs in a highly localized manner,

which could have important implications for achieving precise control over immune responses, as well as improving the safety of tolerogenic therapies involving the administration of disease-associated antigens.

The eventual goal is that such a material system could provide an alternative to cell-based therapies involving *ex vivo* manipulations of autologous cells, some of which are currently in development to treat autoimmunity. The ability to generate antigen-specific tolerance would drastically change the treatment options for autoimmune diseases, as well as for transplantation tolerance.

More generally, this line of work may provide tools to increase our understanding of the mechanisms controlling immunity and tolerance. Biomaterials that serve as a privileged sites for the infiltration of immune cells could be used as *in vivo* systems to study interactions between different cell types and explore the doses and kinetics of antigen presentation that are required to establish, or re-establish, immune tolerance. In addition, the knowledge that is gained may inform the design of other materials-based vaccines, in particular cancer vaccines, to avoid initiating autoimmune diseases as a side effect, which is a growing risk as these vaccines become increasingly potent.

1.5 References

1. Zou, W. Immunosuppressive networks in the tumour environment and their therapeutic relevance. *Nat. Rev. Cancer* **5,** 263–274 (2005).

2. Zitvogel, L., Tesniere, A. & Kroemer, G. Cancer despite immunosurveillance: immunoselection and immunosubversion. *Nat. Rev. Immunol.* **6,** 715–727 (2006).

3. Seliger, B. & Massa, C. The Dark Side of Dendritic Cells: Development and Exploitation of Tolerogenic Activity That Favor Tumor Outgrowth and Immune Escape. *Front. Immunol.* **4,** (2013).

4. Cobbold, S. P. & Waldmann, H. Regulatory Cells and Transplantation Tolerance. *Cold Spring Harb. Perspect. Med.* **3,** a015545 (2013).

5. Sardi, F. *et al.* Alzheimer's disease, autoimmunity and inflammation. The good, the bad and the ugly. *Autoimmun. Rev.* **11,** 149–153 (2011).

6. Herrán-Arita, A. K. D. la *et al.* CD4+ T Cell Autoimmunity to Hypocretin/Orexin and Cross-Reactivity to a 2009 H1N1 Influenza A Epitope in Narcolepsy. *Sci. Transl. Med.* **5,** 216ra176–216ra176 (2013).

7. Ong M, Kohane IS, Cai T, Gorman MP & Mandl KD. Population-level evidence for an autoimmune etiology of epilepsy. *JAMA Neurol.* (2014). doi:10.1001/jamaneurol.2014.188

8. Nucera, S., Biziato, D. & De Palma, M. The interplay between macrophages and angiogenesis in development, tissue injury and regeneration. *Int. J. Dev. Biol.* **55,** 495–503 (2011).

9. Chambers, S. E. J., O'Neill, C. L., O'Doherty, T. M., Medina, R. J. & Stitt, A. W. The role of immune-related myeloid cells in angiogenesis. *Immunobiology* **218,** 1370–1375 (2013).

10. Eming, S. A., Krieg, T. & Davidson, J. M. Inflammation in Wound Repair: Molecular and Cellular Mechanisms. *J. Invest. Dermatol.* **127,** 514–525 (2007).

11. Zgheib, C., Xu, J. & Liechty, K. W. Targeting Inflammatory Cytokines and Extracellular Matrix Composition to Promote Wound Regeneration. *Adv. Wound Care* **3,** 344–355 (2014).

12. Walsh, M. C. *et al.* OSTEOIMMUNOLOGY: Interplay Between the Immune System and Bone Metabolism. *Annu. Rev. Immunol.* **24,** 33–63 (2006).

13. Clowes, J. A., Riggs, B. L. & Khosla, S. The role of the immune system in the pathophysiology of osteoporosis. *Immunol. Rev.* **208,** 207–227 (2005).

14. Takayanagi, H. Osteoimmunology: shared mechanisms and crosstalk between the immune and bone systems. *Nat. Rev. Immunol.* **7,** 292–304 (2007).

15. Germain, R. N. Vaccines and the Future of Human Immunology. *Immunity* **33,** 441–450 (2010).

16. Irvine, D. J., Swartz, M. A. & Szeto, G. L. Engineering synthetic vaccines using cues from natural immunity. *Nat. Mater.* **12,** 978–990 (2013).

17. Jude, B. A. *et al.* Subversion of the innate immune system by a retrovirus. *Nat. Immunol.* **4,** 573–578 (2003).

18. Johnson, W. E. & Desrosiers, R. C. VIRAL PERSISTENCE: HIV's Strategies of Immune System Evasion. *Annu. Rev. Med.* **53,** 499–518 (2002).

19. Bluestone, J. A. & Bour-Jordan, H. Current and Future Immunomodulation Strategies to Restore Tolerance in Autoimmune Diseases. *Cold Spring Harb. Perspect. Biol.* **4,** a007542 (2012).

20. Miller, S. D., Turley, D. M. & Podojil, J. R. Antigen-specific tolerance strategies for the prevention and treatment of autoimmune disease. *Nat. Rev. Immunol.* **7,** 665–677 (2007).

21. Madden, D. R., Gorga, J. C., Strominger, J. L. & Wiley, D. C. The three-dimensional structure of HLA-B27 at 2.1 Å resolution suggests a general mechanism for tight peptide binding to MHC. *Cell* **70,** 1035–1048 (1992).

22. Steinman, R. M. & Witmer, M. D. Lymphoid dendritic cells are potent stimulators of the primary mixed leukocyte reaction in mice. *Proc. Natl. Acad. Sci. U. S. A.* **75,** 5132 (1978).

23. Sakaguchi, S., Sakaguchi, N., Asano, M., Itoh, M. & Toda, M. Immunologic self-tolerance maintained by activated T cells expressing IL-2 receptor alpha-chains (CD25). Breakdown of a single mechanism of self-tolerance causes various autoimmune diseases. *J. Immunol. Baltim. Md 1950* **155,** 1151–1164 (1995).

24. Itoh, M. *et al.* Thymus and Autoimmunity: Production of CD25+CD4+ Naturally Anergic and Suppressive T Cells as a Key Function of the Thymus in Maintaining Immunologic Self-Tolerance. *J. Immunol.* **162,** 5317–5326 (1999).

25. The Autoimmune Diseases Coordinating Committee, National Institute of Allergy and Infectious Diseases & National Institutes of Health. Progress in Autoimmune Disease Research; Report to Congress. *NIH Publ.* (2005). at <http://www.niaid.nih.gov/topics/autoimmune/Documents/adccfinal.pdf>

26. Davis, M. M. & Bjorkman, P. J. T-cell antigen receptor genes and T-cell recognition. *Nature* **334,** 395–402 (1988).

27. Danke, N. A., Koelle, D. M., Yee, C., Beheray, S. & Kwok, W. W. Autoreactive T Cells in Healthy Individuals. *J. Immunol.* **172,** 5967–5972 (2004).

28. Cools, N., Ponsaerts, P., Tendeloo, V. F. I. V. & Berneman, Z. N. Balancing between immunity and tolerance: an interplay between dendritic cells, regulatory T cells, and effector T cells. *J. Leukoc. Biol.* **82,** 1365–1374 (2007).

29. Thompson, A. G. & Thomas, R. Induction of immune tolerance by dendritic cells: Implications for preventative and therapeutic immunotherapy of autoimmune disease. *Immunol. Cell Biol.* **80,** 509–519 (2002).

30. Keir, M. E., Butte, M. J., Freeman, G. J. & Sharpe, A. H. PD-1 and Its Ligands in Tolerance and Immunity. *Annu. Rev. Immunol.* **26,** 677–704 (2008).

31. Alegre, M.-L., Frauwirth, K. A. & Thompson, C. B. T-cell regulation by CD28 and CTLA-4. *Nat. Rev. Immunol.* **1,** 220–228 (2001).

32. Wing, K. & Sakaguchi, S. Regulatory T cells exert checks and balances on self tolerance and autoimmunity. *Nat. Immunol.* **11,** 7–13 (2010).

33. Vignali, D. A. A., Collison, L. W. & Workman, C. J. How regulatory T cells work. *Nat. Rev. Immunol.* **8,** 523–532 (2008).

34. Bluestone, J. A. & Abbas, A. K. Natural versus adaptive regulatory T cells. *Nat. Rev. Immunol.* **3,** 253–257 (2003).

35. Gagliani, N. *et al.* Coexpression of CD49b and LAG-3 identifies human and mouse T regulatory type 1 cells. *Nat. Med.* **19,** 739–746 (2013).

36. Kim, H.-J. & Cantor, H. Regulation of self-tolerance by Qa-1-restricted CD8(+) regulatory T cells. *Semin. Immunol.* **23,** 446–452 (2011).

37. Lu, L. & Cantor, H. Generation and regulation of CD8(+) regulatory T cells. *Cell. Mol. Immunol.* **5,** 401–406 (2008).

38. Kalampokis, I., Yoshizaki, A. & Tedder, T. F. IL-10-producing regulatory B cells (B10 cells) in autoimmune disease. *Arthritis Res. Ther.* **15 Suppl 1,** S1 (2013).

39. Fillatreau, S., Gray, D. & Anderton, S. M. Not always the bad guys: B cells as regulators of autoimmune pathology. *Nat. Rev. Immunol.* **8,** 391–397 (2008).

40. Gabrilovich, D. I. & Nagaraj, S. Myeloid-derived suppressor cells as regulators of the immune system. *Nat. Rev. Immunol.* **9,** 162–174 (2009).

41. Belle, T. L. V., Coppieters, K. T. & Herrath, M. G. V. Type 1 Diabetes: Etiology, Immunology, and Therapeutic Strategies. *Physiol. Rev.* **91,** 79–118 (2011).

42. Trudeau, J. D. *et al.* Neonatal beta-cell apoptosis: a trigger for autoimmune diabetes? *Diabetes* **49,** 1–7 (2000).

43. Benoist, C. & Mathis, D. Autoimmunity provoked by infection: how good is the case for T cell epitope mimicry? *Nat. Immunol.* **2,** 797–801 (2001).

44. Kriegel, M. A. *et al.* Naturally transmitted segmented filamentous bacteria segregate with diabetes protection in nonobese diabetic mice. *Proc. Natl. Acad. Sci. U. S. A.* **108,** 11548–11553 (2011).

45. Chervonsky, A. V. Microbiota and Autoimmunity. *Cold Spring Harb. Perspect. Biol.* **5,** a007294 (2013).

46. Steinman, R. M., Turley, S., Mellman, I. & Inaba, K. The Induction of Tolerance by Dendritic Cells That Have Captured Apoptotic Cells. *J. Exp. Med.* **191,** 411–416 (2000).

47. Steinman, R. M., Hawiger, D. & Nussenzweig, M. C. Tolerogenic Dendritic Cells*. *Annu. Rev. Immunol.* **21,** 685–711 (2003).

48. Belz, G. T. & Nutt, S. L. Transcriptional programming of the dendritic cell network. *Nat. Rev. Immunol.* **12,** 101–113 (2012).

49. Mowat, A. M. Anatomical basis of tolerance and immunity to intestinal antigens. *Nat. Rev. Immunol.* **3,** 331–341 (2003).

50. Coombes, J. L. *et al.* A functionally specialized population of mucosal CD103+ DCs induces Foxp3+ regulatory T cells via a TGF-β– and retinoic acid–dependent mechanism. *J. Exp. Med.* **204,** 1757–1764 (2007).

51. Shklovskaya, E. *et al.* Langerhans cells are precommitted to immune tolerance induction. *Proc. Natl. Acad. Sci.* **108,** 18049–18054 (2011).

52. Shortman, K. & Liu, Y.-J. Mouse and human dendritic cell subtypes. *Nat. Rev. Immunol.* **2,** 151–161 (2002).

53. Coppieters, K. T., Harrison, L. C. & von Herrath, M. G. Trials in type 1 diabetes: Antigen-specific therapies. *Clin. Immunol.* **149,** 345–355 (2013).

54. Hsu, F. J. *et al.* Vaccination of patients with B-cell lymphoma using autologous antigen-pulsed dendritic cells. *Nat. Med.* **2,** 52–58 (1996).

55. Mellman, I., Coukos, G. & Dranoff, G. Cancer immunotherapy comes of age. *Nature* **480,** 480–489 (2011).

56. Tarbell, K. V. *et al.* Dendritic cell-expanded, islet-specific CD4+ CD25+ CD62L+ regulatory T cells restore normoglycemia in diabetic NOD mice. *J. Exp. Med.* **204,** 191–201 (2007).

57. T1DM Immunotherapy Using CD4+CD127lo/-CD25+ Polyclonal Tregs - ClinicalTrials.gov. at <http://clinicaltrial.gov/ct2/show/NCT01210664>

58. Giannoukakis, N., Phillips, B., Finegold, D., Harnaha, J. & Trucco, M. Phase I (Safety) Study of Autologous Tolerogenic Dendritic Cells in Type 1 Diabetic Patients. *Diabetes Care* **34,** 2026–2032 (2011).

59. Autologous Tolerogenic Dendritic Cells for Rheumatoid Arthritis (AutoDECRA) - ClinicalTrials.gov. at <http://www.clinicaltrials.gov/ct2/show/NCT01352858>

60. Bluestone, J. A., Thomson, A. W., Shevach, E. M. & Weiner, H. L. What does the future hold for cell-based tolerogenic therapy? *Nat. Rev. Immunol.* **7,** 650–654 (2007).

61. Vries, I. J. M. de *et al.* Effective Migration of Antigen-pulsed Dendritic Cells to Lymph Nodes in Melanoma Patients Is Determined by Their Maturation State. *Cancer Res.* **63,** 12–17 (2003).

62. Ali, O. A., Huebsch, N., Cao, L., Dranoff, G. & Mooney, D. J. Infection-mimicking materials to program dendritic cells in situ. *Nat. Mater.* **8,** 151–158 (2009).

63. Hori, Y., Stern, P. J., Hynes, R. O. & Irvine, D. J. Engulfing tumors with synthetic extracellular matrices for cancer immunotherapy. *Biomaterials* **30,** 6757–6767 (2009).

64. Ali, O. A., Emerich, D., Dranoff, G. & Mooney, D. J. In situ regulation of DC subsets and T cells mediates tumor regression in mice. *Sci. Transl. Med.* **1,** 8ra19 (2009).

65. Ali, O. A. *et al.* Biomaterial-based vaccine induces regression of established intracranial glioma in rats. *Pharm. Res.* **28,** 1074–1080 (2011).

66. Ali, O. A. *et al.* The efficacy of intracranial PLG-based vaccines is dependent on direct implantation into brain tissue. *J. Controlled Release* **154,** 249–257 (2011).

67. Dendritic Cell Activating Scaffold in Melanoma - ClinicalTrials.gov. at <http://www.clinicaltrials.gov/ct2/show/NCT01753089>

68. Tsai, S. *et al.* Reversal of autoimmunity by boosting memory-like autoregulatory T cells. *Immunity* **32,** 568–580 (2010).

69. Quintana, F. J. *et al.* An endogenous aryl hydrocarbon receptor ligand acts on dendritic cells and T cells to suppress experimental autoimmune encephalomyelitis. *Proc. Natl. Acad. Sci. U. S. A.* **107,** 20768–20773 (2010).

70. Yeste, A., Nadeau, M., Burns, E. J., Weiner, H. L. & Quintana, F. J. Nanoparticle-mediated codelivery of myelin antigen and a tolerogenic small molecule suppresses experimental autoimmune encephalomyelitis. *Proc. Natl. Acad. Sci. U. S. A.* **109,** 11270–11275 (2012).

71. Getts, D. R. *et al.* Microparticles bearing encephalitogenic peptides induce T-cell tolerance and ameliorate experimental autoimmune encephalomyelitis. *Nat. Biotechnol.* **30,** 1217–1224 (2012).

72. Prasad, S., Xu, D. & Miller, S. D. Tolerance Strategies Employing Antigen-Coupled Apoptotic Cells and Carboxylated PLG Nanoparticles for the Treatment of Type 1 Diabetes. *Rev. Diabet. Stud. RDS* **9,** 319–327 (2012).

Chapter 2. A non-inflammatory, pore-forming hydrogel releasing GM-CSF effectively recruits dendritic cells (DCs) *in vivo*

2.1 Introduction

Biomaterials based vaccines are a promising new class of technologies for modulating immune responses in ways that have previously not been possible. As reviewed in Chapter 1, some of the applications being pursued include raising immunity to eradicate tumors, as well as inducing tolerance towards the body's own tissues to treat autoimmune diseases[1]. While a number of groups are developing systemically delivered nanoparticle carriers to target particular cells or tissues[2,3], another promising strategy involves the use of porous material scaffolds that immune cells can infiltrate and where they can be programmed by well-defined, localized cues[4]. Using a scaffold to recruit and program immune cells in a localized manner is appealing for inducing tolerance, since systemic delivery of a disease-related antigen could re-activate effector T cells and exacerbate disease[5]. The scaffold system previously developed by Ali and colleagues as a cancer vaccine[4] is made from poly-lactide-co-glyocolide (PLG), a material that is highly biocompatible, but that may induce some inflammation[6,7]. In addition, surgical implantation is required to introduce this scaffold into the body. These properties are not problematic for applications in which immunity is being raised against tumors or pathogens, since the added inflammation may assist in activating the immune system. However, for the induction of tolerance, even a moderate level of inflammation may run counter to the desired outcome. A new material platform that is inherently non-inflammatory and can be delivered in a minimally invasive manner

would expand the utility of materials based vaccines and make them more amenable for inducing tolerance. This chapter addresses specific aim 1 of this thesis by describing the development and characterization of a non-inflammatory, injectable hydrogel that can effectively recruit DCs.

The material selected for this application is alginate, a highly biocompatible, non-inflammatory polysaccharide composed of alternating blocks of mannuronic and guluronic acid. This polymer is FDA-approved for use as an excipient, a wound dressing material[8], and an additive to common food items. In addition, alginate has been used as a cell carrier in a number of clinical trials without adverse effects[9]. Reports in the literature concerning the immunogenicity of alginate are conflicting, but this is likely a reflection of the fact that many commercially available preparations of alginate contain a number of contaminants. Studies performed using highly purified alginate show that the polymer does not induce immune cell activation[9,10]. Alginate can be crosslinked by divalent cations, such as calcium, to form an ionically crosslinked hydrogel[9]. It is possible to chemically modify alginate in a variety of ways to impart it with different functionalities, such as degradability or cell adhesive properties[9]. Alginate hydrogels are being used for a variety of applications, including therapeutic *in vivo* delivery of single[11,12] or dual[13] growth factors, as well as *in vivo* cell delivery for tissue regeneration[14,15]. One limitation of standard alginate hydrogels is that they are nanoporous and do not allow cell infiltration or migration. Several different techniques have been developed for fabricating alginate gels that contain macro-scale pores[16–18]. More recent innovations have resulted in macroporous scaffolds that can be delivered in a minimally invasive manner through a needle, following either covalent[17] or ionic[18]

crosslinking. Ionically crosslinked macroporous gels can be obtained by incorporating rapidly degrading porogen beads into a bulk gel that will form pores *in situ* as they degrade. Several different parameters can be varied to tune the size, elastic modulus, and degradation rate of the porogens, which will in turn alter the overall structural properties of the pore-forming gels. The composition of the alginate polymer used to fabricate the beads controls both the mechanical properties as well as the degradation of the porogens. Partial oxidation of alginate opens some of the sugar rings in the polysaccharide chain and creates hydrolytically labile bonds[19,20]. However, this chemistry introduces aldehyde groups that can react with primary amines and non-specifically bind proteins *in vivo*, which may cause some inflammation at high degrees of oxidation. To address this issue, the aldehydes in oxidized alginate can be reduced to yield primary alcohols, while still allowing hydrolytic degradation of the polymer. These pore-forming gels are permissive for cell migration and can be used as a cell delivery platform to disperse cells after implantation[18]. Here, these gels are adapted to be used for effective recruitment and redeployment of DCs, which are key orchestrators of immune responses, as discussed in Chapter 1.

Since, by definition, a non-inflammatory material would not mediate immune cell infiltration on its own, a bioactive factor would be required to recruit DCs into the system. Many chemokines and factors involved in lymphocyte recruitment have been extensively studied. One such biomolecule, granulocyte-macrophage colony stimulating factor (GM-CSF) is a potent factor for DC recruitment, differentiation, and proliferation. GM-CSF is a small (14.2 kDa in mouse, 14.6 kDA in human) single-chain glycoprotein. In vitro, GM-CSF is known to promote DC survival, proliferation, and

differentiation. GM-CSF is commonly used as a media supplement to generate DCs from precursors in bone marrow or peripheral blood, and the differentiated DCs remain immature in the absence of other inflammatory cytokines or TLR ligands. It has also been shown to induce chemotaxis and chemokinesis of DCs *in vitro*, confirming its action as a recruitment factor[21]. *In vivo*, GM-CSF is secreted by a number of different cell types[22], including T cells, monocytes, and macrophages, as well as by other non-immune cells such as fibroblasts and endothelial cells. Although GM-CSF is used successfully in cell-based cancer vaccines[23], it can have contradictory effects, ranging from enhancing immune responses to inducing suppressive or toloregenic effects[22], depending on the dose and context in which it is administered. In the setting of autoimmune diseases, there have also been conflicting observations regarding the role of GM-CSF. A previous study has shown that GM-CSF depletion ameliorates disease in a mouse model of rheumatoid arthritis and in experimental autoimmune encephalomyelitis (EAE)[24], suggesting a pathogenic role for GM-CSF in those settings. However, a number of other reports have demonstrated that administration of GM-CSF can have tolerizing effects and delay disease in mouse models of type 1 diabetes[25,26] or experimental autoimmune myasthenia gravis (EAMG)[27]. In particular, these studies observed that GM-CSF treated DCs led to an increase in FoxP3$^+$ Tregs in vitro[28] and in vivo[25]. A role of GM-CSF in diabetes can also be seen from the fact that aged C57Bl/6 mice, which are not normally prone to diabetes, exhibit peri-insulitis when they are deficient in GM-CSF, and they develop diabetes when they are doubly deficient in GM-CSF and IL-3[29].

Achieving substantial DC recruitment likely requires physiologically relevant concentrations of GM-CSF to be released in a sustained manner. Controlling the release of GM-CSF would also limit the amount of GM-CSF reaching systemic circulation. This may be important considering the varying effects that GM-CSF can have depending on the context in which it acts on immune cells. Alginate can interact with heparin-binding proteins, such as VEGF[11,30], which are then released in a sustained manner. Although GM-CSF does contain a heparin-binding domain, binding to heparin only occurs at acidic pH[31,32]. Since GM-CSF has an isoelectic point around 4-5, it will be negatively charged at neutral pH and will not bind to heparin, which has a high negative charge density. Similarly, GM-CSF is not expected to interact with alginate polymer chains, which also bear a negative charge, under normal physiological conditions (pH 7.2-7.4). Based on its small size and its lack of ionic interactions with alginate at neutral pH, GM-CSF is expected to diffuse rapidly through alginate gels. A number of different nano- and micro- particle carriers have been developed in the field of drug delivery and can be used to control the release of proteins. Depending on the method by which the proteins are incorporated, these different types of particles will allow release by different mechanisms. PLG microspheres formed by a simple water-in-oil-in-water (w/o/w) emulsion technique can be used to encapsulate proteins, which are incorporated into the first water phase[4]. Depending on the molecular weight and composition of the PLG polymer, the protein will be released at a defined rate by diffusion through water-filled channels and, at later timepoints, by degradation of the polymer. Mesoporous silica (MPS) particles, on the other hand, are synthesized to contain highly structured pores that can be subsequently loaded with protein[33]. The diffusion of the protein can be restricted and controlled by using particles in which the

pores are only slightly larger than the size of the protein. Gold nanoparticles (AuNPs) form covalent bonds to thiol groups on the surface of proteins, and thus the release of the immobilized protein is dependent on the spontaneous dissociation of the gold-thiol bonds[34]. PLG and MPS, although biocompatible, result in some inflammatory responses in vivo. This is partly due to non-specific protein adsorption and unfolding, which exposes cryptic epitopes and can initiate inflammatory responses[35,36]. Gold has a long track record of safety as a dental filling material, and more recent studies have shown that gold nanoparticles are non-cytotoxic and non-immunogenic to macrophages[37] and DCs[38] in vitro. In addition, gold has been used clinically in the treatment rheumatoid arthritis, an autoimmune disease[39].

The sub-hypothesis for this chapter is that macroporous alginate hydrogels delivering GM-CSF can constitute a platform to effectively recruit DCs for downstream immune modulation. Here, effective recruitment of a highly enriched population of DCs is achieved by controlling the release kinetics of GM-CSF from alginate hydrogels, as well as the pore structure of the gels.

2.2 Materials and Methods

AuNP synthesis

AuNPs were synthesized by a citrate-reduction method[40]. Briefly, a 250mL erlen-meyer flask containing a stir bar were cleaned by first rinsing briefly in aqua regia (1 part nitric acid : 3 parts hydrochloric acid) and subsequently rinsing thoroughly in MilliQ-filtered (Millipore) H_2O. 100mL of 0.01% w/v gold chloride (III) chloride hydrate (Sigma Aldrich #

254169) were added to the flask and brought to a boil on a heating and stirring plate set to 400°C and 500rpm. 3mL of a 1% w/v sodium citrate tribasic dihydrate (Sigma Aldrich # 4641) solution were rapidly added by dispensing forcefully through an 18G needle attached to a 10mL syringe. The solution was removed from the stirring/heating plate once its color changed to red.

The size of the synthesized AuNPs was determined by DLS on a Malvern Zen 3600 Zetasizer, and their concentration was determined by measuring absorbance at 518-519nm on a UV spectrophotometer.

AuNP conjugation

The amount of GM-CSF to be conjugated to AuNPs was determined by calculating the theoretical packing of GM-CSF molecules on the surface of the AuNPs (Appendix A). 150% of the theoretical amount required to obtain 100% coverage was used to ensure complete coverage of AuNPs. A sterile-filtered 45ug/ml AuNP solution was concentrated 157.5 x by centrifuging at 20,000g for 20min and removing supernatant. After resuspending particles by pipetting and sonicating in a water bath sonicator for 10min, concentrated AuNPs were mixed with a 1mg/mL stock of GM-CSF in dH_2O and incubated at 37°C for 1 hour to allow formation of the gold-sulfur bonds.

PLG microsphere fabrication

PLG microspheres were fabricated by a standard double emulsion technique[4]. Briefly, a 100uL solution of GM-CSF in water was added to 1mL of a 5% solution of PLG (85:15, 120 kD copolymer of D, L-lactide and glycolide, Alkermes) in ethyl acetate in a silanized glass test tube. The solution was sonicated at 60% at a continuous setting for 10sec

using a Vibracell probe sonicator (Sonics & Materials). 1mL of 1% PVA / 7% Ethyl Acetate in H_2O was immediately added and the mixture was vortexed for 10sec. The emulsion was added to 200mL of 0.3% PVA / 7% ethyl acetate in H_2O and stirred for 3h. Microspheres were collected and washed in H_2O.

Mesoporous silica particle loading

3ug of GM-CSF, containing a small amount of 125I-labeled GM-CSF as a radioactive tracer, were added to 2mg of mesoporous silica microparticles in 16uL of dH2O. The particles were incubated with GM-CSF for 1h at 37°C before being flash frozen and lyophilized.

***In vitro* GM-CSF release**

3ug per sample of GM-CSF were used for release studies, unless specified otherwise. Particles or gels loaded with GM-CSF were incubated at 37°C in HBSS containining 1% BSA (Roche) to block non-specific protein adsorption and 1% penicillin/streptomycin. Whenever possible, low protein disposables were used, also to minimize non-specific protein adsorption. At each timepoint, the release buffer was collected and replaced with 1mL of fresh buffer. The amount of GM-CSF released was determined either by ELISA or by quantifying a 125I-labeled GM-CSF tracer using a gamma counter.

***In vitro* GM-CSF bioactivity assay**

Cells were isolated from the bone marrow of C57BL/6J mice, resuspended in RPMI-1640 media (supplemented with 10% heat-inactivated FBS, 1% penicillin/streptomycin, 50uM β-mercaptoethanol), and 4 x 10^4 cells/well were seeded in 96 black tissue culture

treated well plates. A standard curve was prepared by performing 4-fold serial dilutions of a 40ng/mL high standard. 100 µl of sample or standard were added, in triplicate, to each well. Cells were incubate at 37°C for 5 days, at which point 10% v/v of AlamarBlue reagent (Life Technologies) was added to each well. After a 4h incubation at 37°C, plates were read on a BioTek plate reader to measure the absorbance at 490nm. The standard curve was used to determine the level of bioactivity of the experimental samples in "ug equivalent". "Percent bioactivity" was calculated by normalizing the "ug equivalent" activity measured in the bioactivity assay to the amount of GM-CSF, in ug, detected by ELISA for the same samples.

Alginate modification

Alginate oxidation and reduction reactions were performed as described previously[15,18].

Alginate porogen fabrication

Pore-forming gels were fabricated using medical grade alginate. Porogens were formed by dispensing an alginate solution through a glass nebulizer, applying a coaxial flow of N2 gas to break up the surface tension, and collecting the beads in a crosslinking solution of 100mM $CaCl_2$ and 100mM HEPES. Beads were washed 3 times by resuspending them in an excess of HBSS (Sigma Aldrich) and pelleting them at 1,800g.

Alginate hydrogel fabrication

A solution of 3% unmodified alginate was first mixed with a solution of GM-CSF or GM-CSF-loaded particles in DMEM without L-cystine (Sigma Aldrich). This mixture, which constituted the bulk phase of the gels, was then mixed with pre-formed porogen beads.

Finally, the bulk gel was crosslinked by mixing with a slurry of $CaSO_4$ dihydrate (8.4g in 40mL H_2O). The volume of $CaSO_4$ crosslinking solution used was 4% v/v relative to the bulk alginate. All mixing steps were performed using 1mL luer-lock syringes joined with luer-lock connectors.

For in vitro studies, the gels were immediately cast between two silanized glass plates separated by 2mm spacers. After allowing the gels to crosslink for 20 min, gel disks were punched out using a sterile 8mm biopsy punch to form ~100uL gels.

For in vivo studies, an 18G needle was attached to the syringe and gels were injected subcutaneously immediately after crosslinking the bulk phase of the gel (within approximately 30-60sec). The gels stayed in place and continued to crosslink fully after injection.

Gel degradation assay

100µL alginate gels were incubated in release buffer at 37°C. At the indicated timepoints, gels were flash frozen and lyophilized to determine their dry mass.

Confocal microscopy

Images were taken using an upright Zeiss LSM 710 confocal microscope, processed using ZEN software (Zeiss), and analyzed using ImageJ software (NIH).

Gel wicking assay

100uL gels were incubated in 1mL of media at 37°C to allow degradation of the porogens. Water wicking was performed by touching an absorbent Kimwipe (Kimberly-Clark) to one side of the gel, allowing the water in the pores to be drawn out by

capillary action. To measure the wicking volume, gels were gently placed on a disposable tray and weighed on a microbalance before and after wicking.

In vivo cell recruitment studies

In vivo studies were done in C57BL/6J female mice between 6-12 weeks of age. Gels were injected subcutaneously into one flank. At various timepoints, gels were removed and dissociated in 40mM EDTA on ice for 10min, with periodic vortexing. For the analysis of lymph nodes, the subcutaneous draining LNs, located on the same side as the gel, as well as the contralateral irrelevant LNs, were also isolated and mechanically disrupted to release the cells. For both gels and LNs, cells were filtered through 40um cell strainers, and live cells were counted using a Countess automated cell counter (Life Technologies).

Flow cytometry

Cells were blocked and stained with antibodies from BD Biosciences, eBioscience, and BioLegend (Appendix B). 7-AAD (BioLegend) or Fixable Live/Dead dyes (Life technologies) were used for live and dead cell discrimination. All antibody staining steps were performed in flow cytometry staining buffer consisting of PBS with 0.5% BSA and 2mM EDTA. Data were collected on either BD LSRII or LSRFortessa flow cytometers and analyzed using FlowJo software (TreeStar).

Immunofluorescent staining of frozen sections

Gels were fixed in fresh, ice-cold 4% PFA in PBS at 4°C for 1h, then rinsed in PBS at 4°C for 2-3h. Sucrose infiltration was performed by incubating the gels in 30% w/v sucrose in

PBS at 4°C overnight. Before embedding, gels were incubated in a 1:1 mixture of 30% w/v sucrose and OCT (Tissue-Tek) for 1h. Gels were embedded in OCT in disposable molds and stored at -80°C until sectioning on a Leica cryostat. 10um sections were cut and collected on Superfrost Plus glass slides (VWR). For staining, sections were first hydrated in PBS for 5min and permeabilized in 0.5% Triton X-100 in PBS for 5min. All subsequent washes were performed using a staining buffer consisting of 0.1% Triton X-100 in PBS. Slides were blocked for 30min at room temperature in blocking buffer (staining buffer + 10% serum from the same species as the secondary antibodies). Primary antibodies were applied to slides in 150uL of blocking buffer and incubated at 4°C overnight, after which the slides were washed for 3-4 hours at 4°C. Secondary antibodies were applied to slides in 300uL of blocking buffer and incubated at room temperature for 1h, then washed for 1h. Nuclei were counterstained using a 1:1000 dilution of Hoechst 33342 (Life Technologies).

Statistical analysis

When comparing two groups, a two-tailed Student's t-test was used. When comparing multiple groups, a one-way or two-way analysis of variance (ANOVA) was performed with corrections for multiple comparisons. When paired biological samples were compared, the parameters of the statistical tests were adjusted accordingly. All statistical analyses were performed using Prism 6 (GraphPad).

2.3 Results

GM-CSF release kinetics were modulated using nano- and micro- particle carriers

As a first step towards achieving effective DC recruitment to alginate hydrogels, GM-CSF release kinetics were engineered to be sustained over several days. When GM-CSF was incorporated directly into a 2% w/v alginate hydrogel, over 90% of the encapsulated protein was released within the first 12 h (Fig. 2.1 A). To achieve a more sustained delivery of GM-CSF, three different nano- or micro- particle carriers were tested. GM-CSF was covalently coupled to AuNPs, encapsulated within PLG microspheres, or incorporated into porous MPS microparticles, following which release of GM-CSF at 37°C was evaluated over time (Fig. 2.1 B). 50% of the GM-CSF was released from AuNPs in first day, whereas 65% and 75% of the GM-CSF were released from the PLG microspheres and MPS, respectively, in the same time period. After 4 weeks, the PLG microspheres had the highest fraction of unreleased GM-CSF still associated with the particles. The final percentages of GM-CSF released at the end of the timecourse were 79% for PLG, 90% for MPS, and 98% for AuNPs. Together, these results demonstrated that GM-CSF release from AuNPs, which requires dissociation of a covalent bond, was the most gradual and sustained over the first few days, as well as the most complete over the course of four weeks. AuNPs were selected for GM-CSF delivery in subsequent work for these reasons, as well as the fact that gold is expected to be the least inflammatory material among the three that were tested.

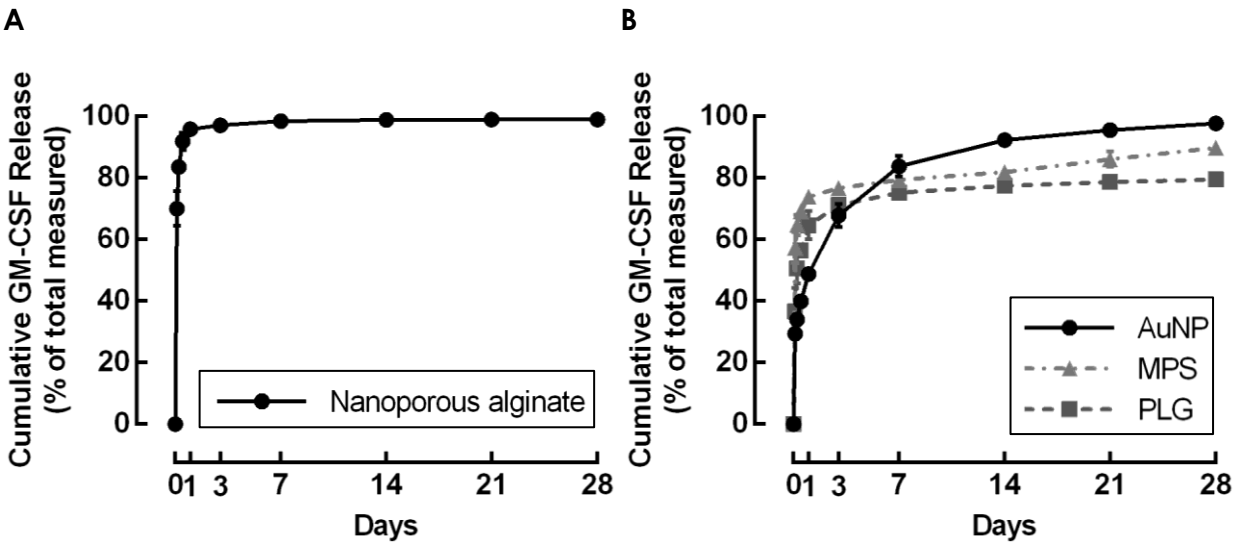

Figure 2.1. Micro- or nano- particle carriers controlled GM-CSF release kinetics. (A) GM-CSF release after direct incorporation in nanoporous alginate gels. 3ug of GM-CSF were encapsulated in ionically crosslinked alginate hydrogels, which were incubated at 37°C in release buffer. GM-CSF release into the supernatant was measured by ELISA. (n = 5; mean ± s.d. shown). (B) GM-CSF release from micro- or nano- particle carriers. For AuNP and PLG, GM-CSF release was quantified by ELISA; for MPS, ^{125}I-labeled GM-CSF was used as a radioactive tracer. (n = 5; mean ± s.d. shown).

Incorporation of GM-CSF conjugated AuNPs in alginate hydrogels resulted in sustained GM-CSF release

AuNPs coated with GM-CSF were incorporated into alginate gels to form a controlled delivery system that could also serve as a physical scaffold for cell infiltration. First, an *in vitro* assay was developed using primary bone marrow cells to test the bioactivity of GM-CSF after conjugation to and release from AuNPs. Across all timepoints, samples of GM-CSF released from AuNPs exhibited greater than 100% bioactivity (Fig. 2.2). At 3h, 6h, and 12h, the bioactivity levels were 166%, 155%, and 141%, respectively. At the subsequent timepoints, from day 1 and on, the bioactivity remained constant, around 125%.

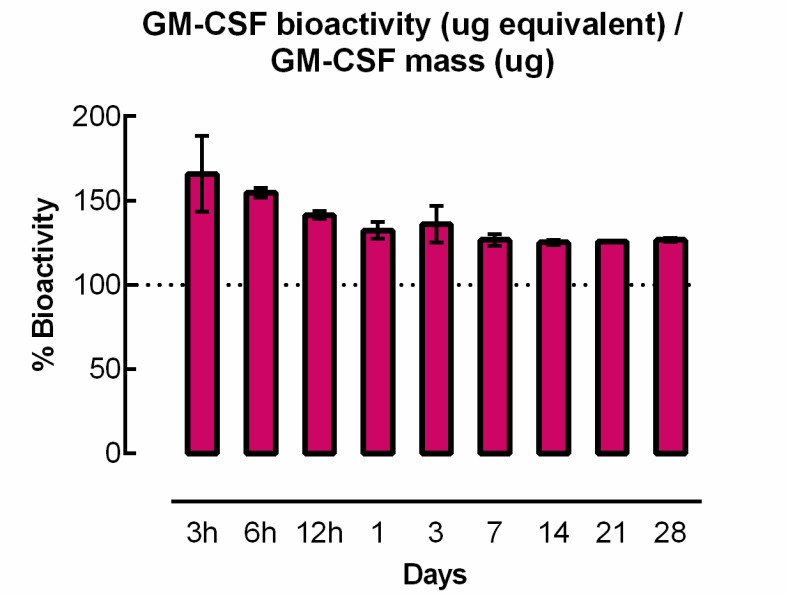

Figure 2.2. GM-CSF remained bioactive following release from AuNPs. GM-CSF-conjugated AuNPs were incubated at 37°C in release buffer and supernatants were removed at each timepoint. Release samples were used in an *in vitro* bioactivity assay and compared to a standard curve to determine their level of bioactivity. The same samples were quantified by ELISA to determine the amount of GM-CSF in ug. (n = 5; mean ± s.e.m. shown).

It was found that GM-CSF dissociated rapidly from AuNPs in the presence of cystine, exhibiting 77% release into the supernatant in only 3 hours, and almost 98% release by 24 hours (Fig. 2.3 A). In contrast, the retention of GM-CSF on AuNPs was significantly higher in cystine-free media (Fig. 2.3 B). After 18 hours, the fraction of GM-CSF that remained conjugated to the AuNPs was 91% in HBSS, and 78% in cystine-free DMEM. For both of these conditions, there was still a statistically significant reduction in the amount of GM-CSF remaining on the AuNPs compared to the 0h control, in which ~96% of the GM-CSF was bound, indicating that the GM-CSF was still being released. In light of these findings, GM-CSF-conjugated AuNPs were incorporated into alginate hydrogels, and the profiles of GM-CSF release were compared between gels formulated with and without cystine (Fig. 2.3 C). When GM-CSF release from cystine-free gels was measured, the resulting GM-CSF release profile was similar to the release from AuNPs alone (Fig 2.1

B). On the other hand, when gels were formulated using standard media containing cystine, the release of GM-CSF was almost identical to the release of free GM-CSF incorporated directly into gels without AuNPs (Fig 2.1 A). Together, these results demonstrated that AuNPs could be used to deliver bioactive GM-CSF from alginate hydrogels, and that the release rate would be gradual and sustained, provided that the gels were formulated without cystine.

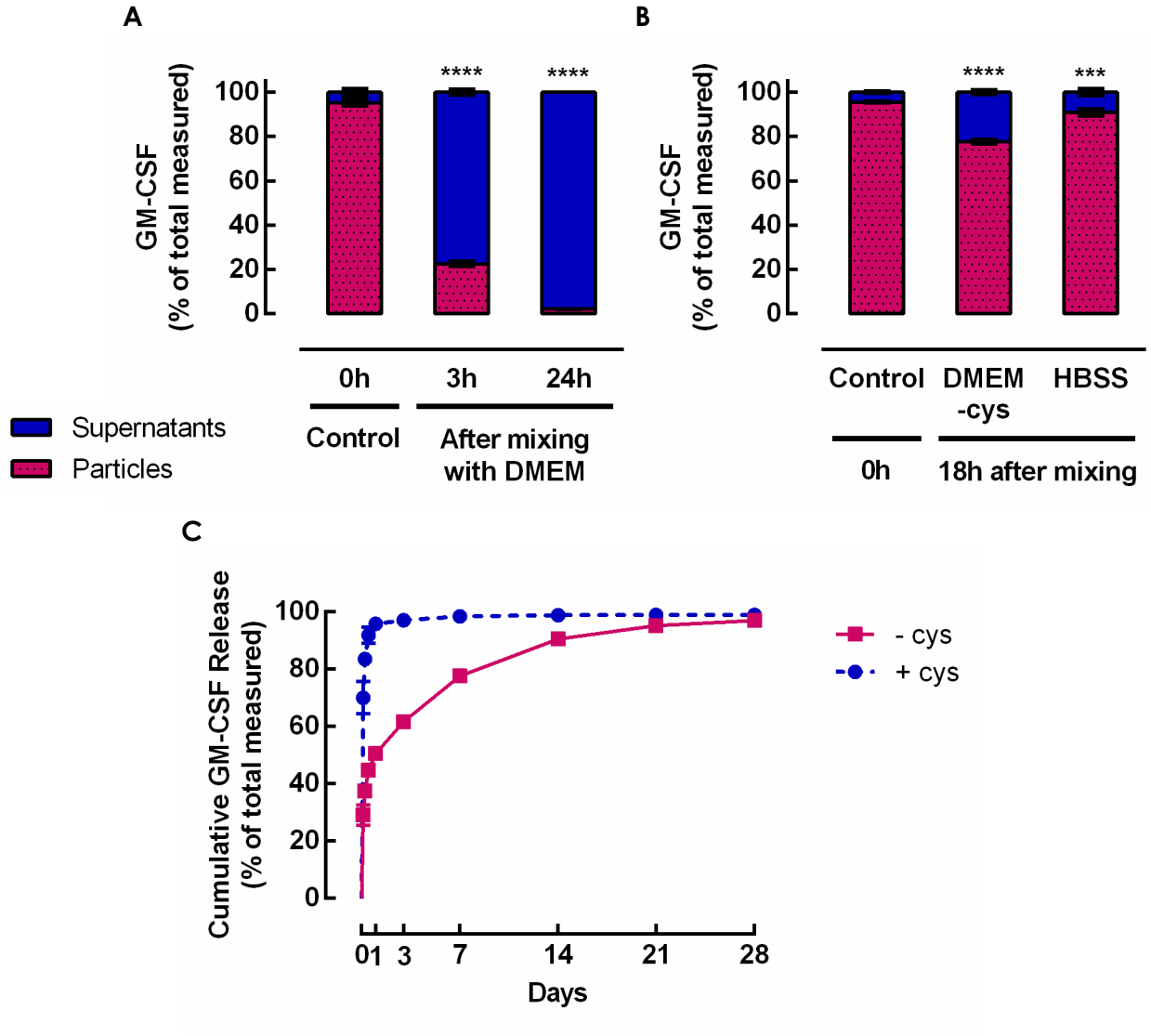

Figure 2.3. GM-CSF release was gradual and sustained when GM-CSF conjugated AuNPs were incorporated into alginate hydrogels formulated without cystine. (A-B) GM-CSF release from AuNPs in cystine containing media, such as standard DMEM (A), or in cystine-free media (B). AuNPs were conjugated to GM-CSF, then mixed with the indicated media and incubated at 37°C for the indicated time. The amounts of GM-CSF released into the media or still associated with the particles were quantified by ELISA. (n = 3; mean ± s.d. shown; *** $p < 0.001$; **** $p < 0.0001$). (C) AuNPs were conjugated to 3µg of GM-CSF and incorporated into 100µL alginate gels formulated either with or without cystine. Gels were incubated at 37°C in 1mL of release buffer, and supernatants were removed at each timepoint to quantify the amount of released GM-CSF by ELISA. (n = 5; mean ± s.d. shown).

Pore-forming gel properties were modulated to allow cell infiltration

Pore-forming alginate hydrogels, which are formed by incorporating rapidly degrading porogen beads into a bulk gel (Fig. 2.4), were characterized and optimized for *in vivo* recruitment of DCs in response to GM-CSF. The effects of varying different fabrication parameters on porogen degradation and size were examined. The degradation kinetics for different alginate formulations at 37°C were determined (Fig. 2.5 A). 2% w/v alginate hydrogels made from 7.5% oxidized/reduced alginate degraded almost completely in only 3 days. In contrast, unmodified alginate gels showed a small initial reduction in dry mass, which was likely due to the diffusion of sulfate ions and unbound calcium ions following crosslinking, but the dry mass then plateaued and remained stable over time, indicating that the gels did not degrade. Binary mixtures of 7.5% oxidized/reduced alginate with a small amount of unmodified alginate exhibited intermediate degradation profiles. A combination of 2% w/v oxidized/reduced alginate together with 0.25% w/v unmodified alginate was selected for subsequent work since it displayed sufficient mechanical stability to withstand the porogen bead fabrication process, yet still degraded rapidly, exhibiting 70% degradation in 5 days. Varying the composition of the polymer affected not only the degradation rate, but also the size of the porogen beads, since oxidized/reduced alginate had a lower molecular weight distribution than unmodified alginate as a result of the oxidation process, and thus a lower viscosity. Increasing the amount of unmodified alginate led to larger diameter porogen beads, while increasing the coaxial airflow rate yielded smaller diameter porogens (Fig. 2.5 B). These porogens formed a separate phase within the gel, even after mixing and crosslinking the bulk gel (Fig. 2.5 C). After incubation at

37°C *in vitro*, the interconnected porosity of pore-forming gels was significantly higher than that of nanoporous gels, indicating that the porogens degraded and formed voids within the bulk gel (Fig. 2.5 D).

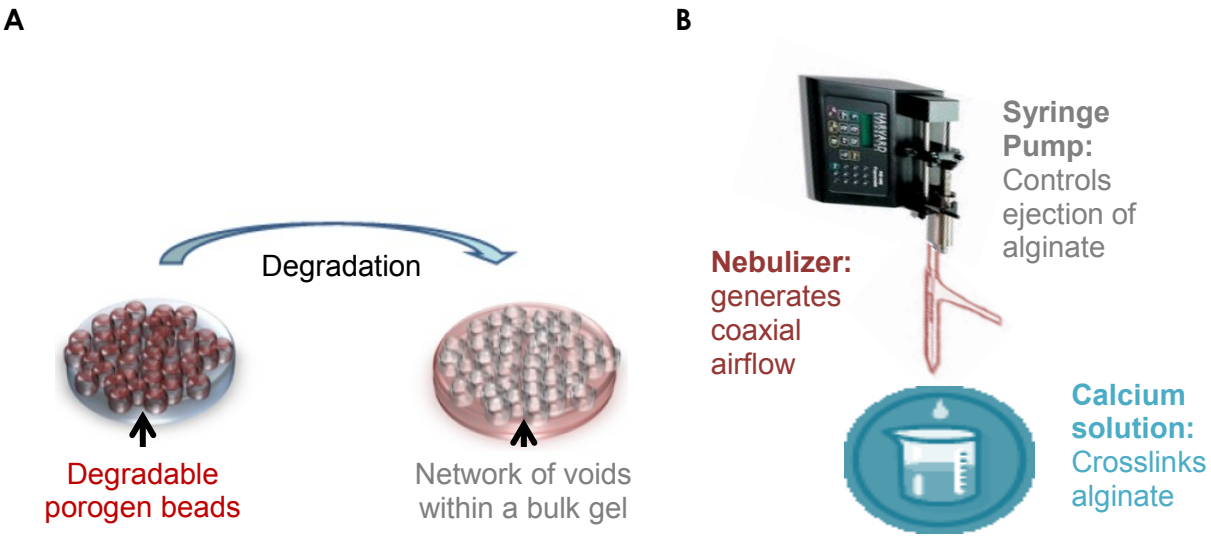

Figure 2.4. Pore-forming hydrogels were created by incorporating rapidly degrading porogen beads into a bulk gel. (A) Formation of a network of voids, or pores, following the degradation of porogen beads within a bulk gel. (B) Setup for porogen fabrication. – Diagrams adapted from Huebsch et al.

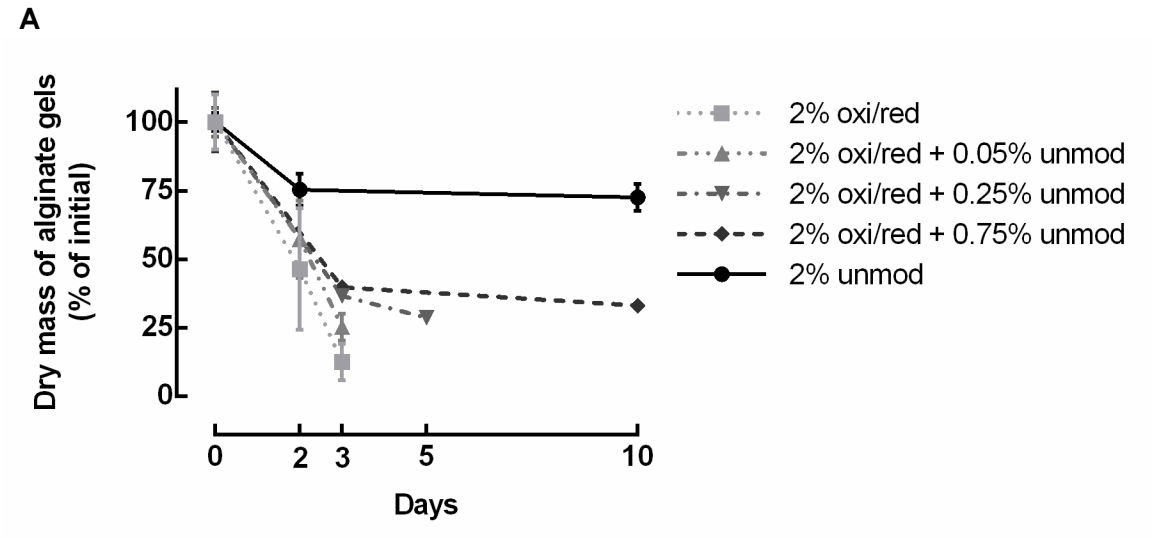

Figure 2.5.

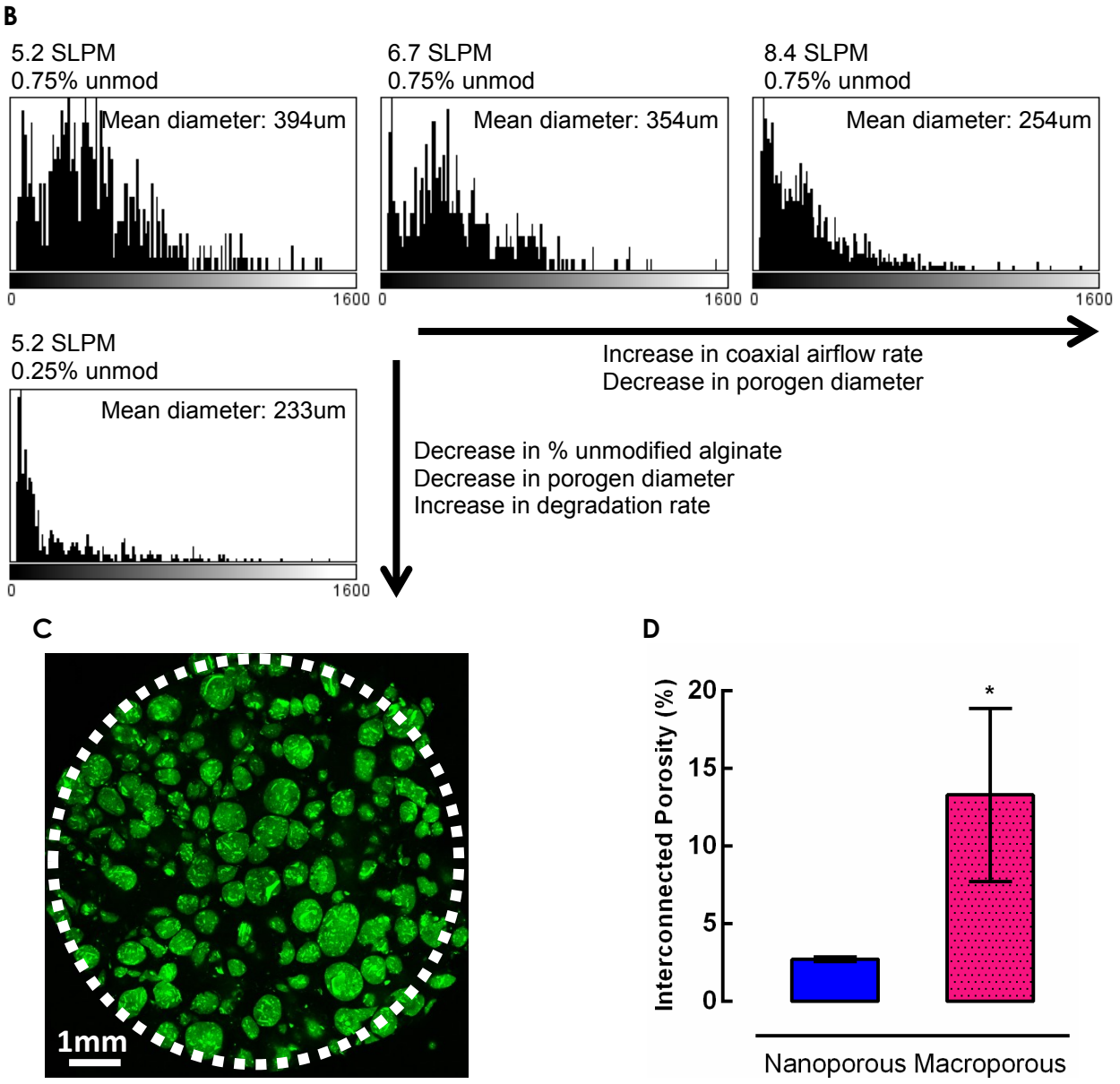

Figure 2.5 (continued). Degradable alginate porogens formed a separate phase within a bulk alginate hydrogel and created a macroporous structure as they degraded. (A) *In vitro* degradation kinetics of alginate gels consisting of 2% w/v unmodified (unmod) alginate, 2% w/v oxidized then reduced (oxi/red) alginate, or binary mixtures of oxi/red and unmod alginate. (n = 3; mean ± s.d. shown). (B) Size distributions of porogens fabricated with different coaxial airflow rates (SLPM of N_2 gas) and percentages of unmod alginate (all conditions contained 2% w/v oxi/red alginate). Labeled porogens were imaged by confocal microscopy. Maximum intensity projections were obtained from confocal Z-stacks and thresholded to analyze particle size (maximum Feret's diameter in um). (C) Confocal Z-slice of a pore-forming gel containing FITC-labeled porogen beads (green) within a bulk gel. White dotted line demarcates gel border. (B) Interconnected porosity of nanoporous and macroporous pore-forming gels, as measured by a wicking assay. (n = 4; mean ± s.d. shown; * $p < 0.05$).

Pore-forming gels delivering GM-CSF *in vivo* mediated substantial cell recruitment

To examine cell recruitment *in vivo*, pore-forming gels delivering GM-CSF conjugated to AuNPs were injected subcutaneously into the flanks of mice. The protein-coated AuNPs were incorporated into the bulk, non-degrading phase of pore forming gels. To test whether the AuNPs exerted any effects independently of GM-CSF, AuNPs were conjugated to a control protein, consisting of Fab fragments from mouse IgG. Mouse Fab fragments are not expected to elicit any biological activity, since they are native proteins, and, unlike Fc fragments, they will not be bound by specialized receptors. Since Fab fragments are larger than GM-CSF (diameters were approximated to be 5nm and 3.4nm, respectively), the amount of protein was reduced to maintain the same surface coverage of the AuNPs while still delivering the same number of AuNPs. Gels that did not contain any GM-CSF, i.e. blank gels and gels containing control AuNPs, did not mediate substantial cell recruitment (Fig. 2.6). Gels delivering soluble GM-CSF showed an accumulation of ~1.6 x 10^6 cells at day 3, and the number of cells in the gels remained higher than in the conditions without GM-CSF for the rest of the timecourse. Strikingly, when GM-CSF was conjugated to AuNPs and delivered in gels, over 5 million cells were recruited into the gels at the peak of cell infiltration (Fig. 2.6 A). While the number of cells in the gels decreased after day 3, there were still close to 3 x 10^6 cells in the gels at day 5, and ~10^6 cells were maintained in the gels up until 14 days after injection. AUCs were calculated to estimate the total number of cells residing in the gels over the course of two weeks (Fig. 2.6 B). Gels delivering GM-CSF conjugated to AuNPs had an AUC of ~24 x 10^6, which was significantly higher than all of the other conditions. The AUC for gels delivering soluble GM-CSF was ~12 x 10^6, which was 2-fold

lower than for the gels delivering GM-CSF conjugated to AuNPs. Although the gels with soluble GM-CSF exhibited more cell infiltration than blank gels or gels with control AuNPs, the differences in AUCs were not statistically significant. These results showed that the delivery of GM-CSF conjugated to AuNPs in pore-forming alginate gels was highly effective at recruiting a large number of cells into the gels over a period of two weeks, with the peak of cell infiltration occurring at day 3. The observation that the number of cells recruited was significantly higher for GM-CSF conjugated to AuNPs compared to soluble GM-CSF demonstrated that control over GM-CSF release kinetics was indeed important for optimal cell recruitment.

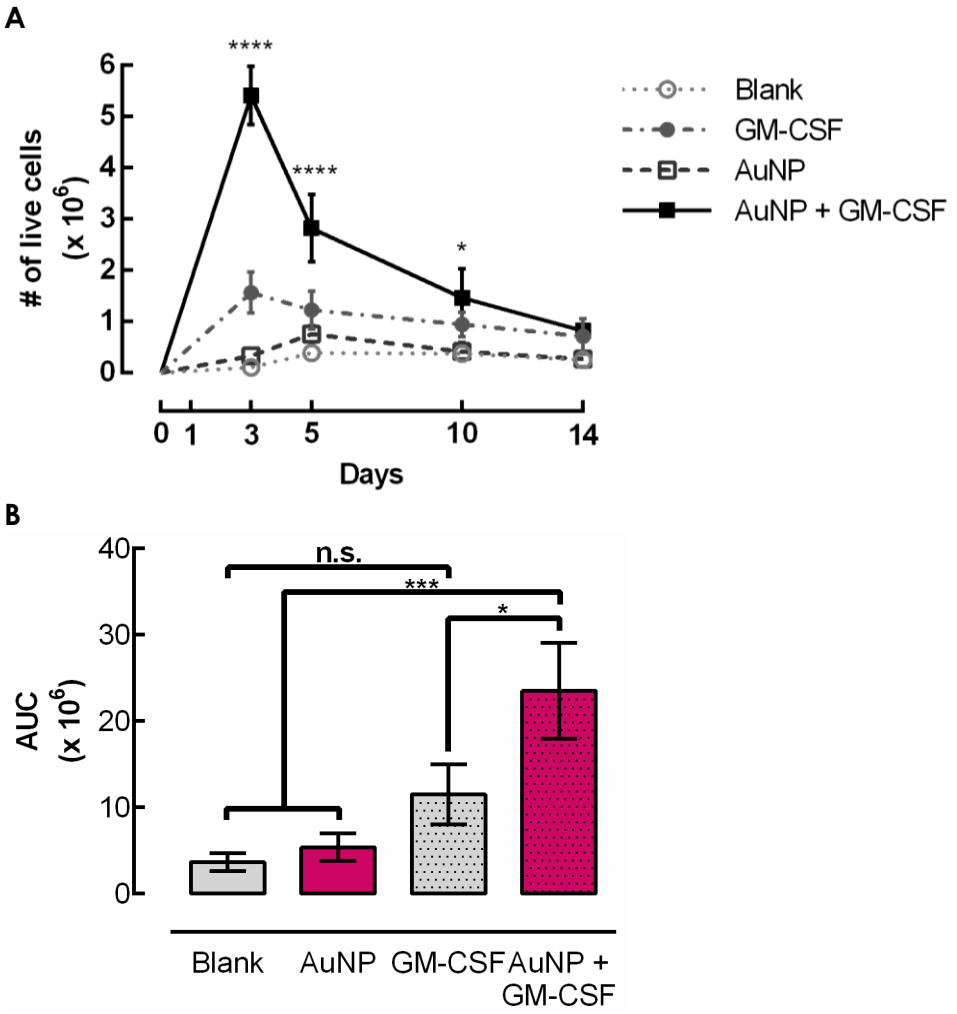

Figure 2.6. Pore-forming gels delivering GM-CSF conjugated to AuNPs mediated substantial cell recruitment in vivo. Gels were injected subcutaneously into the flanks of C57BL/6J mice. At specified timepoints, gels were dissociated to retrieve and quantify infiltrating cells. (A) Number of live cells in gels over time. (n = 3 - 9 per condition per timepoint; mean ± s.d. shown; * $p < 0.05$ compared to Blank and AuNP; **** $p < 0.0001$ compared to all other conditions; AuNP + GM-CSF condition was compared to all other conditions at each timepoint.) (B) Areas under curves corresponding to the cell recruitment data shown in (A). (* $p < 0.05$; *** $p < 0.001$; all conditions were compared to each other.)

To determine whether the structural properties of the pore-forming gels had a significant impact on cell recruitment, the volume fraction of the porogens, as well as the total gel volume, were altered. A porogen volume fraction of 50% led to significantly more cell infiltration than a 25% porogen volume, which indicated that the

incorporation of degradable porogens facilitated cell infiltration into the gels (Fig. 2.7). Unexpectedly, 3 days after injection of the gels, at the peak of cell infiltration, a 50% porogen fraction allowed significantly more cell infiltration than a higher 75% porogen fraction. When the porogen volume fraction was maintained at 50%, doubling the total volume of the gels from 100uL to 200uL led to significantly higher cell infiltration at days 5 and 10, even though the amount of GM-CSF delivered remained constant. The increased accumulation in the 200uL gels may have been a reflection an impaired ability of the cells to migrate out of the larger volume gels and be redeployed, rather than an enhancement in cell recruitment. Based on these data, the 100µL gels with a 50% porogen volume were selected as being optimal for subsequent experiments.

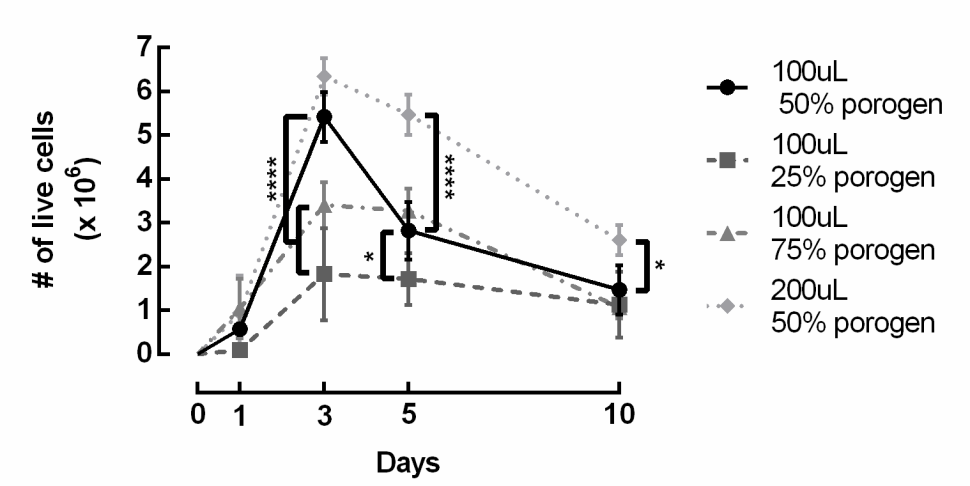

Figure 2.7. Modulating the volume and porogen fraction of pore-forming gels controlled the number of recruited cells. Gels were injected subcutaneously into the flanks of C57BL/6J mice. At specified timepoints, gels were dissociated to retrieve and quantify infiltrating cells. (n = 3 - 9 per condition per timepoint; mean ± s.d. shown; * $p < 0.05$; **** $p < 0.0001$; 100uL 50% porogen condition was compared to all other conditions at each timepoint.)

Recruited cells were highly enriched in CD11c$^+$ dendritic cells

The cells recruited into this gel system were characterized by analyzing a variety of cell surface markers associated with immune cells. For all the timepoints and conditions examined, the vast majority of cells (~80-98%) were CD11b$^+$ (Fig. 2.8 C). A very high percentage of the cells across all timepoints and conditions were also CD11c$^+$ (Fig. 2.8 D). At day 3, the gels delivering GM-CSF conjugated to AuNPs contained 68% CD11c$^+$ cells, which was significantly lower than the 89% CD11c$^+$ cells found in the gels delivering soluble GM-CSF. However, by day 5, the fraction of CD11c$^+$ cells in gels with GM-CSF + AuNP increased to 94%. Histological examination confirmed that the recruited cells expressed CD11c$^+$, and also demonstrated that the cells were able to infiltrate all the way into the center of the gels as early as 3 days after gel injection (Fig. 2.8 B).

A substantial percentage of the CD11b$^+$ CD11c$^+$ double positive cells in the gels also expressed F4/80, a marker of macrophages that is also expressed on some DC subsets (Fig. 2.8 E). The gels delivering GM-CSF conjugated to AuNPs showed a trend towards a lower fraction of F4/80$^+$ cells compared to the other conditions, with some of these differences being statistically significant at days 3 and 10. At day 3, the peak of cell infiltration, around 30% of the cells expressed Gr-1, a marker of monocytes and granulocytes, when GM-CSF conjugated to AuNPs was delivered in the gels (Fig. 2.8 F). This was significantly higher than in the other conditions, which only had ~8-20% Gr-1$^+$ cells at this same timpoint. At later timepoints, this population was reduced and constituted less than 5% of the cells found in gels delivering GM-CSF + AuNP. Finally, the

fraction of cells positive for DX5, an antibody clone that binds to CD49b and labels NK cells, as well as some NKT cells and T cells, was examined. At day 5, the fraction of cells positive for DX5 was only 5% in gels delivering GM-CSF + AuNP, which was significantly lower than in the conditions that did not contain GM-CSF (Fig. 2.8 G). However, at day 14, this relationship was reversed, such that gels delivering GM-CSF + AuNP contained significantly more $DX5^+$ cells than in the other conditions, around ~25%. Overall, the data show that pore-forming gels delivering GM-CSF recruited cells that were predominantly $CD11b^+$ $CD11c^+$ (Fig. 2.8 A), with a large fraction of these also being $F4/80^+$.

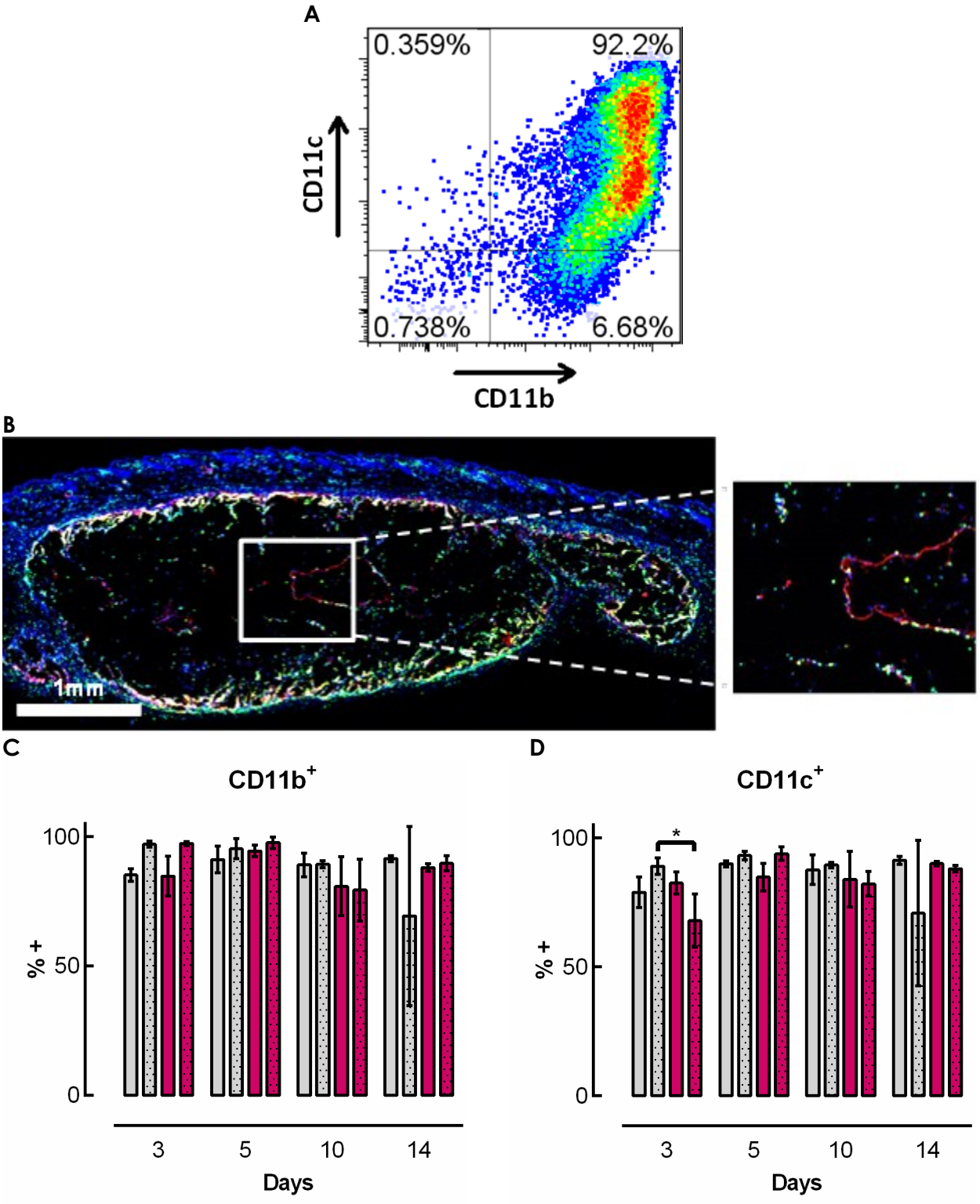
A
0.359%
92.2%
0.738%
6.68%
CD11c
CD11b
B
1mm
C
CD11b+
100
% +
50
0
3
5
10
14
Days
D
CD11c+
*
100
% +
50
0
3
5
10
14
Days

Figure 2.8.

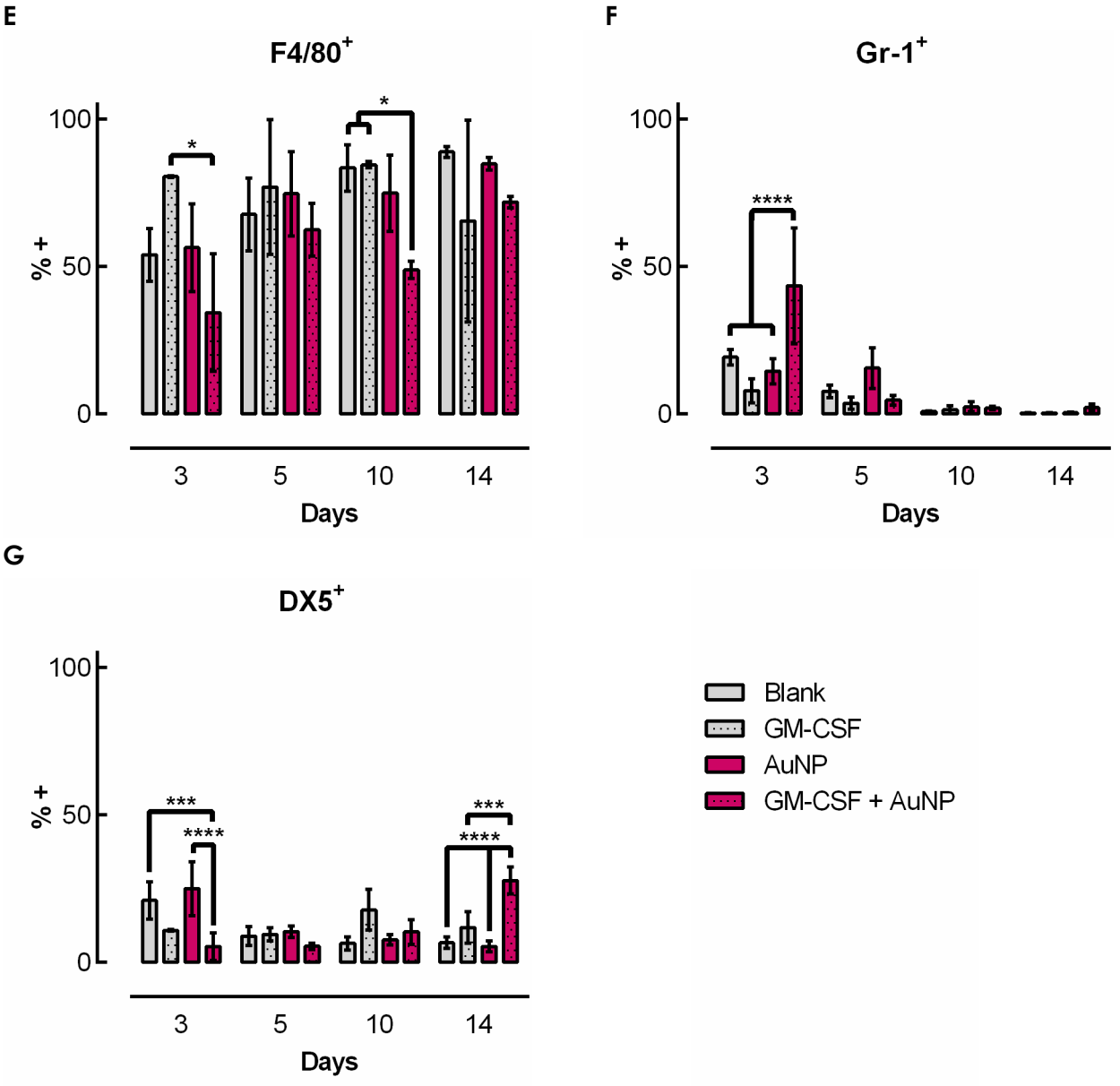

Figure 2.8 (continued). Gels delivering GM-CSF in vivo recruited a highly enriched population of DCs. Gels were injected subcutaneously in the flanks of C57BL/6J mice. At specified timepoints, gels were dissociated to retrieve, quantify, and analyze infiltrating cells. (A) Flow cytometry plot of $CD11b^+$ $CD11c^+$ cells isolated from a gel delivering GM-CSF + AuNPs after 5 days. (B) Immunofluorescent staining of a sectioned gel delivering GM-CSF + AuNPs 3 days after injection. 10um sections were stained for CD11c (red), MHCII (green), and nuclei (blue). (C-G) Frequency of cells expressing cell surface markers CD11b (C), CD11c (D), F4/80 (E), Gr-1 (F), and DX5 (G). (n = 3 per condition per timepoint; mean ± s.d. shown; * $p < 0.05$; *** $p < 0.001$; **** $p < 0.0001$; GM-CSF + AuNP condition was compared to all other conditions at each timepoint.)

Since the percentage of $CD11b^+$ $CD11c^+$ DCs was so high in the first two weeks, conversely, the percentage of other cell types in the gels was low. At later timepoints, i.e. day 17 and 21, the fraction of $CD11b^+$ $CD11c^+$ cells was around 50-60%, and the expression of other immune cell markers was examined. B cells were almost completely absent from the gels, constituting <1% of all cells, while the fraction of T cells was ~5-8% at days 17 and 21 (Fig. 2.9 A). Notably, the majority of the T cells were $CD4^+$ helper T cells, with less than 10% of the T cells being $CD8^+$ cytotoxic T cells (Fig. 2.9 B). Of the $CD4^+$ T cells, > 55% expressed CD25, the high-affinity IL-2 receptor that is expressed on Tregs, as well as transiently on activated T cells (Fig. 2.9 C).

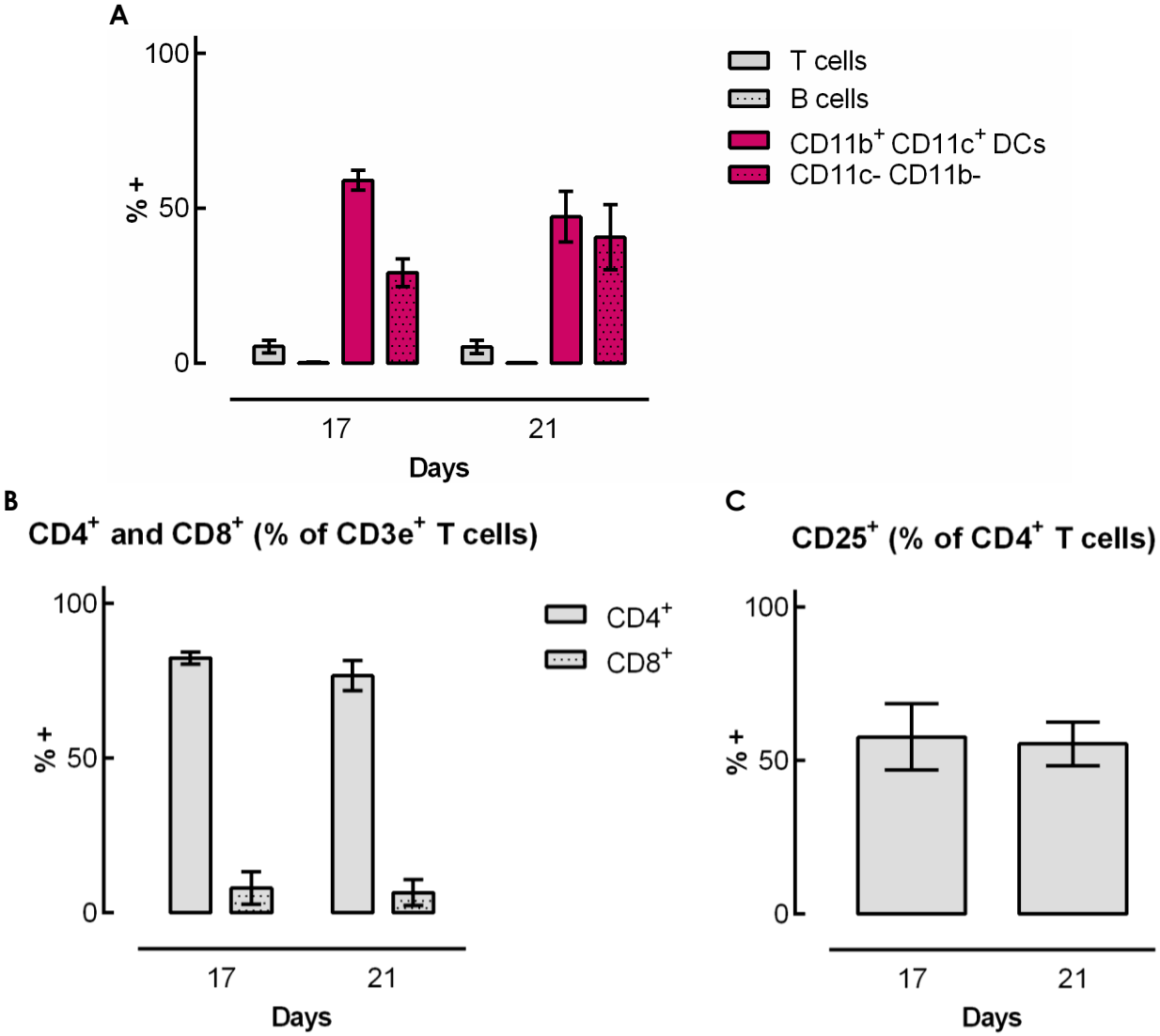

Figure 2.9. A small fraction of CD4+ CD25+ T cells was present in gels delivering AuNP + GM-CSF at later timepoints. Gels were injected subcutaneously in the flanks of C57BL/6J mice. At specified timepoints, gels were dissociated to retrieve, quantify, and analyze infiltrating cells. (A-C) Quantification of flow cytometry data at days 17 and 21 after gel injection. (A) Percentage of T cells, B cells, and DCs found in gels. (B) Percentage of T cells that are CD4+ helper T cells or CD8+ cytotoxic T cells. (C) Percentage of CD4+ T cells expressing CD25. (n = 3 per condition per timepoint; mean ± s.d. shown).

The lymph nodes of mice that received gels delivering GM-CSF conjugated to AuNPs were examined to determine whether any changes in cell number or composition could be observed in the draining lymph nodes. The lymph nodes draining the gels contained significantly more cells than the irrelevant lymph nodes on the contralateral flank at days 5 and 10 (Fig. 2.10 A). In addition, a statistically significantly higher percentage of CD11c$^+$ cells was found in the draining lymph nodes compared to the irrelevant lymph nodes at days 3 and 5 (Fig 2.10 B).

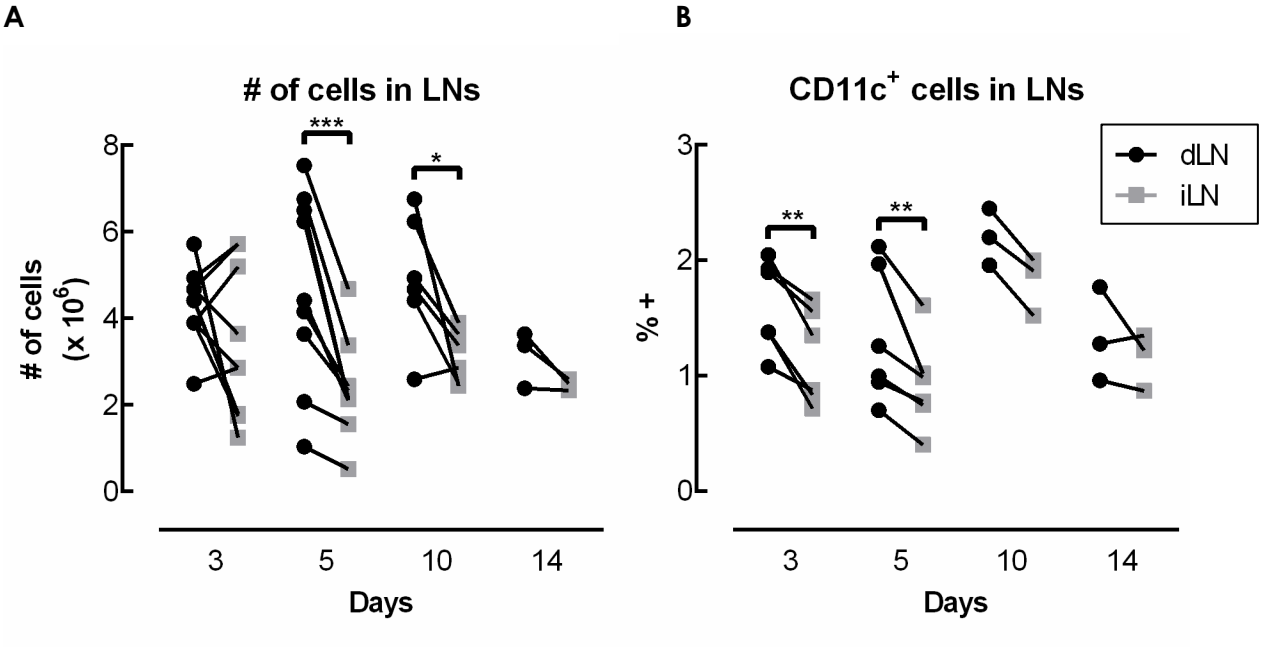

Figure 2.10. Administration of gels delivering GM-CSF led to an increase in the number and percentage of CD11c$^+$ cells in the draining lymph nodes compared to irrelevant lymph nodes. Gels were injected subcutaneously in one flank of C57BL/6J mice. At specified timepoints, the LNs draining the gel (dLN) and the irrelevant LNs (iLN) on the contralateral side were isolated and dissociated to enumerate total cells (A) as well as the percentage of CD11c$^+$ cells (B). (n = 3 - 9 per condition per timepoint; individual data points shown with lines connecting paired samples isolated from the same mouse; * $p < 0.05$; ** $p < 0.01$; *** $p < 0.001$).

2.4 Discussion

The material system developed here, which consisted of an injectable, non-inflammatory, pore-forming hydrogel, mediated an impressive local enrichment of $CD11c^+$ DCs following the release of a DC recruitment factor. Optimal cell accumulation was achieved by controlling both the release kinetics of the recruitment factor, GM-CSF, as well as the physical structure of the hydrogel. Since the hydrogel was engineered to be macroporous, the recruited DCs were able to infiltrate throughout the material, representing an opportunity to control their behavior by exposing them to a defined microenvironment within the hydrogel.

Since GM-CSF does not interact with alginate, several different particle carriers were tested for their ability to delay GM-CSF release from alginate hydrogels. The different types of particles were all able to mediate sustained release of GM-CSF. AuNPs exhibited the most slow and gradual GM-CSF release over the first few days, but also the most complete release at the end of four weeks. The PLG microparticles retained the highest amount of unreleased GM-CSF at the end of four weeks, likely due to the fact that release from PLG is first diffusion controlled, then degradation controlled. For PLG with an 85:15 lactide:glycolide ratio, complete degradation is achieved by 35 weeks, but no significant weight loss occurs until after 10 weeks[41], so the PLG would not have degraded substantially in the timeframe of this release study. AuNPs were selected for subsequent use in the material system because they exhibited a gradual and sustained release of GM-CSF, and also because gold is expected to be inert and non-inflammatory *in vivo*.

The bioactivity of GM-CSF was tested after its release from AuNPs, and it was found to be greater than 100% at all timepoints up until 4 weeks, at which point 98% of the measured GM-CSF had been released from the particles. This demonstrates that the formation and dissociation of gold-thiol bonds did not lead to significant protein unfolding or denaturation. In fact, the samples showed >~125% bioactivity at all timepoints, with the highest percent bioactivity seen in the first 12 hours (166% at 3h, 155% at 6h, and 141% at 12h). The pore size of nanoporous alginate gels is on the order of 5-6nm[19], so the 13nm diameter AuNPs used here were expected to remain entrapped, exhibiting little to no diffusion out of the gels. However, release of AuNPs from the surface of the gel at the earliest timepoints could explain the unexpectedly high percent bioactivity that was observed, since multivalent GM-CSF presentation on the AuNPs may result in more potent bioactivity.

The presence of cystine was found to accelerate the release of GM-CSF from AuNPs, so the gel system was formulated to be free of cystine in order to maintain a more gradual release. Although a very gradual and sustained release of GM-CSF from AuNPs was achieved *in vitro*, it is unclear how closely the measured *in vitro* release profile matches the actual *in vivo* release kinetics. The levels of thiol-containing molecules such as cysteine, cystine, and glutathione were reported to be on the order of 10-100uM in plasma and tissues[42,43], which is a similar order of magnitude to what is found in common media (DMEM and RPMI-1640 contain 200uM of cystine). Upon injection of the gels *in vivo*, endogenous thiol-containing molecules, as well as other proteins, will diffuse into the gel and likely lead to GM-CSF release that is accelerated compared to

the *in vitro* release performed in the absence of cystine. However, additional complexities of the *in vivo* environment, i.e. the presence of many other proteins and biomolecules, make it difficult to predict the resulting *in vivo* release kinetics. Quantifying GM-CSF released from the material directly *in vivo* is challenging, in large part because it is not possible to distinguish the exogenous recombinant murine GM-CSF delivered in the gels from the endogenous murine GM-CSF secreted by immune cells. It would be possible to deliver GM-CSF from another species, such as recombinant human GM-CSF, and quantify it independently from the endogenous murine GM-CSF. However, GM-CSF molecules from different species have slightly different heparin-binding characteristics[31], so this approach would not be entirely representative either. Despite the fact that its *in vivo* release may be more rapid than what was measured *in vitro*, GM-CSF conjugated to AuNPs still has a much more potent biological effect *in vivo* than free GM-CSF. Indeed, significantly more cell infiltration into the gels was observed when GM-CSF was conjugated to AuNPs compared to when it was incorporated directly in the alginate. This effect cannot be attributed to the AuNPs themselves, since gels containing AuNPs conjugated to a control protein were similar to the blank gels and did not induce substantial cell accumulation. The strategy of using AuNPs as a carrier could potentially be applied to control the release of other non-heparin-binding proteins from alginate.

The delivery of GM-CSF conjugated to AuNPs in pore-forming alginate gels led to the infiltration of up to 5 x 10^6 cells into the gels, the majority of which were $CD11b^+$ $CD11c^+$ DCs. In contrast, only ~1.5 x 10^6 cells accumulated in gels delivering free GM-CSF, even at the peak of cell infiltration. In blank gels or gels delivering control AuNPs, barely a

few hundred thousand cells were detected, and a portion of those cells may actually have been scraped off from surrounding tissue in the process of isolating the gels for analysis. The $CD11b^{+}$ $CD11c^{+}$ phenotype of the DCs seen here was consistent with a report showing that administration of PEG-modified GM-CSF, which has an extended circulation time *in vivo*, preferentially expanded $CD11b^{high}CD11c^{high}$ but not $CD11b^{low}CD11c^{high}$ DCs[44]. However, it is unclear exactly how GM-CSF delivery led to the observed accumulation of cells in the gels, since GM-CSF can exert a wide variety of effects on its target cells. It is likely that multiple mechanisms, such as DC migration, pre-DC differentiation, and proliferation, all contributed to some extent. It was interesting to note that, while delivery of GM-CSF conjugated to AuNPs had a striking effect on the number of cells that accumulated in the gels, the overall surface marker expression of the cells was not significantly altered. This suggests that GM-CSF induced proliferation may be playing an important role in expanding recruited DCs. In addition, immune cells such as monocytes and DCs secrete their own chemokines, including GM-CSF. It is possible that endogenous factors produced by cells infiltrating the gels in the initial stages of cell recruitment amplified the effect of the delivered GM-CSF and contributed to the observed cell accumulation.

Tuning the physical properties of the hydrogel had a significant impact on cell recruitment. In these studies, an intermediate porogen volume fraction of 50% was optimal for achieving maximal recruitment of DCs. At a lower porogen volume fraction, fewer cells were able to infiltrate the gels, supporting the importance of creating a macroporous structure to achieve effective cell recruitment. However, increasing the porogen volume fraction beyond 50% did not further improve cell infiltration, possibly

because the bulk gel may collapse as the porogens degrade if the porogen fraction is too high, resulting in sub-optimal cell infiltration. Although the incorporation of 50% degradable porogens by volume led to a significant increase in the interconnected porosity of the gels, the level of interconnected porosity achieved (~13%) was not as high as what has been seen in other macroporous gel systems[17]. However, cells are still able to infiltrate into the center of the gels after only 3 days *in vivo*, so even a modest level of interconnected porosity appears to be sufficient for effective cell infiltration in this particular system. In addition, the effective interconnected porosity may actually be greater *in vivo*, since the gels are subject to mechanical stresses exerted by tissues and infiltrating cells, which may lead to the formation of local fractures within the gels and the creation of new connections between pores.

Strikingly, this material system recruited not only a large number, but also a very high purity of DCs. At D3, more that 90% of the cells in the gels were double positive for CD11b, a broadly expressed marker for leukocytes, and CD11c, a characteristic marker of conventional DCs. This percentage is higher than what was achieved in other material systems using comparable doses of GM-CSF[4] (other unpublished data from the Mooney lab). One possible explanation for this pronounced enrichment of DCs may be that the intentional absence of adhesion ligands on the alginate polymer forming the gels favors infiltration by immune cells. Most other mammalian cell types require adhesion ligands for survival and migration. Leukocytes, on the other hand, can traffic in an integrin-independent manner by amoeboid migration[45–47]. As a result, the gels may be selectively restricting infiltration by fibroblasts and other cells from neighboring tissues, such that the gels are infiltrated almost exclusively by DCs. It would be of great

interest and utility to extend this approach to recruit other immune cell types, such as T and B cells, using different chemokines or recruitment factors.

A characterization of several other immune cell surface markers in addition to CD11b and CD11c revealed that many of the $CD11b^+$ $CD11c^+$ double positive cells also expressed F4/80, which is often cited as a macrophage marker, but is also expressed on certain subsets of DCs, including BMDCs[48], Langerhans cells, some skin-draining DCs[49], and some less mature splenic DCs[50]. Some of the $CD11b^+$ cells also expressed Gr-1, a marker of monocytes and granulocytes, particularly at early timepoints. The $Gr\text{-}1^+$ cells isolated from these gels had a forward scatter (FSC) / side scatter (SSC) profile when analyzed by flow cytometry that appeared consistent with monocytes. It is interesting to note that day 3, the timepoint at which the fraction of $Gr\text{-}1^+$ cells was the highest in the gels delivering GM-CSF conjugated to AuNPs, was also the same day at which the fraction of $CD11c^+$ cells was the lowest. Observing the trends in the percentage of $CD11c^+$ and $Gr\text{-}1^+$ cells for the different conditions at each timepoint suggests that these markers may vary in an inversely proportional manner. Indeed, the expression of these two markers on the cells was segregated, with few cells coexpressing CD11c and Gr-1. It could be speculated that these $Gr\text{-}1^+$ cells represent a population of monocytes or pre-DCs that migrate and differentiate into $CD11c^+$ DCs upon exposure to GM-CSF. Finally, a small fraction of the cells were found to be positive for DX5, an antibody clone that binds to CD49b and is typically used as a marker of NK cells. It is unclear whether all of the $DX5^+$ cells here are *bona fide* NK cells, since a number of them coexpress CD11c and have higher FSC and SSC than would be expected for NK cells, which usually have the low FSC/SSC profile that is typical of lymphocytes. These cells may be

an intermediate cell type, perhaps similar to the CD11c$^+$ DX5$^+$ bitypic NK/DC regulatory cells that were described as being protective in a model of virally induced type 1 diabetes[51]. An additional barrier to distinguishing NK cells from NKT cells or T cells without a more extensive analysis is that these lymphocytes all have a similar FSC / SSC profile, and that some subsets of T cells, such as Tr1 cells, express CD49b[52].

Preliminary evidence suggests that these DCs were redeployed into the local draining lymph nodes, since the number of cells in the LNs draining the gels, as well as the percentage of CD11c$^+$ cells, were significantly increased compared to the contralateral irrelevant LNs. DC homing to the LNs is critical for generating downstream immune responses, since LNs are the meeting points where DCs interact with large numbers of T cells, greatly increasing their chances of encountering antigen-specific T cells. It must be noted that the increase in the total cell number was not fully accounted for by the increase in the percentage of CD11c$^+$ DCs. Since no exogenous antigens were provided here, the increase in T and B cells was not expected to be a result of proliferation. It is speculated that an increase in the number of DCs trafficking to the LNs may result in increased LN homing of the other cell types, rather than proliferation.

The material system introduced here represents a platform that can be used to recruit a highly enriched population of CD11c$^+$ DCs in a non-inflammatory environment, possibly enabling the development of a materials-based tolerogenic vaccine.

2.5 References

1. Irvine, D. J., Swartz, M. A. & Szeto, G. L. Engineering synthetic vaccines using cues from natural immunity. *Nat. Mater.* **12,** 978–990 (2013).

2. Getts, D. R. *et al.* Microparticles bearing encephalitogenic peptides induce T-cell tolerance and ameliorate experimental autoimmune encephalomyelitis. *Nat. Biotechnol.* **30,** 1217–1224 (2012).

3. Yeste, A., Nadeau, M., Burns, E. J., Weiner, H. L. & Quintana, F. J. Nanoparticle-mediated codelivery of myelin antigen and a tolerogenic small molecule suppresses experimental autoimmune encephalomyelitis. *Proc. Natl. Acad. Sci. U. S. A.* **109,** 11270–11275 (2012).

4. Ali, O. A., Huebsch, N., Cao, L., Dranoff, G. & Mooney, D. J. Infection-mimicking materials to program dendritic cells in situ. *Nat. Mater.* **8,** 151–158 (2009).

5. Miller, S. D., Turley, D. M. & Podojil, J. R. Antigen-specific tolerance strategies for the prevention and treatment of autoimmune disease. *Nat. Rev. Immunol.* **7,** 665–677 (2007).

6. Anderson, J. M. & Shive, M. S. Biodegradation and biocompatibility of PLA and PLGA microspheres. *Adv. Drug Deliv. Rev.* **28,** 5–24 (1997).

7. Athanasiou, K. A., Niederauer, G. G. & Agrawal, C. M. Sterilization, toxicity, biocompatibility and clinical applications of polylactic acid/ polyglycolic acid copolymers. *Biomaterials* **17,** 93–102 (1996).

8. Kim, W. S. *et al.* Adipose Tissue Engineering Using Injectable, Oxidized Alginate Hydrogels. *Tissue Eng. Part A* **18,** 737–743 (2011).

9. Lee, K. Y. & Mooney, D. J. Alginate: properties and biomedical applications. *Prog. Polym. Sci.* **37,** 106–126 (2012).

10. Zimmermann, U. *et al.* Production of mitogen-contamination free alginates with variable ratios of mannuronic acid to guluronic acid by free flow electrophoresis. *Electrophoresis* **13,** 269–274 (1992).

11. Silva, E. A. & Mooney, D. J. Spatiotemporal control of vascular endothelial growth factor delivery from injectable hydrogels enhances angiogenesis. *J. Thromb. Haemost.* **5,** 590–598 (2007).

12. Silva, E. A. & Mooney, D. J. Effects of VEGF temporal and spatial presentation on angiogenesis. *Biomaterials* **31,** 1235–1241 (2010).

13. Hao, X. *et al.* Angiogenic effects of sequential release of VEGF-A165 and PDGF-BB with alginate hydrogels after myocardial infarction. *Cardiovasc. Res.* **75,** 178–185 (2007).

14. Borselli, C., Cezar, C. A., Shvartsman, D., Vandenburgh, H. H. & Mooney, D. J. The role of multifunctional delivery scaffold in the ability of cultured myoblasts to promote muscle regeneration. *Biomaterials* **32,** 8905–8914 (2011).

15. Silva, E. A., Kim, E.-S., Kong, H. J. & Mooney, D. J. Material-based deployment enhances efficacy of endothelial progenitor cells. *Proc. Natl. Acad. Sci. U. S. A.* **105,** 14347–14352 (2008).

16. Hill, E., Boontheekul, T. & Mooney, D. J. Regulating activation of transplanted cells controls tissue regeneration. *Proc. Natl. Acad. Sci.* **103,** 2494–2499 (2006).

17. Bencherif, S. A. *et al.* Injectable preformed scaffolds with shape-memory properties. *Proc. Natl. Acad. Sci.* **109,** 19590–19595 (2012).

18. Huebsch, N. *et al.* Matrix elasticity controls bone formation by transplanted stem cells. *Rev.*

19. Boontheekul, T., Kong, H.-J. & Mooney, D. J. Controlling alginate gel degradation utilizing partial oxidation and bimodal molecular weight distribution. *Biomaterials* **26,** 2455–2465 (2005).

20. Bouhadir, K. H. *et al.* Degradation of Partially Oxidized Alginate and Its Potential Application for Tissue Engineering. *Biotechnol. Prog.* **17,** 945–950 (2001).

21. Ali, O. A., Tayalia, P., Shvartsman, D., Lewin, S. & Mooney, D. J. Inflammatory Cytokines Presented from Polymer Matrices Differentially Generate and Activate DCs In Situ. *Adv. Funct. Mater.* **23,** 4621–4628 (2013).

22. Parmiani, G. *et al.* Opposite immune functions of GM-CSF administered as vaccine adjuvant in cancer patients. *Ann. Oncol.* **18,** 226–232 (2007).

23. Dranoff, G. GM-CSF-based cancer vaccines. *Immunol. Rev.* **188,** 147–154 (2002).

24. Hamilton, J. A. GM-CSF in inflammation and autoimmunity. *Trends Immunol.* **23,** 403–408 (2002).

25. Cheatem, D., Ganesh, B. B., Gangi, E., Vasu, C. & Prabhakar, B. S. Modulation of dendritic cells using granulocyte-macrophage colony-stimulating factor (GM-CSF) delays type 1 diabetes by enhancing CD4+CD25+ regulatory T cell function. *Clin. Immunol. Orlando Fla* **131,** 260–270 (2009).

26. Gaudreau, S. *et al.* Granulocyte-macrophage colony-stimulating factor prevents diabetes development in NOD mice by inducing tolerogenic dendritic cells that sustain the suppressive function of CD4+CD25+ regulatory T cells. *J. Immunol. Baltim. Md 1950* **179,** 3638–3647 (2007).

27. Sheng, J. R. *et al.* Suppression of experimental autoimmune myasthenia gravis by granulocyte-macrophage colony-stimulating factor is associated with an expansion of FoxP3+ regulatory T cells. *J. Immunol. Baltim. Md 1950* **177,** 5296–5306 (2006).

28. Zou, T., Caton, A. J., Koretzky, G. A. & Kambayashi, T. Dendritic Cells Induce Regulatory T Cell Proliferation through Antigen-Dependent and -Independent Interactions. *J. Immunol.* **185,** 2790–2799 (2010).

29. Enzler, T. *et al.* Functional deficiencies of granulocyte-macrophage colony stimulating factor and interleukin-3 contribute to insulitis and destruction of β cells. *Blood* **110,** 954–961 (2007).

30. Lee, K. Y., Peters, M. C., Anderson, K. W. & Mooney, D. J. Controlled growth factor release from synthetic extracellular matrices. *Nature* **408,** 998–1000 (2000).

31. Sebollela, A. *et al.* Heparin-binding sites in granulocyte-macrophage colony-stimulating factor. Localization and regulation by histidine ionization. *J. Biol. Chem.* **280,** 31949–31956 (2005).

32. Wettreich, A. *et al.* Acidic pH modulates the interaction between human granulocyte-macrophage colony-stimulating factor and glycosaminoglycans. *J. Biol. Chem.* **274,** 31468–31475 (1999).

33. Slowing, I. I., Vivero-Escoto, J. L., Wu, C.-W. & Lin, V. S.-Y. Mesoporous silica nanoparticles as controlled release drug delivery and gene transfection carriers. *Adv. Drug Deliv. Rev.* **60,** 1278–1288 (2008).

34. Bhatt, N., Huang, P.-J. J., Dave, N. & Liu, J. Dissociation and Degradation of Thiol-Modified DNA on Gold Nanoparticles in Aqueous and Organic Solvents. *Langmuir* **27,** 6132–6137 (2011).

35. Hu, W.-J., Eaton, J. W., Ugarova, T. P. & Tang, L. Molecular basis of biomaterial-mediated foreign body reactions. *Blood* **98,** 1231–1238 (2001).

36. Lynch, I., Dawson, K. A. & Linse, S. Detecting Cryptic Epitopes Created by Nanoparticles. *Sci. Signal.* **2006,** pe14 (2006).

37. Shukla, R. *et al.* Biocompatibility of Gold Nanoparticles and Their Endocytotic Fate Inside the Cellular Compartment: A Microscopic Overview. *Langmuir* **21,** 10644–10654 (2005).

38. Villiers, C. L., Freitas, H., Couderc, R., Villiers, M.-B. & Marche, P. N. Analysis of the toxicity of gold nano particles on the immune system: effect on dendritic cell functions. *J. Nanoparticle Res.* **12,** 55–60 (2009).

39. Thakor, A., Jokerst, J., Zaveleta, C., Massoud, T. & Gambhir, S. GOLD NANOPARTICLES: A REVIVAL IN PRECIOUS METAL ADMINISTRATION TO PATIENTS. *Nano Lett.* **11,** 4029–4036 (2011).

40. Perrault, S. D. & Chan, W. C. W. Synthesis and Surface Modification of Highly Monodispersed, Spherical Gold Nanoparticles of 50−200 nm. *J. Am. Chem. Soc.* **132,** 11824–11824 (2010).

41. Mooney, D. J., Breuer, C., McNamara, K., Vacanti, J. P. & Langer, R. Fabricating Tubular Devices from Polymers of Lactic and Glycolic Acid for Tissue Engineering. *Tissue Eng.* **1,** 107–118 (1995).

42. Wu, G., Fang, Y.-Z., Yang, S., Lupton, J. R. & Turner, N. D. Glutathione Metabolism and Its Implications for Health. *J. Nutr.* **134,** 489–492 (2004).

43. Chen, T. S., Richie, J. P. & Lang, C. A. Life span profiles of glutathione and acetaminophen detoxification. *Drug Metab. Dispos.* **18,** 882–887 (1990).

44. Daro, E. *et al.* Polyethylene Glycol-Modified GM-CSF Expands CD11bhighCD11chigh But Not CD11blowCD11chigh Murine Dendritic Cells In Vivo: A Comparative Analysis with Flt3 Ligand. *J. Immunol.* **165,** 49–58 (2000).

45. Wolf, K., Müller, R., Borgmann, S., Bröcker, E.-B. & Friedl, P. Amoeboid shape change and contact guidance: T-lymphocyte crawling through fibrillar collagen is independent of matrix remodeling by MMPs and other proteases. *Blood* **102,** 3262–3269 (2003).

46. Lämmermann, T. *et al.* Rapid leukocyte migration by integrin-independent flowing and squeezing. *Nature* **453,** 51–55 (2008).

47. Friedl, P. & Weigelin, B. Interstitial leukocyte migration and immune function. *Nat. Immunol.* **9,** 960–969 (2008).

48. Nguyen, M. T. A. *et al.* A Subpopulation of Macrophages Infiltrates Hypertrophic Adipose Tissue and Is Activated by Free Fatty Acids via Toll-like Receptors 2 and 4 and JNK-dependent Pathways. *J. Biol. Chem.* **282,** 35279–35292 (2007).

49. Heng, T. S. P. *et al.* The Immunological Genome Project: networks of gene expression in immune cells. *Nat. Immunol.* **9,** 1091–1094 (2008).

50. Hoyo, G. M. del, Martín, P., Arias, C. F., Marín, A. R. & Ardavín, C. CD8a+ dendritic cells originate from the CD8a− dendritic cell subset by a maturation process involving CD8a, DEC-205, and CD24 up-regulation. *Blood* **99,** 999–1004 (2002).

51. Homann, D. *et al.* CD40L Blockade Prevents Autoimmune Diabetes by Induction of Bitypic NK/DC Regulatory Cells. *Immunity* **16,** 403–415 (2002).

52. Gagliani, N. *et al.* Coexpression of CD49b and LAG-3 identifies human and mouse T regulatory type 1 cells. *Nat. Med.* **19,** 739–746 (2013).

Chapter 3. DCs recruited to alginate gels releasing GM-CSF *in vivo* are immature and have the capacity to induce antigen-specific T cell responses

3.1 Introduction

The immune system has an exquisite capacity to mount highly antigen-specific responses, both for the purposes of generating immunity against pathogens, as well as for maintaining tolerance to self. Vaccination, which has been used successfully for over ~200 years now, since the introduction of the smallpox vaccine by Edward Jenner[1], is highly antigen specific. Through the administration of an attenuated pathogen accompanied by an adjuvant, vaccination evokes precisely targeted immunity. On the other hand, still today in 2014, the therapies in the clinic for treating autoimmune diseases involve coarser manipulations of the immune system that are not antigen specific. The use biomaterials may greatly enhance our ability to induce antigen-specific tolerogenic responses by controlling the presentation of defined self-antigens and by co-delivering cues that program immune cells for tolerance. This chapter addresses specific Aim 2 of this thesis by examining the ability of the material system described in the previous chapter to induce antigen-specific T cell responses.

The development of antigen-specific tolerogenic therapies would be transformative in the areas of autoimmunity, as well as transplantation tolerance. Although broad immunosuppression can alleviate autoimmune disease, it would be preferable to specifically block self-reactive immunity, while maintaining the full capacity of the immune system to clear foreign antigens and pathogens. While individuals predisposed

to autoimmunity may have some underlying defects in components of their immune systems, the fact that not all such individuals progress to the disease state suggests that it could be possible to restore tolerance, even in the context of genetic predispositions. A number of clinical trials have attempted to treat human autoimmune diseases in an antigen-specific manner by taking advantage of the known tolerogenic properties of mucosal DCs. These studies, which involved delivering disease-associated proteins either orally or nasally, have essentially all failed, despite the fact that these treatment strategies were effective in many pre-clinical models[2]. One possible reason for this discrepancy is that in pre-clinical models, these antigen-specific therapies have primarily been used prophylactically, prior to the onset of disease, while most clinical studies have been done in patients with recent-onset disease, largely for ethical reasons[2]. Research in this area is still ongoing, and a large parameter space still remains to be explored for translating these treatments into humans, such as antigen dose, formulation, and frequency of administration, as well as the stage of disease at which the therapy should be administered. Recently, though, significant concerns have been raised regarding the safety of administering autoimmune disease-associated antigens through systemic routes, which include intravenous, oral, and nasal administration. In animal models of multiple sclerosis (MS), delivery of soluble disease-associated peptides was shown to induce fatal anaphylaxis in some mouse models, as well as lead to disease exacerbation in a non-human primate study[3]. The ability to deliver peptides in a localized and controlled manner could be key to developing successful antigen-specific tolerogenic therapies.

DCs are an ideal cell type to target for eliciting antigen-specific immune tolerance, since they integrate multiple signals from their environment, present peptides to antigen-specific T cells, and direct T cell differentiation and activation. DCs are critical for maintaining self-tolerance in steady state conditions, as demonstrated by the fact that depletion of $CD11c^+$ DCs breaks this tolerance, leading to spontaneous and fatal autoimmunity[4]. In another study, depletion of $CD11c^+$ DCs led to greater severity in EAE[5], whereas, in contrast, inducing DCs to present self-antigens led to disease prevention by a PD-1 dependent mechanism. In the steady state, DCs are immature, expressing low levels of costimulatory molecules, such as CD80, CD86, and CD40[6,7]. Immature DCs have a high capacity for capturing and processing antigen, as well as high levels of intracellular MHCII, but low levels of surface MHCII. When DCs are exposed to DAMPs or PAMPs, they undergo maturation, which is characterized by an increase in the levels of surface MHCII and an upregulation of costimulatory molecule expression[6,7]. While antigen uptake is downregulated upon maturation, migration is increased, allowing the DCs to rapidly home to LNs where they can induce downstream T cell activation. Although it is clear that inflammatory, fully mature DCs induce immunity rather than tolerance, there is not complete consensus in the field as to which type of DCs is ideal for inducing tolerance. Previously, it has been held that immature DCs are the most appropriate to induce tolerance, since their role in steady-state settings is to maintain peripheral tolerance. However, this is in conflict with the fact that completely immature DCs do not effectively present antigen or migrate to LNs, which limits their ability to interact with T cells. More recently, studies have shown that, even in the steady-state, DCs acquire certain features of maturation as they migrate, such as higher expression of CCR7, MHCII, and even some costimulatory molecules.

Such DCs have been termed semi-mature DCs[8], and it has been suggested that these DCs induce IL-10 producing regulatory T cells, whereas immature DCs induce T cell anergy. In vivo targeting of antigen to immature or semi-mature DCs via endocytic receptors such as DEC-205 has been shown to induce deletion or hyporesponsiveness of antigen-specific T cells[9–12]. In addition, tolerogenic factors may be used to prime DCs for tolerance[13], generating what are termed tolerogenic DC (tolDC) or induced tolerogenic DC (itDC).

The ability of DCs to induce antigen-specific tolerance has been tested in preclinical models for several different autoimmune diseases, including type 1 diabetes. Non-obese diabetic (NOD) mice are the most widely used animal model of type 1 diabetes, among several existing models. Some of the other mouse models, RIP-OVA (ovalbumin) and RIP-LCMV (lymphocytic choriomeningitis virus) are immune mediated, but rely on the tissue-specific transgenic expression of foreign proteins to raise a cytotoxic immune response, thus breaking tolerance and triggering the specific destruction of beta cells. NOD mice are seen as the most relevant disease model since diabetes is spontaneously occurring, has a genetic association, and bears a number of similarities to human type 1 diabetes. In both cases, insulitis, or infiltration of pancreatic islets by lymphocytes, is followed by β cell destruction and a loss of insulin secretion[14]. Hyperglycemia does not occur until the majority (estimated to be ~90%) of beta cells have already been destroyed[14]. In both mice and humans, the disease is primarily T cell-driven, implicating both $CD4^+$ and $CD8^+$ T cells, but B cells producing auto-antibodies also play a role in disease progression[14]. Genetic susceptibility to type 1 diabetes is strongly associated with specific MHC and HLA alleles in mice and humans, respectively, and structural

similarities have been noted between the peptide binding pockets of MHCII I-A^{g7} in NOD mice and human diabetes-associated HLA alleles[15]. As in humans, environmental factors affect disease development in NOD mice, as illustrated by differences in disease incidence rates among different colonies or facilities. Even within a single colony, the age of disease onset varies widely, and some mice never develop overt diabetes.

In order to dissect the role of T cells with single antigen specificities in disease progression, a number of islet-reactive T cell clones were established from NOD derived T cells[16]. The TCR α- and β-chain genes from the BDC2.5 $CD4^+$ clone were used to generate transgenic mice expressing islet antigen-specific $CD4^+$ T cells[17]. While these BDC2.5 transgenic mice exhibit a lower incidence of diabetes than NOD mice, BDC2.5 T cells clearly have the capacity to be diabetogenic, since adoptive transfer of *in vitro* pre-activated BDC2.5 T cells induces rapid disease progression in young non-diabetic NOD mice[18] and in NOD-*scid* mice[19]. On the other hand, BDC2.5 T cells can also develop into functional Tregs, making them appropriate for studies investigating the induction of tolerance. BDC2.5 Tregs that were expanded *in vitro* by DCs were found to be >100-fold more effective at preventing diabetes in pre-diabetic NOD mice upon adoptive transfer as compared to polyclonal Tregs from NODs[20]. In addition, these same BDC2.5 Tregs were effective therapeutically in NODs with new-onset diabetes, leading to long-lasting reversal of hyperglycemia in 50% of the mice[21]. In another report, BDC2.5 T cells transduced with FoxP3 to endow them with Treg function were able to home to the pancreatic LNs and reverse disease in NOD mice with recent-onset diabetes, while FoxP3-transduced polyclonal T cells were unable to do so[22]. These studies demonstrate not only that antigen specificity is important for Treg function, but

also that it is possible for Tregs with a single antigen specificity to effectively suppress disease, both in prophylactic and therapeutic settings. BDC2.5 T cells respond to a number of peptide sequences presented in association with the I-A^{g7} molecule. The endogenous antigen recognized by BDC2.5 cells was initially unknown, and for some time it was thought to identify a peptide derived from Glutamic Acid Decarboxylase 65 (GAD65)[23]. Recently, the true endogenous peptide recognized by BDC2.5 was identified as being derived from Chromogranin A[24]. For the studies described in this chapter, the high affinity BDC13 peptide mimetope sequence[25] was used. While there are many other antigens implicated in diabetes progression, the BDC2.5 system is highly useful for elucidating mechanisms of antigen-specific T cell responses in NOD mice.

In this chapter, the sub-hypothesis is that the material system developed in Chapter 2 can, in addition to effectively recruiting DCs, present the DCs with a peptide antigen in a localized manner and redeploy them to the LNs to elicit antigen-specific T cell responses. Here, the NOD model of T1D together with BDC2.5 TCR-transgenic T cells were used to study antigen-specific responses that occur following delivery of the BDC13 (BDC) peptide.

3.2 Materials and Methods

In vivo cell characterization studies

In vivo cell characterization studies were performed as described in Chapter 2.

Flow cytometry

Flow cytometry was performed as described in Chapter 2.

PLG microsphere fabrication

Peptide-loaded PLG microspheres were fabricated following the procedure described in Chapter 2, the only difference being that the BDC peptide (AAVRPLWVRMEAA; Peptide 2.0 or 21st Century Biochemicals) was dissolved in 100uL of DMSO instead of in H_2O.

***In vitro* peptide release**

Peptide-loaded PLG particles were gas-foamed into porous scaffolds as described previously[26]. The resulting peptide-loaded scaffolds were incubated at 37°C in 1mL of release buffer. At the indicated timepoints, the release buffer was collected and replaced with 1mL of fresh buffer. The amount of released peptide was quantified by peptide ELISA, as described below.

***In vivo* peptide biodistribution**

Peptide-loaded scaffolds were implanted subcutaneously into the left flanks of C57BL/6J mice, as described previously[26]. At the indicated timepoints, scaffolds and tissue samples were isolated. Samples were taken from muscle tissue directly underlying the material, as well as 4mm, 8mm, and >3cm (i.e. on the right flank) away from the implanted material. The left inguinal and axillary LNs were also isolated. The scaffold was cut into small (~1mm) pieces, and 500uL of T-Per reagent (Pierce) was used to extract proteins from the tissue infiltrating the scaffold, following the manufacturer's

instructions. The pieces of polymer, which were insoluble, were separated by centrifugation. Proteins were extracted from the other tissue samples using 500uL of T-Per reagent, as for the scaffolds. All samples were analyzed by peptide ELISA, as described below.

Peptide ELISA

To enable detection of full length, non-degraded peptide, biotin and DNP tags were incorporated at the N- and C- termini of the peptide, respectively (Biotin-AAVRPLWVRMEAAK(DNP); Peptide 2.0). Peptide was detected using a customized ELISA assay. StreptaWell (High Bind, Roche) 96 well plates were incubated in blocking buffer (1% BSA in PBS) at room temperature for 1h, then the blocking buffer was removed. 50uL of fresh blocking buffer + 50uL of standards or samples (in T-Per reagent) were added to the wells and incubated for 1h at room temperature. The DNP tag on the peptide was detected using 100uL of anti-DNP antibody (10ug/mL), followed by 100uL of anti-rat IgG-HRP secondary antibody (10ug/mL). Detection steps were performed by diluting reagents in blocking buffer, incubating at room temperature for 1h, and washing wells 5 times in wash buffer (0.05% Tween-20 in PBS) in between each step. 100uL of a standard ELISA chromogenic substrate (R&D Systems or BioLegend) were allowed to develop for 20-30min before the addition of 100uL 1N sulfuric acid stop solution. Plates were read for absorbance at 450nm within 30 min, and absorbance at 540nm was used for wavelength correction.

T cell culture

Primary T cells isolated from mice were cultured in RPMI-1640 medium (with L-glutamine; Sigma Aldrich) supplemented with 10% heat-inactivated FBS, 1% penicillin/streptomycin, 10mM HEPES, and 50uM β-mercaptoethanol. This T cell medium was also used for cocultures of T cells and DCs.

BMDC culture

Bone marrow cells were isolated using a standard procedure. Briefly, the femur and tibia bones were isolated and flushed with HBSS using a 25G needle. Cells were dissociated and filtered through a 40um cell strainer. For NOD BMDCs, 5 x 10^6 cells were plated in 10mL of medium in bacteriological Petri dishes. The medium used for BMDC differentiation consisted of RPMI-1640 medium (with L-glutamine; Sigma Aldrich) supplemented with 10% heat-inactivated FBS, 1% penicillin/streptomycin, 50uM β-mercaptoethanol, and 20ng/mL GM-CSF. At day 3, 10mL of fresh medium were added to each dish, and at day 6, 10mL of medium were removed from each dish and replaced with 10mL of fresh medium.

***In vivo* peptide presentation**

Gels were injected subcutaneously into the flanks of NOD/ShiLtJ mice. At the indicated timepoints, gels and LNs were isolated and dissociated, as described for the *in vivo* cell characterization studies. The cells were resuspended in medium and irradiated with 5krad to inhibit their proliferation. Separately, $CD4^+$ T cells were isolated from the spleen and lymph nodes of BDC2.5 mice and sorted using an untouched $CD4^+$ MACS sorting kit (Miltenyi). Each of the irradiated cell samples was plated into 6 separate wells of a

96 well plate. 3 wells per sample were used for background subtraction, and 10^5 BDC2.5 $CD4^+$ T Cells were added to the other 3 wells. After 48h, 1uCi of ^3H-thymidine was added to each well. After an 18h pulse, the samples were harvested on a Tomtec cell harvester and ^3H counts were read using a Microbeta 1450 scintillation counter.

***In vivo* T cell proliferation**

BDC2.5 T cells were labeled with a cell proliferation dye (CFSE or eFluor 670, eBioscience) and 1-2 x 10^6 cells were adoptively transferred into NOD recipients i.v. by tail vein injection. One day later, gels delivering peptide were injected. LNs were isolated at various timepoints, and the dilution of the cell proliferation dye was analyzed by flow cytometry.

***In vivo* T cell cytokine secretion**

Gels were injected subcutaneously into the flanks of NOD/ShiLtJ mice. At the indicated timepoints, LNs were isolated and dissociated as described for the *in vivo* cell characterization studies. The samples were enriched for $CD4^+$ T cells using an untouched $CD4^+$ MACS sorting kit (Miltenyi). The enriched T cells were cocultured with 7.5 x 10^4 NOD BMDCs, and 1uM peptide was added for restimulation. A BMDC culture was started 7 days in advance of the coculture according to the procedure described above, and 24h before the start of the coculture, 50ng/mL LPS was added to mature the BMDCs. Supernatants from the DC : T cell cocultures were collected after 24h and stored at -20°C until cytokine analysis was performed, as described below.

qPCR

Cells were stained for CD11b, CD11c, CD3e, DX5. Calcein blue (eBioscience) was added to a final concentration of 10 uM to discriminate live cells and sorted on a Beckman Coulter MoFlo Astrios. RNA was extracted using TRIzol reagent (Life Technologies) according to a standardized protocol recommended by the Immunological Genome Project[27]. cDNA was synthesized using the High Capacity cDNA Reverse Transcription Kit (Applied Biosystems). The RT-PCR reaction was carried out using TaqMan gene expression assays with the TaqMan Fast Advanced Master Mix on an ABI 7900 HT Real-Time PCR System (Applied Biosystems).

Cytokine analysis

Gels or cell culture supernatants were analyzed by performing BioPlex assays, using either the mouse cytokine 23-plex or 8-plex (Bio-Rad) according to the manufacturer's instructions. The samples were run on a BioPlex 3D System (Bio-Rad). To extract proteins from gels for cytokine analysis, 500uL of T-Per reagent (Pierce) were added to 100uL gels, and protein extraction was performed according to the manufacturer's instructions.

Statistical analysis

Statistical analyses were performed as described in Chapter 2.

3.3 Results

DCs recruited into pore-forming gels exhibited a non-inflammatory phenotype

The material system that was presented in Chapter 2 demonstrated the ability to recruit a significant number and percentage of $CD11b^+$ $CD11c^+$ DCs. To achieve a better understanding of the maturation level of these DCs, a number of cell surface markers associated with DC maturation were examined over time (Fig. 3.1). Over 50% of the $CD11b^+$ $CD11c^+$ DCs recruited to the gels expressed MHCII, confirming their status as professional APCs (Fig. 3.1 A). These cells also expressed CD86 (Fig. 3.1 C) and CCR7 (Fig. 3.1 E), with 30-40% $CD86^+$ cells and ~10-25% $CCR7^+$ cells in gels delivering GM-CSF conjugated AuNPs. At day 3, both the percentage of $CD86^+$ cells, as well as the level of expression of the $CD86^+$ cells, were significantly lower in gels delivering GM-CSF (either GM-CSF alone or GM-CSF + AuNP) compared to control gels (blank or control AuNP) (Fig. 3.1 C-D). This trend was also visible at day 5, although not all of the differences were statistically significant. Over time, the percentage and expression levels of the $CD86^+$ cells in the control gels decreased and normalized to the levels seen in the GM-CSF loaded gels. For MHCII, a similar trend was seen for the expression levels, where the DCs infiltrating the gels delivering GM-CSF expressed significantly less surface MHCII compared to the controls at day 3 (Fig. 3.1 B). As with CD86, the expression of MHCII eventually normalized to the same low level for all conditions at later timepoints. In terms of the percentage of $MHCII^+$ cells, however, a different trend was observed (Fig. 3.1 A). At day 3, gels delivering GM-CSF alone had the highest percentage of $MHCII^+$ DCs. At day 5, the fraction of $MHCII^+$ DCs increased for all conditions. At days 10 and

14, the fraction of MHCII$^+$ cells was maintained for the control conditions, but decreased significantly in the gels delivering GM-CSF. CCR7 expression was seen on ~12% of cells at day 3, and the fraction of CCR7$^+$ cells increased to approximately 20-30% at the subsequent timepoints (Fig. 3.1 E-F). There were no significant differences in the percentage or expression levels of CCR7 between conditions.

To further characterize the phenotype of the DCs infiltrating these gels, a number of markers associated with different DC subsets were examined at day 3 (Fig. 3.1 G). CD11c$^+$ DCs isolated from the gels expressed high levels of the negative costimulatory molecules PD-L1 and PD-L2. Gels delivering GM-CSF + AuNP contained over 90% PD-L1$^+$ and ~55% PD-L2$^+$ DCs, which was significantly higher than in the AuNP only control gels. At the same timepoint, a significant fraction of CD11c$^+$ DCs also expressed PDCA-1, a marker for plasmacytoid dendritic cells (pDCs). In this case, GM-CSF delivery led to reduced PDCA-1 expression, since only ~40% of the DCs in gels delivering GM-CSF were PDCA-1$^+$, compared to ~80% in control gels. A low percentage of DCs expressed the endocytic receptor CD205 (DEC-205) (~12%), even fewer expressed CD103 (4-7%), and essentially none of the DCs were CD8a$^+$. In addition, most of the cells were negative for CD207 (langerin), a marker of Langerhans cells. Gels delivering AuNP alone contained around 20% CD207$^+$ cells, compared to only 5% in gels delivering GM-CSF.

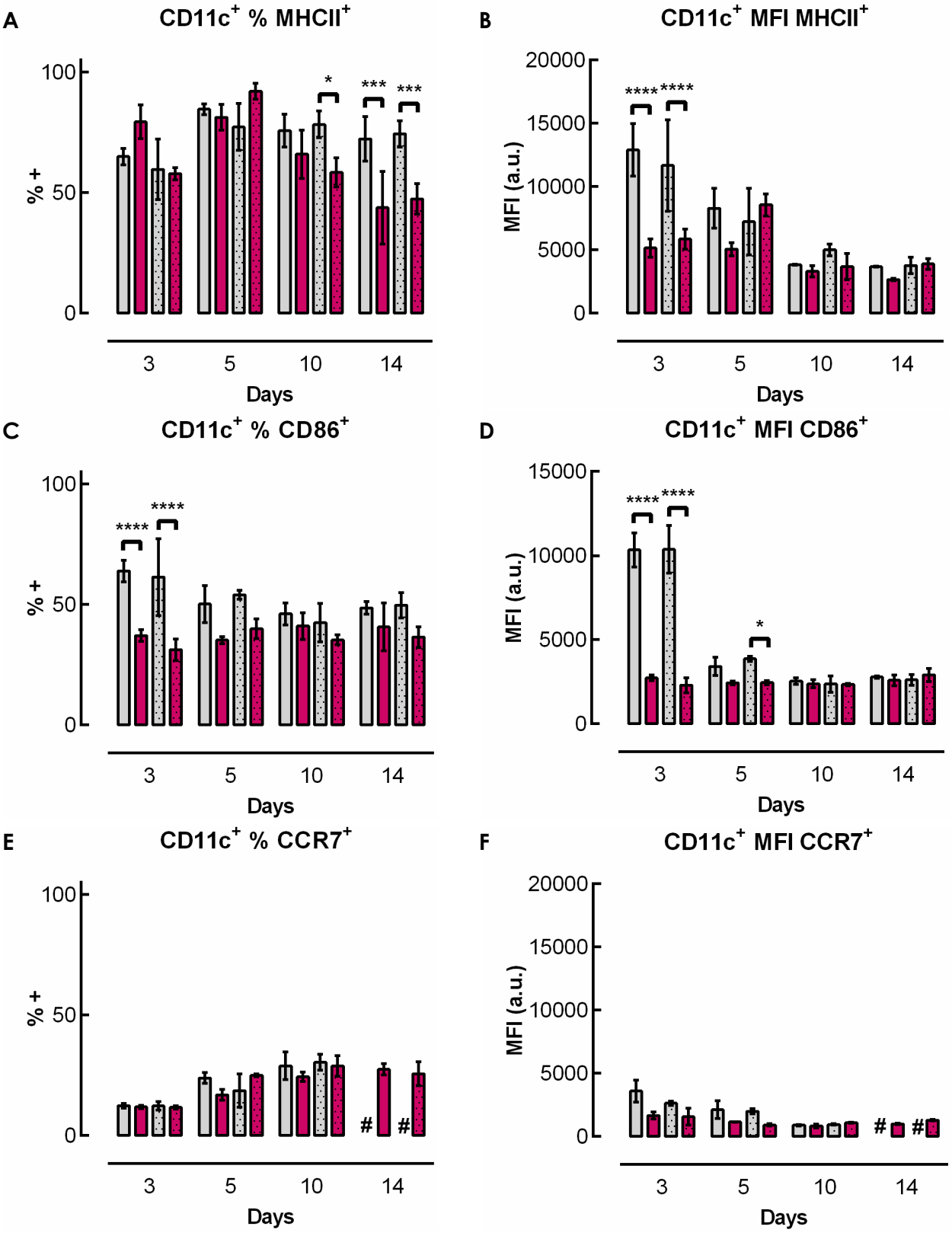
A
CD11c+ % MHCII+
% +
100
50
0
*
***
***
3
5
10
14
Days
B
CD11c+ MFI MHCII+
MFI (a.u.)
20000
15000
10000
5000
0
****
****
3
5
10
14
Days
C
CD11c+ % CD86+
% +
100
50
0
****
****
3
5
10
14
Days
D
CD11c+ MFI CD86+
MFI (a.u.)
15000
10000
5000
0
****
****
*
3
5
10
14
Days
E
CD11c+ % CCR7+
% +
100
50
0
#
#
3
5
10
14
Days
F
CD11c+ MFI CCR7+
MFI (a.u.)
20000
15000
10000
5000
0
#
#
3
5
10
14
Days

Figure 3.1.

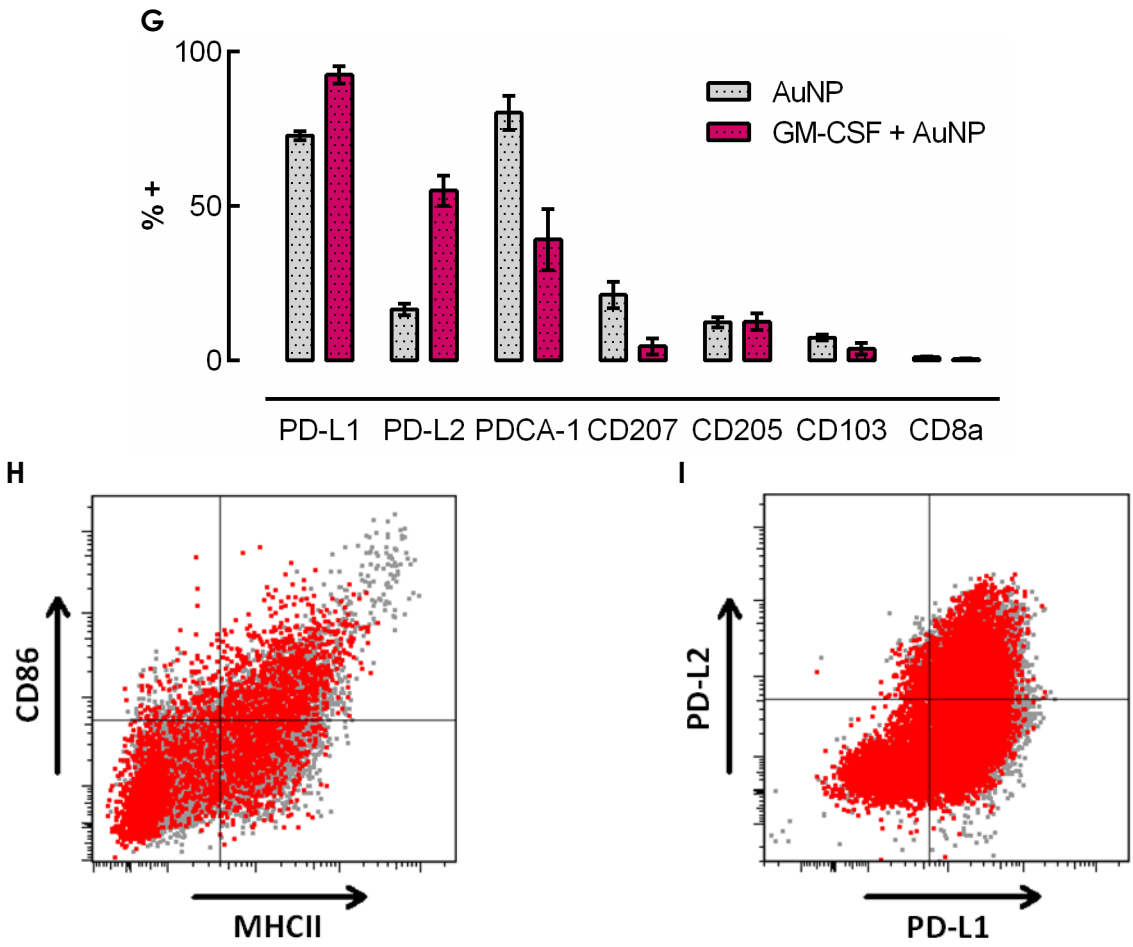

Figure 3.1 (continued). DCs recruited to the gels exhibited a semi-mature phenotype, with low expression of activation markers and high expression of negative costimulatory molecules. Gels were injected subcutaneously into the flanks of C57BL/6J mice; at specified timepoints, gels were isolated and dissociated to analyze infiltrating cells by flow cytometry. (A-F) Quantification of flow cytometry data showing the percentage (A) and MFI (B) of MHCII$^+$ cells, the percentage (C) and MFI (D) of CD86$^+$ cells, and the percentage (E) and MFI (F) of CCR7$^+$ cells. Illustrative FACS plots can be found in Appendix C. (G) Percentage of DCs expressing negative costimulatory molecules (PD-L1 and PD-L2) and markers associated with various DC subtypes (PDCA-1, CD207, CD205, CD103, and CD8a). (H-I) Flow cytometry plots comparing cell surface marker expression by immature BMDCs (grey) and by cells isolated from gels at day 3 (red, overlaid). (H) Expression of MHCII and CD86. (I) Expression of PD-L1 and PD-L2. (n = 3 per condition per timepoint; mean ± s.d. shown; * $p < 0.05$; *** $p < 0.001$; **** $p < 0.0001$; # data not available).

Encapsulation of peptide antigen in PLG allowed localized delivery and presentation *in vivo*

The ability of the DCs recruited into the material system to elicit specific T cell responses was tested by incorporating the BDC MHCII restricted peptide antigen into the material. Encapsulation of peptide in PLG microspheres allowed relatively hydrophobic peptides to be readily incorporated into the gel and released gradually. The release of peptide from PLG was first measured in vitro; for ease of handling, the particles were gas-foamed into scaffolds. Peptide was released at a very slow and sustained rate, with only 1.5ug being released over the first week (Fig. 3.2 A). Next, PLG scaffolds loaded with peptide were implanted subcutaneously to examine the distribution of this peptide *in vivo* (Fig. 3.2 B-C). A variety of tissue samples were analyzed for the presence of intact, i.e. full-length and non-degraded, peptide. Intact peptide was consistently detected in the tissue infiltrating the scaffold at all assayed timepoints (Fig. 3.2 C). The highest levels, around 100ng, were detected at day 1, followed by fairly constant levels, around 20ng, persisting from day 3 to day 14. However, no peptide could be detected in any of the other tissues analyzed, including the muscle directly underlying the material and the draining lymph nodes, indicating that the peptide was not diffusing into adjacent tissues or passively draining through lymphatic vessels. Together, these results show that a peptide antigen could be delivered at a controlled rate and in a highly localized manner, with no detectable spread of the peptide into neighboring tissues or into systemic circulation.

To determine whether BDC peptide delivered locally from a material *in vivo* would be taken up and functionally presented by DCs, peptide-loaded PLG microspheres were incorporated into pore-forming alginate gels delivering GM-CSF. After subcutaneous injection of these gels, the ability of DCs from various tissues to present peptides that they acquired *in vivo* was examined by isolating these DCs and coculturing them with BDC2.5 responder T cells. When OVA, a control peptide, was delivered in the gels, the responder T cells did not proliferate, since they did not encounter their cognate antigen (Fig. 3.2 D). In contrast, when BDC peptide was delivered *in vivo*, the DCs infiltrating the gels were clearly able to acquire and present the peptide, as demonstrated by the observed responder T cell proliferation (Fig. 3.2 D). An increase in peptide presentation was also seen for DCs isolated from the lymph nodes draining the gels delivering BDC peptide, but this difference was not statistically significant. Peptide presentation was not observed in other, more distant lymph nodes, supporting the notion that the peptide was not being disseminated systemically. In the pancreatic LNs, where the endogenous antigen from beta cells can be presented by DCs, there appeared to be a small increase in peptide presentation. However, as for the draining LNs, this difference was not statistically significant.

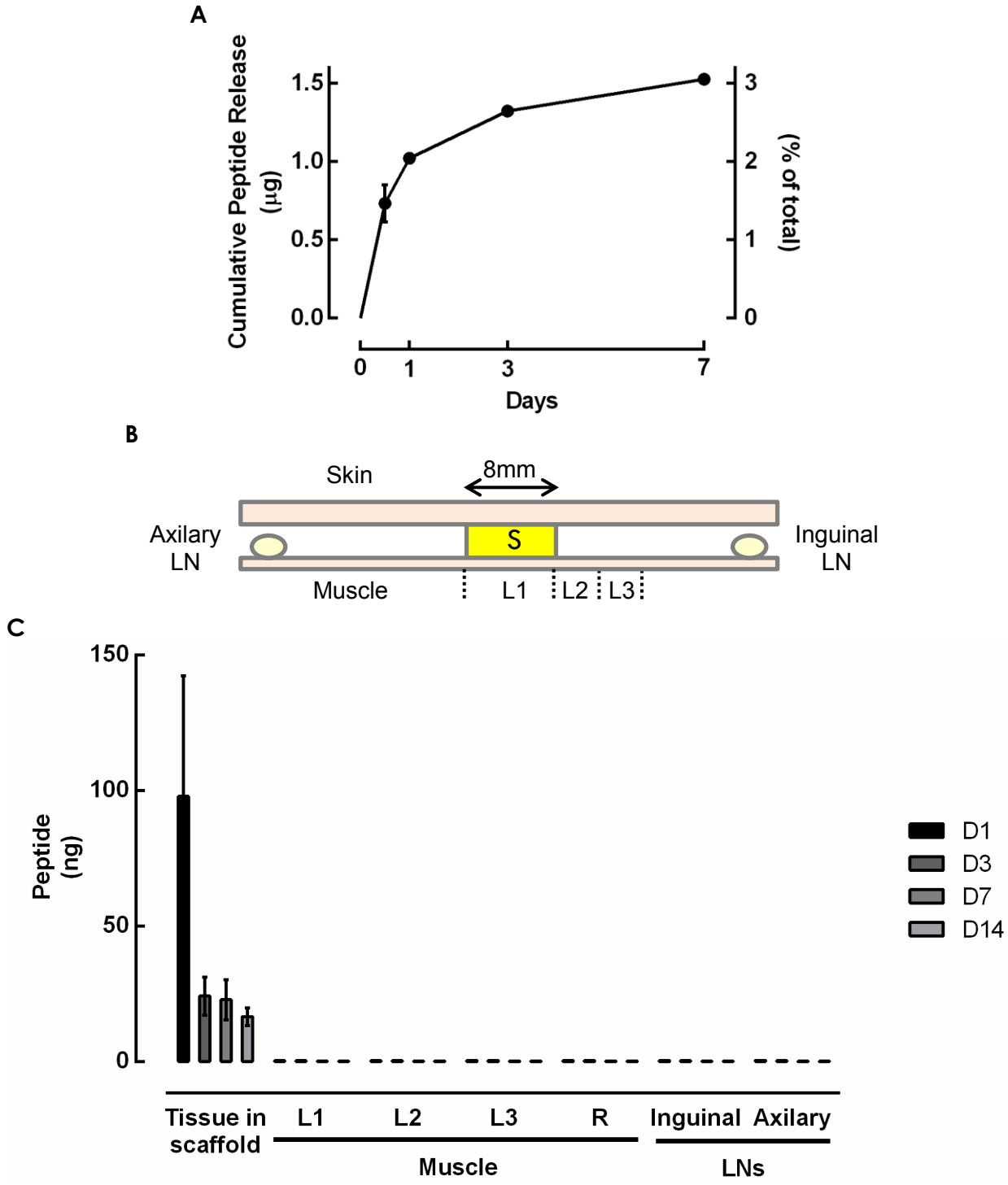
A
Cumulative Peptide Release (µg)
1.5
1.0
0.5
0.0
3
2
1
0
(% of total)
0
1
3
7
Days
B
Skin
8mm
Axilary LN
S
Inguinal LN
Muscle
L1
L2
L3
C
150
100
50
0
Peptide (ng)
D1
D3
D7
D14
Tissue in scaffold
L1
L2
L3
R
Inguinal
Axilary
Muscle
LNs

Figure 3.2.

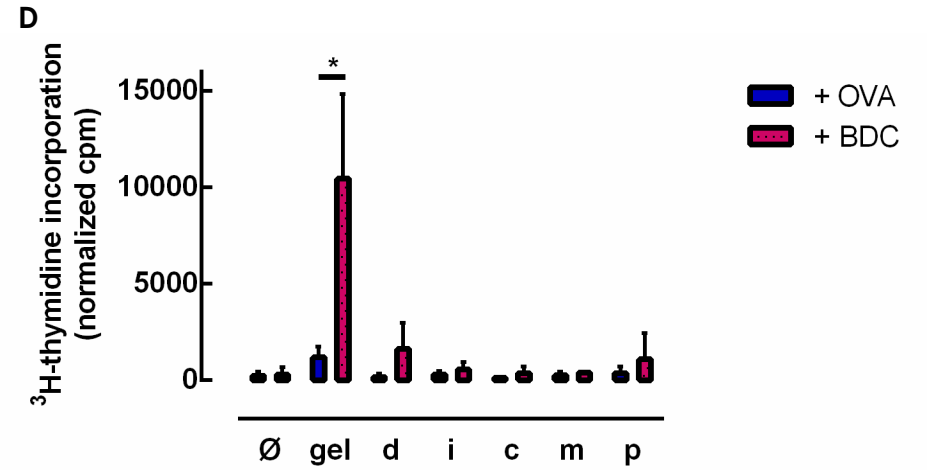

Figure 3.2 (continued). Sustained delivery of peptide antigen *in vivo* led to localized antigen presentation in the gel and draining lymph nodes. (A) *In vitro* release of a peptide antigen from PLG at 37°C. (n = 3 per condition per timepoint; mean ± s.d. shown). (B-C) *In vivo* peptide biodistribution. (B) Peptide-loaded PLG scaffolds (S) were implanted subcutaneously into the left flank. (C) Peptide was quantified by ELISA at the indicated timepoints in various tissues, including the muscle underlying the gel (L1), as well as 4mm (L2), 8mm (L3), and >3cm (R) away from the material (n = 4 per condition per timepoint; mean ± s.d. shown). (D) Antigen presentation by APCs isolated from gels delivering GM-CSF + AuNP and peptide-loaded PLG particles, as well as from the draining (d), irrelevant (i), cervical (c), mesenteric (m), and pancreatic (p) LNs, as indicated by the proliferation of BDC2.5 responder T cells. T cells only, without APCs, were used as a negative control (Ø). (n = 5 per condition per timepoint; mean ± s.d. shown).

In vivo delivery of peptide resulted in antigen-specific T cell proliferation and cytokine secretion

Delivery of peptide from the material system *in vivo* led to clear proliferation and expansion of antigen-specific BDC2.5 T cells (Fig. 3.3). In both control animals that did not receive a gel and in animals that received a gel with OVA control peptide, the proliferation of adoptively transferred antigen-specific cells was only seen in the pLN, where the endogenous peptide from chromogranin A would be found. In contrast, upon delivery of BDC peptide, robust proliferation of the transferred cells was seen in

the lymph nodes draining the gel (Fig. 3.3 A). Proliferating antigen-specific T cells were also detected in more distant lymph nodes, but the amount of proliferation was highest in the draining lymph nodes, as indicated by a greater extent of CFSE dilution.

An increase in the frequency of adoptively transferred, antigen-specific $CD4^+$ T cells was observed in the draining lymph nodes and spleen 5 days after the delivery of BDC peptide in the gel system (n.s.) (Fig. 3.3 B). At day 10, the frequency of $tetramer^+$ T cells was significantly higher in the draining lymph nodes of mice that received BDC peptide (Fig. 3.3 C). By day 20, the population of antigen-specific T cells found in the LNs contracted, returning to baseline levels similar to those in the mice that received OVA peptide (Fig. 3.3 D). Importantly, the expansion of endogenous antigen-specific T cells could be detected in NOD mice even without the adoptive transfer of $BDC2.5^+$ T cells (Fig. 3.3 E). The overall frequency of cells detected was lower than when the adoptive transfer was performed, but an increase in the frequency of $tetramer^+$ cells was still observed for the spleen and dLN (n.s.).

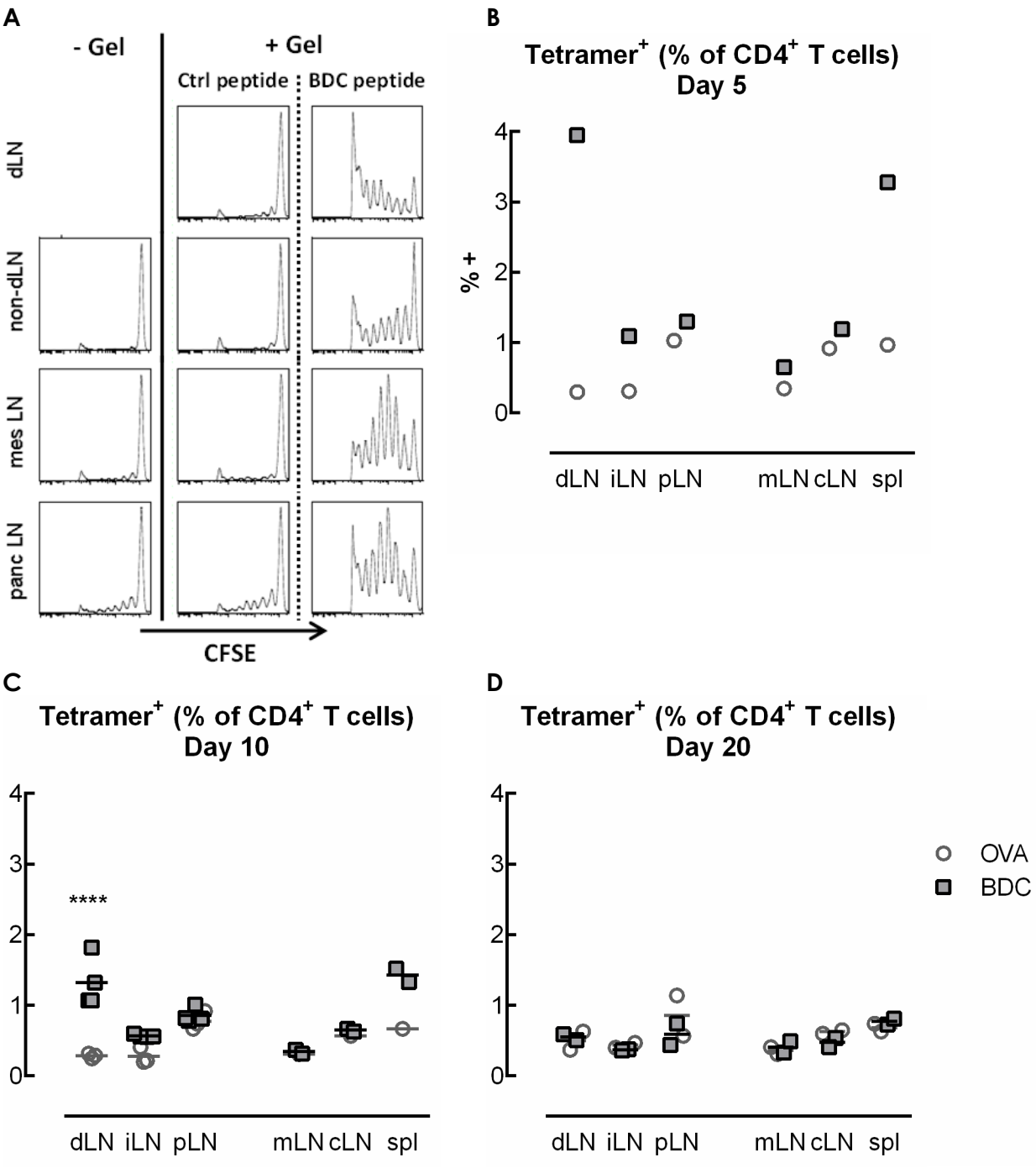
A
- Gel
+ Gel
Ctrl peptide
BDC peptide
dLN
non-dLN
mes LN
panc LN
CFSE
B
Tetramer+ (% of CD4+ T cells)
Day 5
% +
dLN iLN pLN mLN cLN spl
C
Tetramer+ (% of CD4+ T cells)
Day 10
****
dLN iLN pLN mLN cLN spl
D
Tetramer+ (% of CD4+ T cells)
Day 20
dLN iLN pLN mLN cLN spl
OVA
BDC

Figure 3.3.

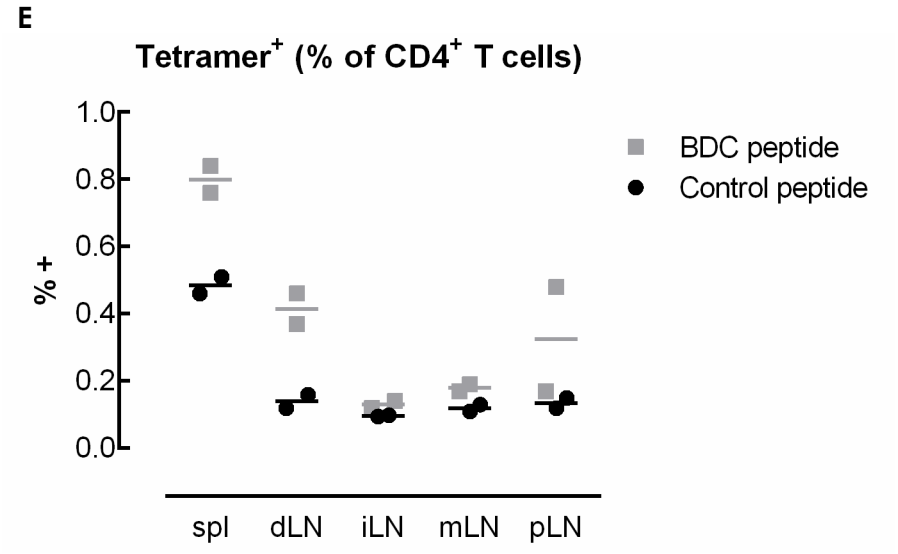

Figure 3.3 (continued). T cells proliferated and expanded in an antigen-specific manner *in vivo* following delivery of BDC peptide in the material system. (A) Proliferation of adoptively transferred BDC2.5 T cells, as indicated by dilution of the CFSE cell tracking dye. (B-D) Percentage of tetramer+ antigen-specific T cells, which include both adoptively transferred and endogenous cells, in the draining LNs (dLN), irrelevant (iLN), mesenteric (mLN), and pancreatic (pLN) LNs, as well as in the spleen (spl), at days 5 (B), 10 (C), and 20 (D). (E) Frequency of endogenous tetramer+ antigen-specific T cells, without any adoptive transfer, at day 9. (n = 1 - 4 per condition per timepoint; individual data points and mean shown; **** $p < 0.0001$; statistical tests comparing BDC to control were only performed for the conditions at day 5 where n >= 3).

To define the functional status of the proliferating, antigen-specific T cells in this system, CD4+ T cells were isolated and restimulated *in vitro* to characterize their cytokine secretion. Either BDC or OVA (control) peptides were delivered in the material system *in vivo*, and, for each of these conditions, the isolated T cells were restimulated *in vitro* with either BDC or OVA peptides. *In vitro* restimulation with the OVA control peptide did not lead to cytokine secretion, even for T cells isolated from mice that received OVA *in vivo* (Fig. 3.4 A & C). In contrast, restimulation with BDC peptide did trigger cytokine secretion in an antigen-specific manner (Fig. 3.4 B & D). Specifically, T cells isolated from the draining LNs of mice that received BDC-loaded gels secreted high levels of IL-2 upon restimulation with BDC peptide (Fig. 3.4 B). T cells isolated from other lymph nodes

in these same mice also secreted IL-2 in response to restimulation with BDC, but to a much lesser extent (Fig. 3.4 B). Analysis of other pertinent cytokines showed that they were also secreted in an antigen-specific manner, only by T cells isolated from mice that were injected with gels delivering BDC *in vivo* (Fig. 3.4 C-D). The greatest fold increase in antigen-specific secretion, around 27-fold, was seen for IL-10 (Fig. 3.4 D). IFN-γ exhibited the second highest increase in secretion, with a 16-fold increase, while the other cytokines assayed only showed more modest increases between 2- to 8-fold. Cells isolated from gels that received OVA in vivo did not exhibit such antigen-specific cytokine secretion (Fig. 3.4 C).

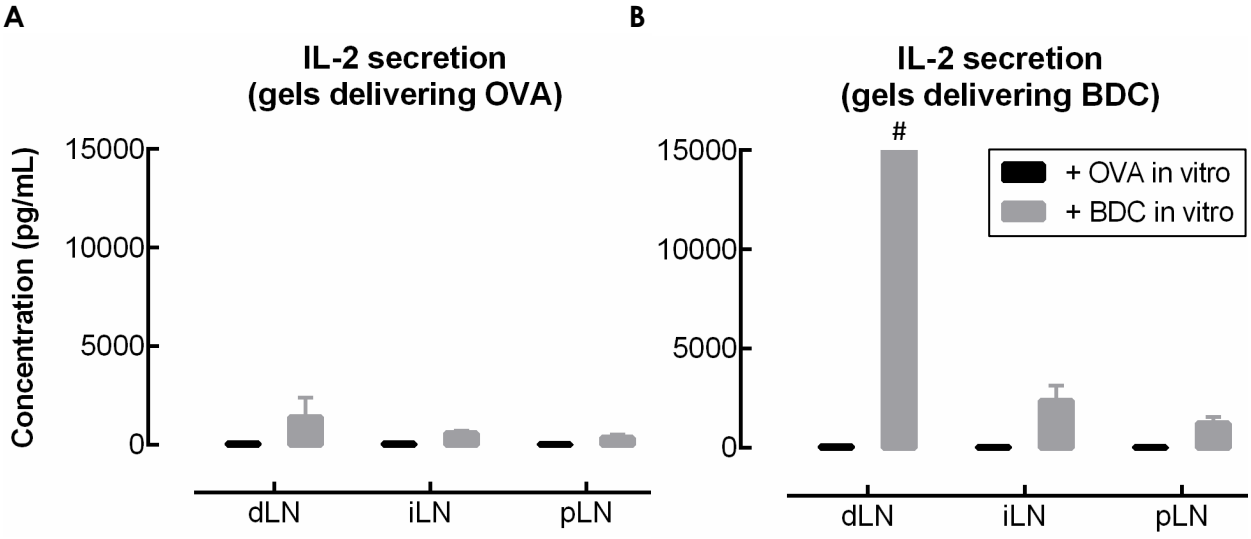

Figure 3.4.

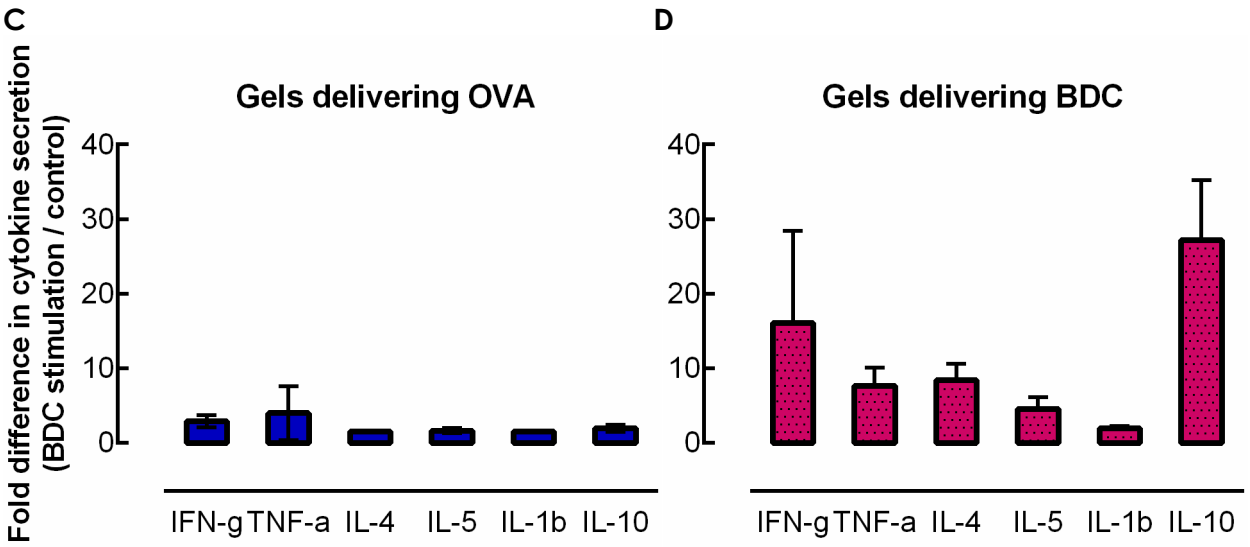

Figure 3.4 (continued). T cells secreted cytokines in an antigen-specific manner following delivery of peptide in the gel system. (A-D) 5 days after administration of gels delivering GM-CSF and peptide, T cells were isolated from the draining (dLN), irrelevant (iLN), and pancreatic (pLN) lymph nodes. T cells were restimulated *in vitro* by BMDCs pulsed with either BDC peptide or control peptide (OVA). Coculture supernatants were analyzed to determine the cytokine secretion profile of the T cells. (A-B) IL-2 secretion by T cells isolated from mice that received control OVA peptide-loaded gels (A) or BDC peptide-loaded gels (B) *in vivo*. (C-D) Secretion of cytokines associated with Th1, Th2, Th17, and Treg phenotypes by T cells isolated from the draining LNs of mice that received OVA (C) or BDC (D) in gels *in vivo*, represented as a fold difference in secretion between BDC restimulation and OVA restimulation. (n = 3; mean ± s.d. shown; # data out of range).

Incorporation of PLG particles in pore-forming gels altered the phenotype of recruited DCs

The impact of using PLG as a vehicle for delivering peptide on the phenotype of cells recruited into the material system was investigated. In gels delivering GM-CSF conjugated to AuNPs, either with or without PLG particles, >~95% of the cells were consistently $CD11b^+$ across all timepoints (Fig. 3.5 A). However, substantial differences in expression were seen for the other markers assayed. In gels that recruited DCs using only GM-CSF conjugated to AuNPs, the percentage of $CD11c^+$ (Fig. 3.5 B), $F4/80^+$ (Fig.

3.5 C), and MHCII$^+$ (Fig. 3.5 D) cells was initially low at day 1, but these populations increased significantly at days 3 and 5. In contrast, for gels also delivering peptide-loaded PLG particles, the fraction of these cell populations started at similar low levels at day 1, but failed to increase substantially over time. The fraction of F4/80$^+$ and MHCII$^+$ cells remained almost the same as at day 1, and the CD11c$^+$ population only showed a modest increase. At day 5, gels delivering PLG and peptide contained 3.5-fold, 28-fold, and 12-fold lower fractions of CD11c$^+$, F4/80$^+$, and MHCII$^+$ cells, respectively. Intriguingly, the opposite trend was seen for Gr-1$^+$ cells (Fig. 3.5 E). At day 1, around 90% of the cells were Gr-1$^+$, in addition to being CD11b$^+$, for both conditions. At subsequent timepoints, the fraction of Gr-1$^+$ cells decreased significantly in gels without PLG particles, reaching less than 5% at day 5. In gels with PLG, the population of Gr-1$^+$ cells remained higher than 90% through day 5, at which point the fraction of Gr-1$^+$ cells was 20-fold higher than in gels without PLG.

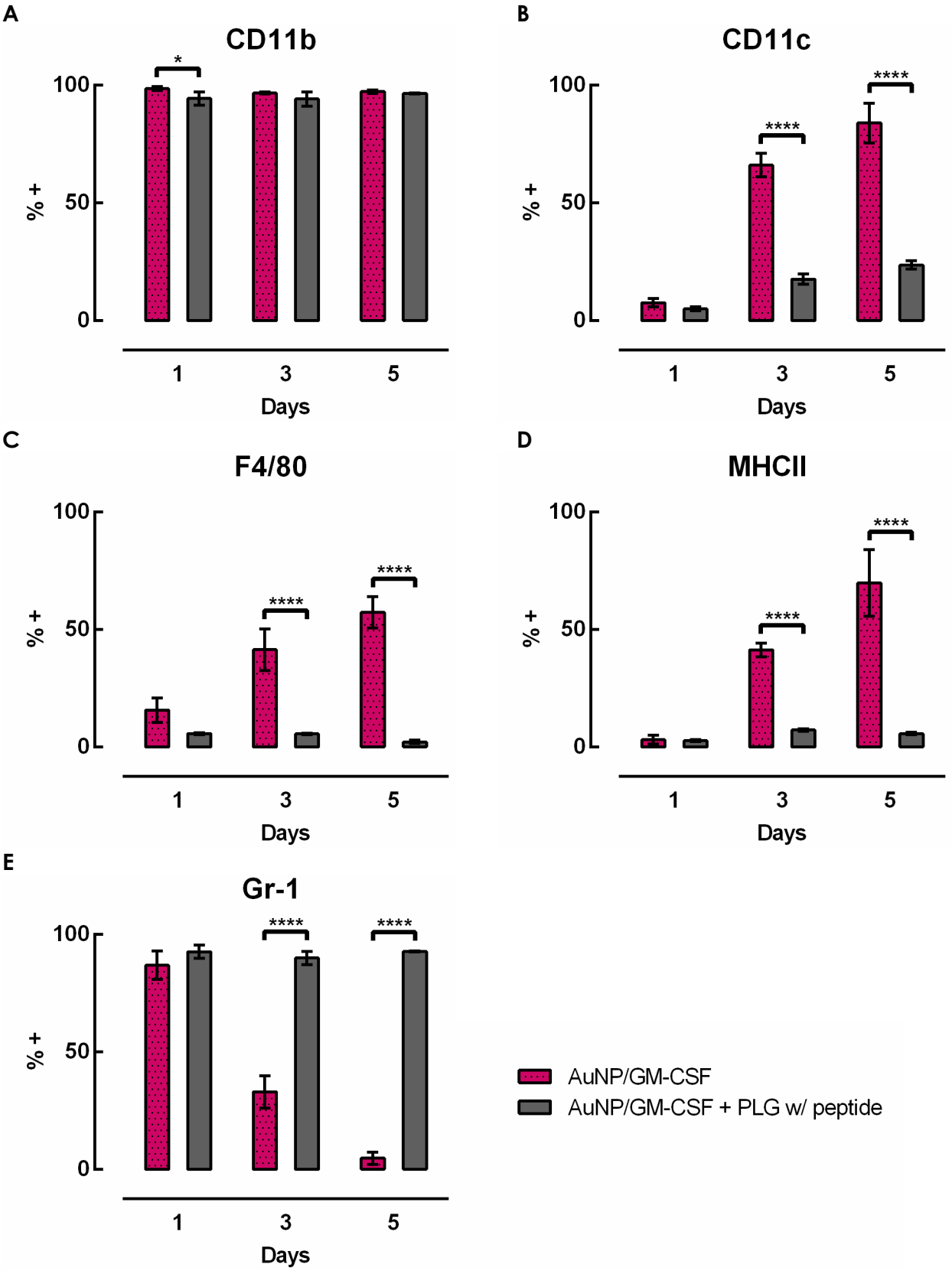
A
CD11b
*
100
50
0
% +
1
3
5
Days
B
CD11c
****
****
100
50
0
% +
1
3
5
Days
C
F4/80
****
****
100
50
0
% +
1
3
5
Days
D
MHCII
****
****
100
50
0
% +
1
3
5
Days
E
Gr-1
****
****
100
50
0
% +
1
3
5
Days
AuNP/GM-CSF
AuNP/GM-CSF + PLG w/ peptide

Figure 3.5.

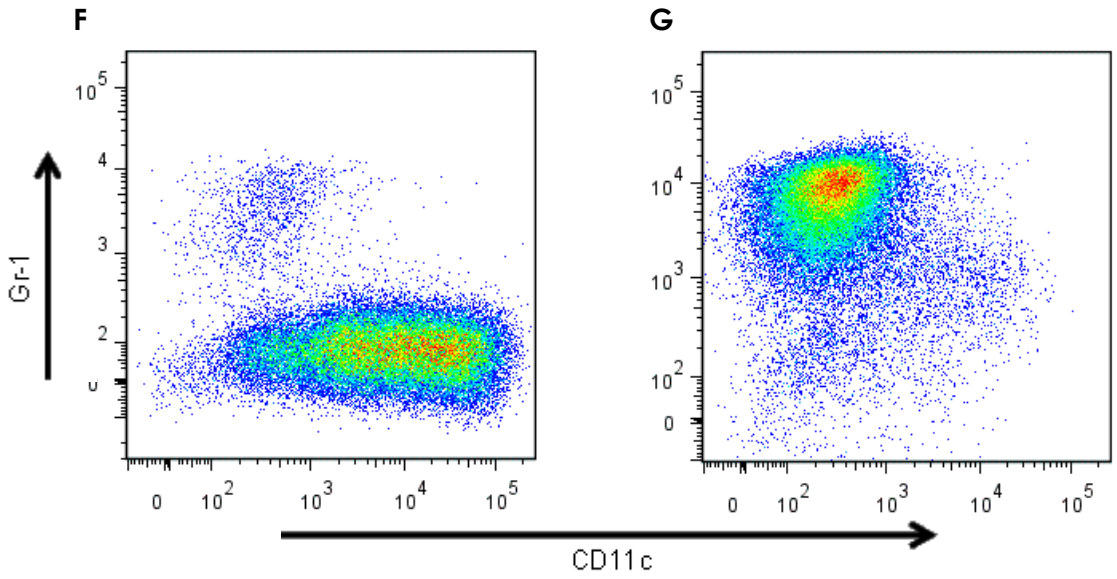

Figure 3.5 (continued). Incorporation of PLG particles in the gels significantly altered the phenotype of cells recruited in response to GM-CSF. Gels delivering GM-CSF, either with or without peptide-loaded PLG particles, were injected subcutaneously in the flanks of C57BL/6J mice; at specified timepoints, gels were isolated and dissociated to analyze infiltrating cells by flow cytometry. (A-E) Percentage of cells expressing $CD11b^+$ (A), $CD11c^+$ (B), $F4/80^+$ (C), $MHCII^+$ (D), and $Gr\text{-}1^+$ (E). (F-G) Flow cytometry plots showing expression of CD11c and Gr-1 by cells isolated from gels delivering only AuNP/GM-CSF (F) or AuNP/GM-CSF with peptide-loaded PLG particles (G) at 5 days. (n = 3; mean ± s.d. shown; * $p < 0.05$; **** $p < 0.0001$).

Higher levels of inflammatory cytokines were expressed in gels containing PLG particles

To further assess the maturation status of the cells in the gels, the expression of inflammatory cytokines was examined at both the mRNA and protein levels at day 3, the peak of cell infiltration. For gene expression analysis, live cells were sorted on the basis of CD11b and CD11c to separate $CD11b^+$ $CD11c^+$ double positive "DCs" from $CD11b^+$ $CD11c^-$ single positive "myeloid" cells (Fig. 3.6 A). The cells that did not fit into those populations, i.e. lymphocytes ($CD3e^+$ and $DX5^+$ cells) and $CD11b^-$ cells, were pooled together and excluded. Splenocytes from naïve mice were used as a basis for comparison, and these cells were also separated into different populations using the

same sorting strategy (Fig. 3.6 A). The CD11b$^+$ CD11c$^+$ splenic DCs were used as a control representing immature DCs, and all other samples were normalized to this one. As a positive control for inflammatory DCs, CD11b$^+$ CD11c$^+$ splenic DCs were stimulated with LPS for 4h. As expected, the LPS-stimulated splenocytes showed a significant increase in the expression of transcripts for the inflammatory cytokines, such as *Il23a*, *Il27*, *Il33*, and *Il6*. Expression of *Il12b* and *Il1a* was also increased in the LPS-stimulated controls, but not in a statistically significant manner (Fig. 3.6 B). Cells isolated from gels delivering GM-CSF exhibited similar or lower expression levels for all the assayed genes, as compared to the immature CD11b$^+$ CD11c$^+$ splenocyte controls (Fig. 3.6 C-D). Some of the transcripts, such as *Il12b*, were several orders of magnitude less abundant than in the splenic DC control. In cells isolated from gels delivering peptide-loaded PLG, the expression levels were also lower than in the splenic DCs for many of the genes. However, *Il1a* expression was significantly increased when peptide-loaded PLG particles were present in the gels (Fig. 3.6 C-D). Within each experimental condition, comparing the CD11b$^+$ CD11c$^-$ "myeloid" cells and the CD11b$^+$ CD11c$^+$ "DCs" did not reveal any significant differences in gene expression for the transcripts that were examined here.

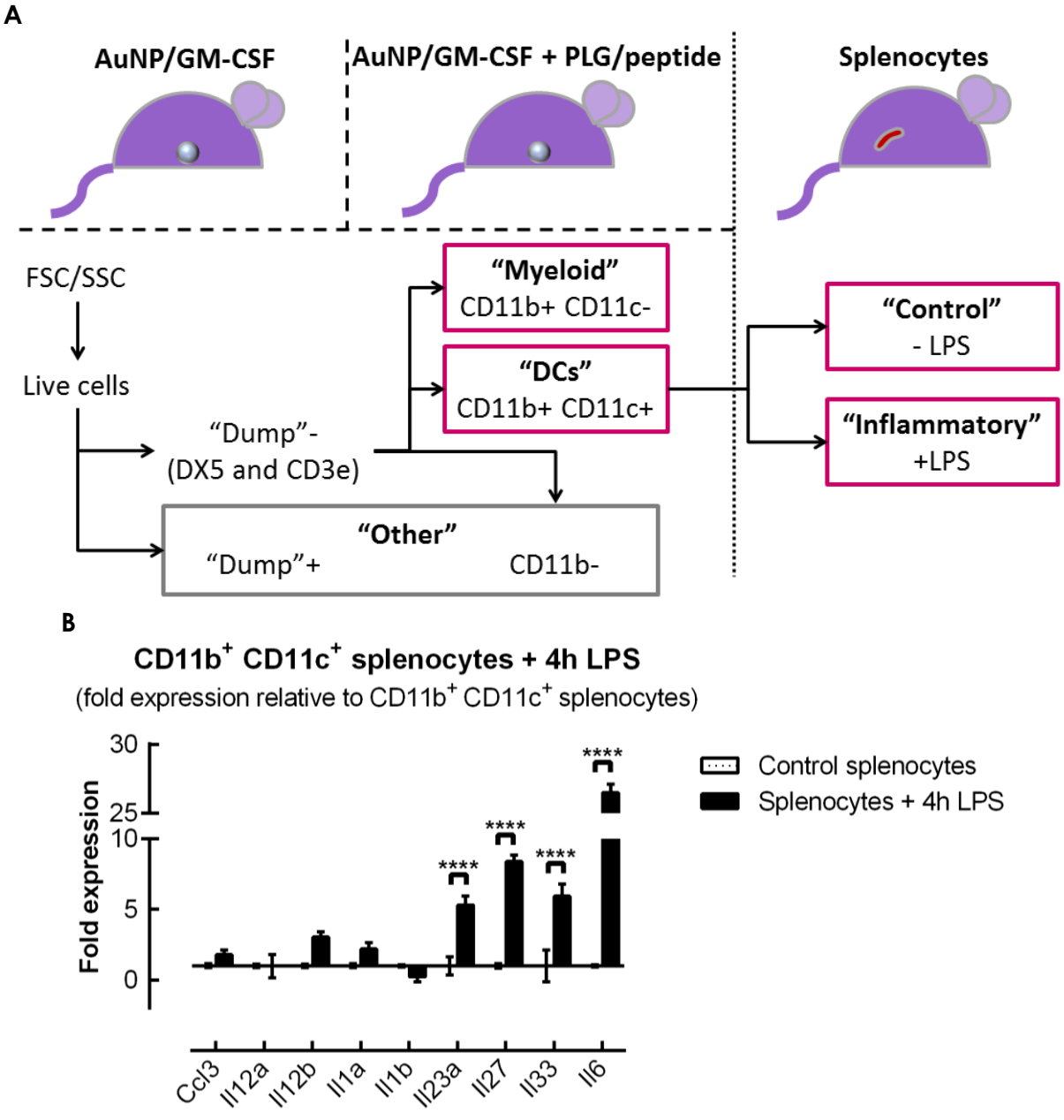
A
AuNP/GM-CSF
AuNP/GM-CSF + PLG/peptide
Splenocytes
FSC/SSC
Live cells
"Dump"-
(DX5 and CD3e)
"Myeloid"
CD11b+ CD11c-
"DCs"
CD11b+ CD11c+
"Other"
"Dump"+
CD11b-
"Control"
- LPS
"Inflammatory"
+LPS
B
CD11b+ CD11c+ splenocytes + 4h LPS
(fold expression relative to CD11b+ CD11c+ splenocytes)
Fold expression
30
25
10
5
0
****
Control splenocytes
Splenocytes + 4h LPS
Ccl3
Il12a
Il12b
Il1a
Il1b
Il23a
Il27
Il33
Il6

Figure 3.6.

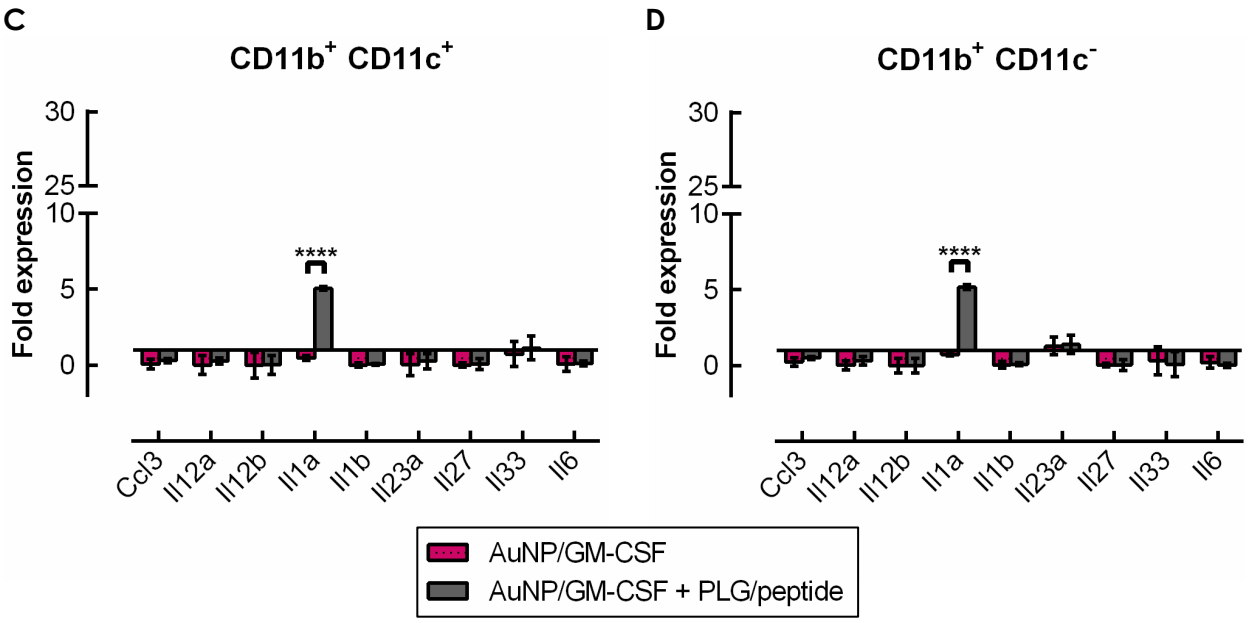

Figure 3.6 (continued). Cells in gels containing peptide-loaded PLG particles expressed higher levels of *Il1a* mRNA. Gene expression analysis of cells isolated from gels delivering GM-CSF with or without peptide-loaded PLG particles. Gels were injected subcutaneously into the flanks of C57BL/6J mice; after 3 days, gels were isolated, cells were sorted, and gene expression was analyzed by qPCR. (A) Cell sorting strategy to separate $CD11b^+$ $CD11c^-$ "myeloid" cells from $CD11b^+$ $CD11c^+$ "DCs" for analysis. (B-D) Fold differences in gene expression, normalized to splenic DC controls. (B) Control splenocytes before or after 4h LPS stimulation. (C-D) Comparison of gene expression in cells isolated from gels either with or without peptide-loaded PLG particles. The $CD11b^+$ $CD11c^-$ "myeloid" (C) and $CD11b^+$ $CD11c^+$ "DC" (D) subsets were analyzed separately. (n = 3; mean ± s.e.m. shown; **** $p < 0.0001$).

A BioPlex assay was performed to examine the expression of a broad panel of immunologically relevant cytokines and growth factors (Fig. 3.7). An overview of all 23 cytokines assayed revealed that the gels contained very low levels of inflammatory cytokines that induce Th1 (i.e. IL-12p70 and IFN-γ) or Th17 (i.e. IL-6) responses, as well as low levels of IL-10 and Th2-inducing cytokines (i.e. IL-4, IL-13) (Fig. 3.7 A). The concentrations of some of the assayed cytokines were near or below the lower limit of detection. The most abundant proteins detected in this panel were chemokine (C-C motif) ligand 3 (CCL3 or MIP-1a), followed by GM-CSF. Several other CC family

chemokines were also expressed, such as CCL4 (MIP-1b), CCL2 (MCP-1), CCL5 (RANTES), and CCL11 (eotaxin). IL-12p40 and IL-1b were detectable, but at low levels. As a positive control for inflammatory conditions, LPS was incorporated into gels delivering GM-CSF, which resulted in a substantial and expected increase in the production of several inflammatory cytokines. Gels containing peptide-loaded PLG particles did not exhibit significant differences in the quantity of inflammatory cytokines detected, as compared to AuNP/GM-CSF gels (Fig. 3.7 B-D). However, gels containing control (i.e. blank) PLG particles exhibited levels of inflammatory cytokines that were significantly higher than in the gels only delivering GM-CSF. For IL-12p70 (Fig. 3.7 B) and IL-1b (Fig. 3.7 D), this increase was statistically significant, whereas for IL-1a (Fig. 3.7 C), the same trend was observed, but was not statistically significant. For all of these cytokines, the levels found in gels delivering control PLG particles still remained lower than in the inflammatory LPS control.

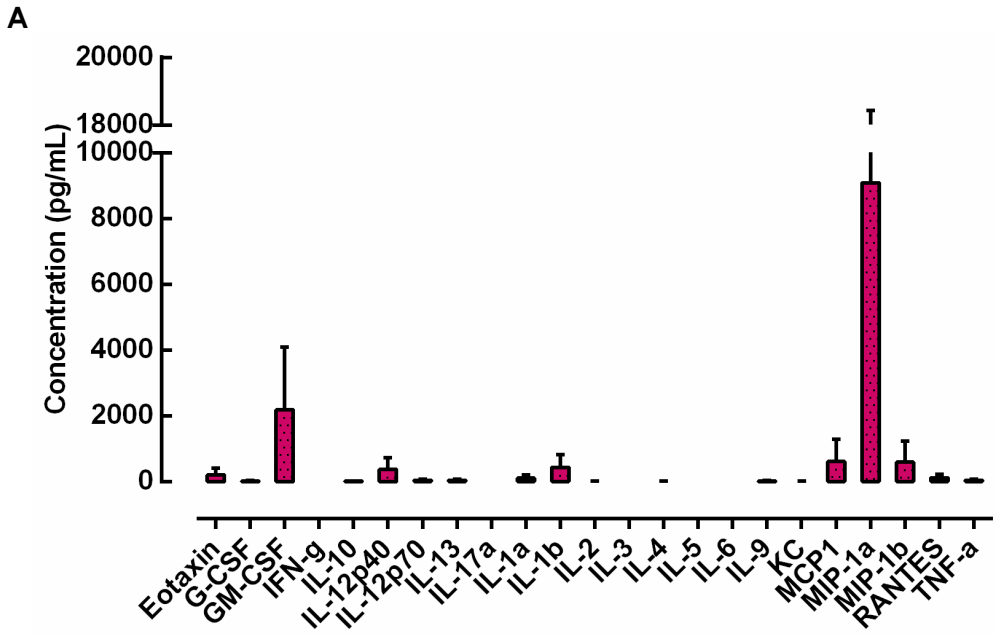

Figure 3.7.

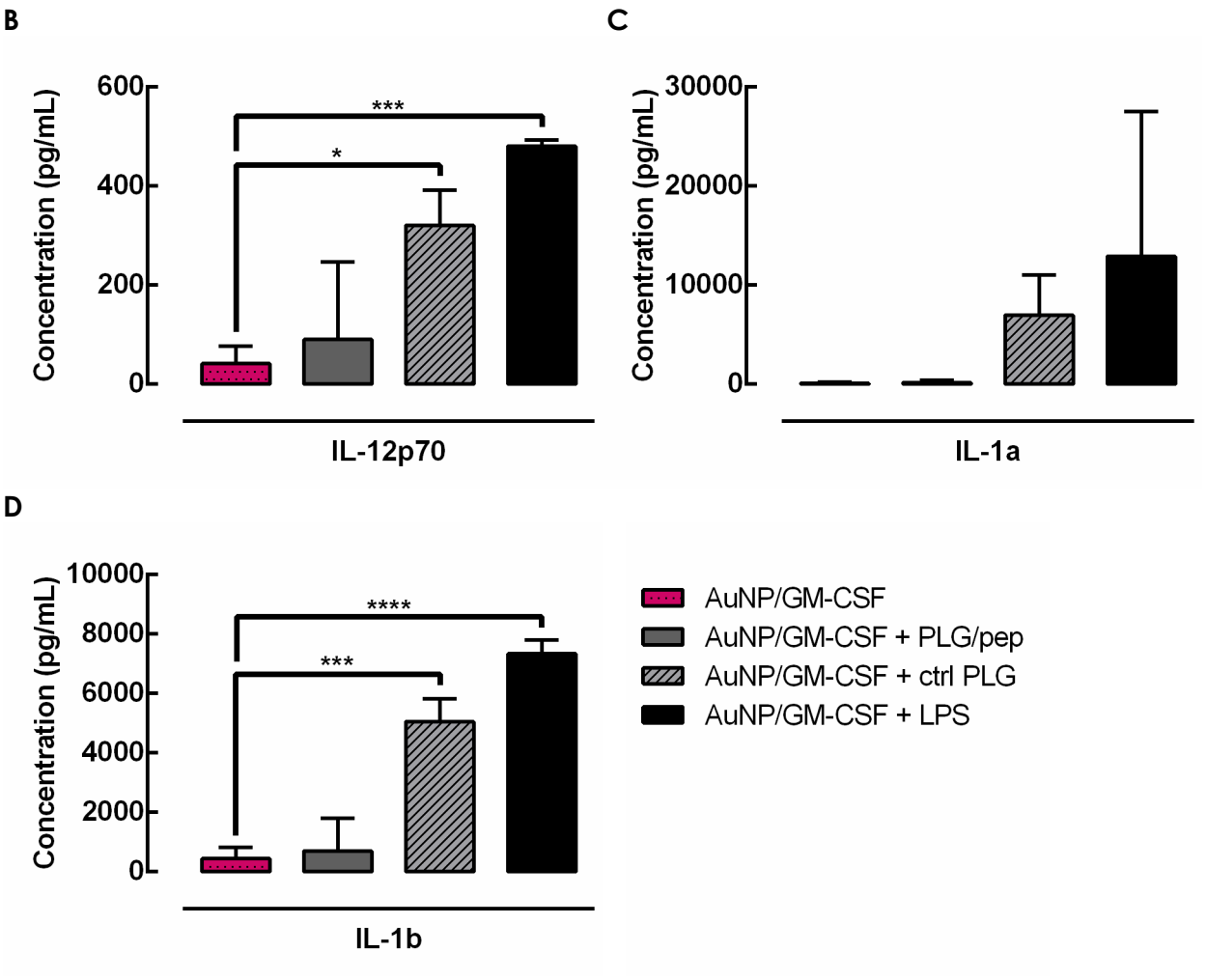

Figure 3.7 (continued). Gels containing blank PLG particles, but not peptide-loaded PLG particles, expressed higher levels of inflammatory cytokines than gels without PLG particles. Gels were injected subcutaneously in the flanks of C57BL/6J mice; at day 3, gels were isolated and subjected to protein extraction for cytokine analysis. (A) Overview of 23 different cytokines measured in gels delivering GM-CSF conjugated to AuNPs. (B-D) Concentrations of the inflammatory cytokines IL-12p70 (B), IL-1a (C), and IL-1b (D) in gels delivering either AuNP/GM-CSF alone, or AuNP/GM-CSF together with blank PLG particles or peptide-loaded PLG particles. Gels delivering AuNP/GM-CSF + 3ug LPS were used as a positive control for inflammatory conditions. (n = 3; mean ± s.d. shown; * $p < 0.05$; *** $p < 0.001$; **** $p < 0.0001$; AuNP/GM-CSF condition was compared to all other conditions.)

3.4 Discussion

The material system described in Chapter 2 achieved effective recruitment of millions of $CD11b^+$ $CD11c^+$ DCs. In this chapter, further characterization revealed that these DCs exhibited a cell surface marker phenotype consistent with immature or semi-mature DCs. To harness the potential of these DCs to induce antigen-specific T cells, the material system was further adapted to deliver a defined peptide antigen at a slow rate, which resulted in localized delivery. DCs were found to present peptide in a localized manner, which elicited antigen-specific $CD4^+$ T cell proliferation and cytokine secretion in the draining LNs. However, the use of PLG particles to deliver the peptide antigen significantly altered the phenotype of the recruited cells, leading to a much lower abundance of $CD11b^+$ $CD11c^+$ DCs and an increase in cytokines associated with inflammation.

The $CD11c^+$ DCs recruited to the material system in response to GM-CSF delivery expressed MHCII, CD86, and CCR7, but at relatively low levels, suggesting that they were immature or semi-mature. When expressed at high levels, these markers are indicative of DC maturation. However, some level of MHCII expression may be important for inducing antigen-specific tolerogenic responses, since MHCII is necessary for peptide presentation by DCs to $CD4^+$ T cells. Similarly, some level of CCR7 expression may also be desirable, since CCR7 mediates homing to the lymph nodes, where the DCs interact with T cells. Interestingly, CD86 expression levels were significantly lower in gels delivering GM-CSF, either with or without AuNPs, compared to gels without GM-CSF, suggesting that GM-CSF may be suppressing maturation. The levels of MHCII and CD86

expressed on cells recruited into gels delivering GM-CSF were comparable to those seen on immature BMDCs.

Despite a thorough characterization of the cell surface markers expressed by DCs recruited using this system, the specific subtype and lineage of these cells remains unclear. These DCs were found to express high levels of PD-L1 and PD-L2, two negative costimulatory molecules that signal through PD-1 on T cells and are important for tolerance mechanisms[28,29]. This is a promising indication that the DCs infiltrating the gels may have the capacity to induce tolerance. On the other hand, only ~12% of the DCs in this system expressed DEC-205 (CD205), an endocytic receptor that has been associated with DCs that have tolerogenic potential[30]. A significant fraction of the cells consisted of PDCA-1$^+$ cells, which was unexpected since PDCA-1$^+$ pDCs are usually described as expressing low levels of CD11c[31]. CD8a$^+$ DCs, which are particularly effective at cross-presentation and may not be the best targets for modulating CD4$^+$ cells[32], were not present in this system. Few of the DCs expressed CD207, i.e. langerin, or CD103, two markers found on dermal DCs. This suggests that, despite the fact that the gels were injected subcutaneously and were adjacent to the dermis, the majority of DCs infiltrating the gels did not consist of specialized dermal DCs known as Langerhans cells. Gels delivering control AuNPs, without GM-CSF, contained a higher percentage of CD207$^+$ cells, which was likely a reflection of the fact that the total number of cells in those gels was significantly lower, so the same number of CD207$^+$ would represent a greater fraction of the total cells. It is speculated that the DCs in this material system may be CD11b$^+$ CD103$^-$ migratory DCs or monocyte-derived DCs that would have migrated, differentiated, and proliferated in response to GM-CSF. However,

determining the lineage of these cells with certainty would require extensive studies that are beyond the scope of this work.

A peptide antigen was incorporated into the material delivery system by first encapsulating it in PLG microspheres, allowing it to be released at a slow and sustained rate. An *in vivo* biodistribution study detected intact peptide in the tissue infiltrating the material delivery system, but not in the adjacent tissue. Despite the fact that molecules and particles under ~100-200nm[33–35] can be passively transported through lymphatic vessels, the delivered peptide antigen was also not detected in the LNs draining the material. This precise localization at the site of the material may be explained by the fact that the peptide was released at a very slow rate from the material, such that free peptide would be either captured by DCs or proteolytically degraded before it reached other tissues. An assay for peptide presentation determined that DCs recruited to the material system were able to capture the peptide antigen *in vivo* and functionally present it to T cells. Clear peptide presentation was observed for cells isolated from the gels, and an increase, although not statistically significant, was also seen in the dLN. Together, these data suggest that only cells infiltrating the material were exposed to a local concentration of peptide within the material, allowing them to acquire the peptide and transport it to the draining LNs. The ability to deliver peptide in a localized manner is an important feature from a safety perspective, since it eliminates the risk of antigen being disseminated to a site of disease where it could potentially precipitate or exacerbate autoimmunity[3]. In addition, maintaining a local concentration of peptide exclusively within the material would be desirable if

tolerogenic factors were added to this system, since DCs would only be exposed to the peptide in the context of tolerogenic signals.

As a result of *in vivo* peptide presentation by DCs, $CD4^+$ T cells proliferated and expanded in an antigen-specific manner. This was shown both for adoptively transferred BDC2.5 T cells, as well as for endogenous antigen-specific T cells. Although peptide presentation by DCs remained localized to the material and the draining LNs, proliferating antigen-specific T cells were found not only in the draining LNs, but also in the spleen and other LNs. The use of a cell proliferation dye showed that the T cells in the draining LNs underwent a greater number of divisions than those in the other lymphoid organs, strongly suggesting that the T cells proliferated upon contact with peptide-bearing DCs in the draining LNs and subsequently trafficked to other tissues. These results demonstrate that DCs programmed by a biomaterial in a localized manner interacted with antigen-specific T cells that were able to traffic systemically and could potentially home to sites of disease.

After an initial expansion, the population of antigen-specific T cells found in the LNs contracted back to baseline levels. One possibility is that these cells simply died after an initial proliferation phase. Other studies showing a similar effect have attributed this to an active T cell deletion process[11,36]. In this system, the antigen-specific T cells did not disappear completely, suggesting that deletion was not the cause of the population contraction, or that any deletion that may have occurred was incomplete. Mechanistic studies would be required to determine whether active deletion, rather than simple apoptosis, is playing any role. Another interesting possibility is that these

expanded antigen-specific T cells may have migrated into peripheral tissues. Although the antigen-specific cells did not accumulate in the pancreatic LNs, it is possible that some of these T cells may have homed to the pancreatic islets, where their endogenous antigen is found. The islets themselves were not examined in this set of studies, but antigen-specific T cells infiltrating the islets could be analyzed by flow cytometry or by immunohistochemistry, both of which would be associated with some technical challenges.

In addition to undergoing proliferation, T cells also secreted cytokines in an antigen-specific manner following the administration of gels delivering BDC peptide. In agreement with the observed T cell proliferation, cells from the draining LNs secreted high levels of IL-2 in response to restimulation with BDC peptide. Other cytokines were also secreted in an antigen specific manner, in particular IL-10 and IFN-γ, which are suggestive of a Tr1 secretion profile[38]. Importantly, restimulation with OVA, which was used here as a control peptide, did not induce cytokine secretion, even in the T cells isolated from mice that received gels delivering OVA peptide *in vivo*. This demonstrates that, even though OVA(323-339) can be presented on the I-A^{g7} molecule[37], this material system did not raise immunity towards OVA, which is a foreign peptide.

Upon investigation, it was found that incorporating PLG microspheres into the gels led to significant differences in the phenotype of the cells recruited to the gels, as well as the expression of cytokines by these cells. When PLG microspheres were introduced into the gels, the majority of recruited cells were still $CD11b^+$ myeloid cells. However, a significantly lower fraction of cells expressed the DC-associated marker CD11c, and

even greater reductions in expression were seen for MHCII and F4/80. The low abundance of $CD11c^+$ and $MHCII^+$ cells indicated that only a small fraction of these cells were DCs and that they may have a more limited ability to present delivered antigens. Gr-1, which labels monocytes and granulocytes, appeared to vary inversely with CD11c. In gels delivering GM-CSF without PLG, the fraction of $Gr\text{-}1^+$ was high at day 1, but decreased at subsequent timepoints as the fraction of $CD11c^+$ cells increased. In gels with PLG particles, the percentage of $Gr\text{-}1^+$ cells remained high for all the timepoints examined. It is unclear what the functional differences were between the $CD11b^+$ $CD11c^+$ cells and the $CD11c^+$ $Gr\text{-}1^+$ cells seen in the presence of PLG particles. In spite of the low frequency of $CD11c^+$ $MHCII^+$ cells found in gels delivering peptide-loaded PLG particles, clear antigen-specific T cell proliferation was observed *in vivo*, indicating that, even in the presence of PLG, at least some of the recruited cells were competent to present antigen to T cells.

When PLG particles were incorporated into the gels, the recruited cells expressed higher levels of cytokines associated with inflammation at both the mRNA and protein levels. Strikingly, cells isolated from gels delivering only GM-CSF expressed similar or lower levels of many genes encoding inflammatory cytokines as compared to immature $CD11b^+$ $CD11c^+$ splenic DCs, which were used as a control cell population. When PLG particles containing peptide were delivered in addition to GM-CSF, *Il1a* expression was significantly increased. It was interesting to observe that the overall pattern of gene expression was similar between the sorted $CD11c^-$ "myeloid" and $CD11c^+$ "DC" populations.

At the protein level, gels delivering GM-CSF conjugated to AuNPs exhibited low or undetectable levels of most inflammatory cytokines, but they did contain a number of different CC family chemokines. Surprisingly, CCL3 (MIP-1a) was the most abundant protein detected in gels delivering GM-CSF, even though the abundance of *Ccl3* mRNA was several fold lower than in control splenocytes. The incorporation of peptide-loaded PLG particles did not have a significant impact on the production of inflammatory cytokines in the gels. In contrast, incorporation of blank PLG particles significantly increased the levels of IL-1b and IL-12p70 protein, with a similar trend also seen for IL-1a. This difference between peptide-loaded and blank PLG particles could be attributed to the fact that PLG is known to mediate non-specific protein adsorption, which may be greatly reduced when peptide is incorporated into the particles. However, this raises questions about effects that may occur at later timepoints, as the peptide diffuses out of the particles. Another point of consideration is that the cells within the gels were lysed, so these data are not necessarily representative of protein secretion. In addition, some cytokines, like IL-1b, are secreted in an inactive precursor form (pro-IL-1b). Since the BioPlex assay used here was not designed to exclusively detect the mature forms of proteins like IL-1a and IL-1b, it is assumed that there could be cross-reactivity with their precursor forms (pro-IL-1a and pro-IL-1b).

Taken together, the gene and protein expression data demonstrate that the delivery of PLG microspheres had a significant impact on cell phenotype, even though the particles were encapsulated in the alginate hydrogel. The changes in cell phenotype and the increases in inflammatory cytokine expression were consistent with the qualitative observations that gels containing peptide-loaded PLG particles became

vascularized in a 5-10 day timeframe and were surrounded by a thickened capsule, which was not the case for gels delivering only GM-CSF conjugated to AuNPs. The differences in cytokine expression seen here, while statistically significant, were not as drastic as might have been expected based on the stark differences in cell surface marker expression. The gels were analyzed 3 days after injection because this represented the peak of cell infiltration for gels delivering GM-CSF, but this may not be the timepoint at which the differences in cytokine expression are the most pronounced. However, the observed differences in cell phenotype and the shift in cytokine expression may impact the function of the recruited DCs in ways that alter their ability to induce tolerogenic responses.

While peptide delivery from PLG microspheres in alginate gels demonstrated desirable characteristics of localized delivery and functional antigen presentation by DCs, further optimization will likely be required to enable the induction of robust tolerogenic responses. In particular, devising a different strategy for localized delivery of peptide from the biomaterial may be a promising next step.

3.5 References

1. Germain, R. N. Vaccines and the Future of Human Immunology. *Immunity* **33,** 441–450 (2010).

2. Coppieters, K. T., Harrison, L. C. & von Herrath, M. G. Trials in type 1 diabetes: Antigen-specific therapies. *Clin. Immunol.* **149,** 345–355 (2013).

3. Miller, S. D., Turley, D. M. & Podojil, J. R. Antigen-specific tolerance strategies for the prevention and treatment of autoimmune disease. *Nat. Rev. Immunol.* **7,** 665–677 (2007).

4. Ohnmacht, C. *et al.* Constitutive ablation of dendritic cells breaks self-tolerance of CD4 T cells and results in spontaneous fatal autoimmunity. *J. Exp. Med.* **206,** 549–559 (2009).

5. Yogev, N. *et al.* Dendritic Cells Ameliorate Autoimmunity in the CNS by Controlling the Homeostasis of PD-1 Receptor+ Regulatory T Cells. *Immunity* **37,** 264–275 (2012).

6. Banchereau, J. & Steinman, R. M. Dendritic cells and the control of immunity. *Nature* **392,** 245–252 (1998).

7. Shortman, K. & Liu, Y.-J. Mouse and human dendritic cell subtypes. *Nat. Rev. Immunol.* **2,** 151–161 (2002).

8. Lutz, M. B. & Schuler, G. Immature, semi-mature and fully mature dendritic cells: which signals induce tolerance or immunity? *Trends Immunol.* **23,** 445–449 (2002).

9. Hawiger, D. *et al.* Dendritic Cells Induce Peripheral T Cell Unresponsiveness under Steady State Conditions in Vivo. *J. Exp. Med.* **194,** 769 (2001).

10. Bonifaz, L. *et al.* Efficient Targeting of Protein Antigen to the Dendritic Cell Receptor DEC-205 in the Steady State Leads to Antigen Presentation on Major Histocompatibility Complex Class I Products and Peripheral CD8+ T Cell Tolerance. *J. Exp. Med.* **196,** 1627–1638 (2002).

11. Mukhopadhaya, A. *et al.* Selective delivery of β cell antigen to dendritic cells in vivo leads to deletion and tolerance of autoreactive CD8+ T cells in NOD mice. *Proc. Natl. Acad. Sci.* **105,** 6374–6379 (2008).

12. Price, J. D. *et al.* CD8+ dendritic cell-mediated tolerance of autoreactive CD4+ T cells is deficient in NOD mice and can be corrected by blocking CD40L. *J. Leukoc. Biol.* jlb.0113013 (2013). doi:10.1189/jlb.0113013

13. Creusot, R. J., Giannoukakis, N., Trucco, M., Clare-Salzler, M. J. & Fathman, C. G. It's Time to Bring Dendritic Cell Therapy to Type 1. *Diabetes* **63,** 20–30 (2014).

14. Belle, T. L. V., Coppieters, K. T. & Herrath, M. G. V. Type 1 Diabetes: Etiology, Immunology, and Therapeutic Strategies. *Physiol. Rev.* **91,** 79–118 (2011).

15. Muixí, L. *et al.* The peptide-binding motif of HLA-DR8 shares important structural features with other type 1 diabetes-associated alleles. *Genes Immun.* **12,** 504–512 (2011).

16. Haskins, K., Portas, M., Bergman, B., Lafferty, K. & Bradley, B. Pancreatic islet-specific T-cell clones from nonobese diabetic mice. *Proc. Natl. Acad. Sci. U. S. A.* **86,** 8000–8004 (1989).

17. Katz, J. D., Wang, B., Haskins, K., Benoist, C. & Mathis, D. Following a diabetogenic T cell from genesis through pathogenesis. *Cell* **74,** 1089–1100 (1993).

18. Haskins, K. & McDuffie, M. Acceleration of Diabetes in Young NOD Mice with a CD4$^+$ Islet-Specific T Cell Clone. *Science* **249,** 1433–1436 (1990).

19. Mueller, R., Bradley, L. M., Krahl, T. & Sarvetnick, N. Mechanism Underlying Counterregulation of Autoimmune Diabetes by IL-4. *Immunity* **7,** 411–418 (1997).

20. Tarbell, K. V., Yamazaki, S., Olson, K., Toy, P. & Steinman, R. M. CD25+ CD4+ T cells, expanded with dendritic cells presenting a single autoantigenic peptide, suppress autoimmune diabetes. *J. Exp. Med.* **199,** 1467–1477 (2004).

21. Tarbell, K. V. *et al.* Dendritic cell-expanded, islet-specific CD4+ CD25+ CD62L+ regulatory T cells restore normoglycemia in diabetic NOD mice. *J. Exp. Med.* **204,** 191–201 (2007).

22. Jaeckel, E., Boehmer, H. von & Manns, M. P. Antigen-Specific FoxP3-Transduced T-Cells Can Control Established Type 1. *Diabetes* **54,** 306–310 (2005).

23. Judkowski, V. *et al.* Identification of MHC Class II-Restricted Peptide Ligands, Including a Glutamic Acid Decarboxylase 65 Sequence, that Stimulate Diabetogenic T Cells from Transgenic BDC2.5 Nonobese Diabetic Mice. *J. Immunol.* **166,** 908–917 (2001).

24. Stadinski, B. D. *et al.* Chromogranin A is an autoantigen in type 1 diabetes. *Nat. Immunol.* **11,** 225–231 (2010).

25. Jang, M.-H., Seth, N. P. & Wucherpfennig, K. W. Ex Vivo Analysis of Thymic CD4 T Cells in Nonobese Diabetic Mice with Tetramers Generated from I-Ag7/Class II-Associated Invariant Chain Peptide Precursors. *J. Immunol.* **171,** 4175–4186 (2003).

26. Ali, O. A., Huebsch, N., Cao, L., Dranoff, G. & Mooney, D. J. Infection-mimicking materials to program dendritic cells in situ. *Nat. Mater.* **8,** 151–158 (2009).

27. Heng, T. S. P. *et al.* The Immunological Genome Project: networks of gene expression in immune cells. *Nat. Immunol.* **9,** 1091–1094 (2008).

28. Keir, M. E. *et al.* Tissue expression of PD-L1 mediates peripheral T cell tolerance. *J. Exp. Med.* **203,** 883–895 (2006).

29. Keir, M. E., Butte, M. J., Freeman, G. J. & Sharpe, A. H. PD-1 and Its Ligands in Tolerance and Immunity. *Annu. Rev. Immunol.* **26,** 677–704 (2008).

30. Steinman, R. M., Hawiger, D. & Nussenzweig, M. C. Tolerogenic Dendritic Cells*. *Annu. Rev. Immunol.* **21,** 685–711 (2003).

31. Reizis, B., Bunin, A., Ghosh, H. S., Lewis, K. L. & Sisirak, V. Plasmacytoid Dendritic Cells: Recent Progress and Open Questions. *Annu. Rev. Immunol.* **29,** 163–183 (2011).

32. Belz, G. T. & Nutt, S. L. Transcriptional programming of the dendritic cell network. *Nat. Rev. Immunol.* **12,** 101–113 (2012).

33. Bachmann, M. F. & Jennings, G. T. Vaccine delivery: a matter of size, geometry, kinetics and molecular patterns. *Nat. Rev. Immunol.* **10,** 787–796 (2010).

34. Manolova, V. *et al.* Nanoparticles target distinct dendritic cell populations according to their size. *Eur. J. Immunol.* **38,** 1404–1413 (2008).

35. Reddy, S. T. *et al.* Exploiting lymphatic transport and complement activation in nanoparticle vaccines. *Nat. Biotechnol.* **25,** 1159–1164 (2007).

36. Annoni, A. *et al.* The immune response to lentiviral-delivered transgene is modulated in vivo by transgene-expressing antigen-presenting cells but not by CD4+CD25+ regulatory T cells. *Blood* **110,** 1788–1796 (2007).

37. Stratmann, T. *et al.* The I-Ag7 MHC Class II Molecule Linked to Murine Diabetes Is a Promiscuous Peptide Binder. *J. Immunol.* **165,** 3214–3225 (2000).

38. Gagliani, N. *et al.* Coexpression of CD49b and LAG-3 identifies human and mouse T regulatory type 1 cells. *Nat. Med.* **19,** 739–746 (2013).

Chapter 4. Conjugation of a peptide antigen to alginate represents a promising delivery strategy for generating antigen-specific tolerogenic responses *in vivo*

4.1 Introduction

The spatio-temporal presentation, dose, and affinity of a peptide antigen play an important role in directing immune responses, in addition to the critical signals provided by damage associated molecular patterns (DAMPs), pathogen associated molecular patterns (PAMPs), and various cytokines. The notion that strong immune responses are elicited when there is a temporal difference, or discontinuity, in the appearance of an antigen has been modeled and formulated into a "discontinuity theory" of immunity[1]. This theory captures the phenomena that an invading pathogen is associated with the acute introduction of a foreign antigen, potentially at high local concentrations, and that the successful elimination of an infection by the immune system removes the source of antigen. In contrast, the presence of antigens at low but persistent levels favors tolerance, as in the steady state. Accordingly, a materials-based vaccine would be most effective at inducing tolerance if it could deliver antigen at a low but sustained rate. This chapter addresses specific Aim 3 of this thesis by developing a technique for localized and cell-triggered delivery of peptide to DCs that infiltrate the non-inflammatory material system characterized in Chapters 2 and 3.

Several studies have investigated experimentally the effects of peptide dose and affinity on the induction of Tregs[2–7]. Two separate studies found that low doses of peptide antigen presented by DC *in vitro* were far more effective than high doses at

inducing and expanding suppressive Foxp3$^+$ Tregs in mouse[3] and human[4] T cells. The doses considered to be "low" varied by 3-4 orders of magnitude depending on affinity of the peptide mimetopes[3]. Taking this further, *in vivo* studies found that low doses of a high affinity antigen induced FoxP3$^+$ Tregs[5,6], while high doses of a low affinity antigen induced deletion of the antigen-specific cells after an initial proliferation[6]. The FoxP3$^+$ Tregs induced by *in vivo* delivery of low dose, high-affinity peptide were shown to be functional, since they were able to prevent disease in the NOD model of T1D[7]. Together, these studies highlight the importance of regulating peptide dose and presentation for the induction of tolerance.

In view of the findings described in Chapter 3, a method was sought to localize the delivery of peptide *in vivo* by covalently coupling it directly to alginate, thus avoiding the use any additional material that might cause phenotypic changes in the recruited DCs. As part of this strategy, it was necessary to incorporate a mechanism by which the peptide antigen could be released from the material to be loaded onto MHCII molecules and presented by DCs to T cells. A number of biocompatible degradable linkers have been characterized and used in the field of bioengineering. Several different types of linkers simply rely on the gradual breaking of chemical bonds, including hydrolytically labile bonds such as esters, acid-labile acetal linkers[8], or dithiol bonds that are cleaved in biological settings in the presence of glutathione[9]. For the particular application investigated here, the most appropriate strategy was to engineer cell-triggered degradation of the linker, such that release of peptide would be coordinated with cell infiltration, allowing effective capture of the peptide by the recruited DCs. Among the enzymes present *in vivo*, matrix metalloproteinases (MMPs)

are particularly good candidates to mediate cell-triggered release. MMPs are a family of proteases used by cells to degrade a wide variety of extracellular matrix (ECM) proteins, including many types of collagen, as well as fibronectin, laminin, elastin, and aggrecan; as a result, MMPs are critical for cell migration and tissue remodeling[10]. MMPs are also important for modifying a number of other bioactive molecules, performing functions such as cleaving cell surface receptors or activating chemokines/cytokines, thus affecting other important cell functions such as proliferation and differentiation[10]. Many different cell types express different MMPs, and, in particular, dermal DCs were shown to express MMP-9 and MMP-2 on their cell surface, which are important for their migration through the dermis[11]. MMP-cleavable peptide sequences have been incorporated into several types of synthetic hydrogels, creating cell-degradable matrices that deliver bioactive factors[12–14] and/or cells[15] for tissue engineering applications. A number of peptide sequences with different specificities and cleavage kinetics have been characterized and optimized to act as substrates for different MMPs[16,17].

The sub-hypothesis tested in this Chapter was that a defined peptide antigen could be coupled to and delivered from the hydrogel system for localized uptake by DCs in a non-inflammatory environment. An MMP-cleavable peptide sequence was selected to enable cell-triggered release of the covalently coupled peptide from alginate, allowing DCs to present the peptide and induce antigen-specific T cell responses.

4.2 Materials and Methods

In vivo MMP activity assay

Gels were injected subcutaneously in the flanks of NOD/ShiLtJ mice. 4 days later, 10uL of MMPSense 750 FAST (Perkin Elmer) were injected directly into the middle of the gels using 27G needles. As recommended by the manufacturer, baseline images were taken before injection of the MMPSense reagent, and mice were imaged again 4h after injection. Fluorescent *in vivo* imaging was performed using an IVIS Spectrum system (Perkin Elmer), and images were analyzed using Living Image software (Perkin Elmer).

Alginate conjugation and characterization

BDC-CMR peptide (CGGDDDDGPQGIWGQAAVRPLWVRMEAAKK(Rho_B); Peptide 2.0) was mixed at a 1:1:1 molar ratio with heterobifunctional (maleimide and amine) 7.5kDa PEG (JenKem Technology USA) and tris(2-carboxyethyl)phosphine (TCEP) in DMSO. The DMSO solvent was removed and the peptide-PEG conjugate was resuspended in H_2O. Coupling of the amine on the PEG to alginate was performed using EDC/Sulfo-NHS as described previously[18]. Peptide coupling was assayed by measuring the absorbance and/or fluorescence of the rhodamine B label using a BioTek plate reader.

In vitro peptide presentation

Bone marrow cells from NOD mice were isolated and differentiated as described in Chapter 3. On day 6 of the BMDC culture, 50ng/mL LPS was added to mature the BMDCs for 24h. On day 7, $CD4^+$ T cells were isolated from the spleen and lymph nodes

of BDC2.5 mice and sorted using an untouched $CD4^+$ MACS sorting kit (Miltenyi). Cocultures were set up by plating 10^5 BDC2.5 $CD4^+$ T cells and 2.5 10^4 BMDCs per well in 96 well plates. The indicated concentrations of BDC peptide or peptide-conjugated alginate were added in a total volume of 250uL/well. The proliferation of the BDC2.5 T cells was analyzed after 3 days. As a positive control for proliferation, T cells were cultured at a 1:4 ratio with mouse anti- CD3/CD28 activation beads (Dynabeads, Life Technologies).

In vivo peptide presentation

In vivo peptide presentation assays were performed as described in Chapter 3.

In vivo cell characterization studies

In vivo cell characterization studies were performed as described in Chapter 2.

Flow cytometry

Flow cytometry was performed as described in Chapter 2.

Statistical analysis

Statistical analyses were performed as described in Chapter 2.

4.3 Results

A peptide antigen was covalently coupled to alginate for localized delivery and cell-triggered release

First, to determine whether the DCs recruited to the material system would be able to degrade an MMP-cleavable linker and mediate release of covalently conjugated peptide, MMP activity in the gels was assayed *in vivo*. A fluorogenic MMP substrate was injected directly into the gels around the peak of DC infiltration. Gels delivering GM-CSF exhibited significantly enhanced MMP activity *in vivo* compared to control gels (Fig. 4.1), validating the use of an MMP-cleavable linker to mediate release of a covalently coupled peptide antigen from the alginate gels.

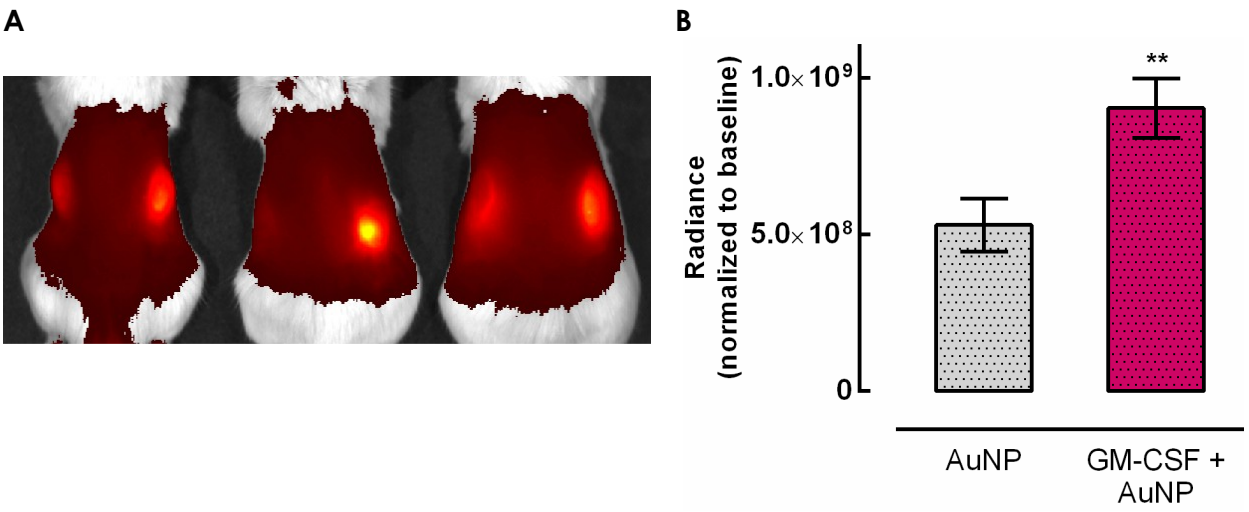

Figure 4.1. Pore-forming alginate gels delivering GM-CSF exhibited higher MMP activity than control gels. AuNP control gels and gels delivering GM-CSF + AuNPs were injected subcutaneously in the left and right flanks, respectively, of NOD/ShiLtJ mice. (A) 4 days after administration of the gels, a fluorogenic MMP substrate was injected directly into the gels and 3 replicate mice were imaged. (B) Quantification of the image shown in (A). Regions of interest (ROIs) of the same size were centered over each gel for analysis of the fluorescent signal. (n = 3; mean ± s.d. shown; ** $p < 0.01$.)

The BDC peptide antigen was modified to include an N-terminal cysteine for use in coupling reactions, followed by a short linker and an MMP-cleavable peptide sequence, as well as a C-terminal Rhodamine B label for detection (Fig. 4.2 A). This modified version of the BDC peptide was termed BDC-CMR (cysteine, MMP-cleavable, Rhodamine). Despite the addition of aspartic acid residues in the linker region to increase the hydrophilicity of the BDC-CMR peptide, it only dissolved in water to a concentration of 2.8 mg/mL (Fig. 4.2 B). To make the peptide more amenable for aqueous coupling chemistries, a 7.5kDa heterobifunctional polyethylene glycol (PEG) chain was conjugated to the BDC-CMR peptide to increase its solubility in water. After reacting the maleimide on the PEG with the cysteine on the peptide, the resulting peptide-PEG conjugate was soluble in water at a concentration of at least 5mg/mL (Fig. 4.2 B). The peptide-PEG conjugate was then coupled to alginate using standard EDC/NHS chemistry. The coupling efficiency, which was determined by quantifying the rhodamine label on the peptide, was approximately 60% (Fig. 4.2 C).

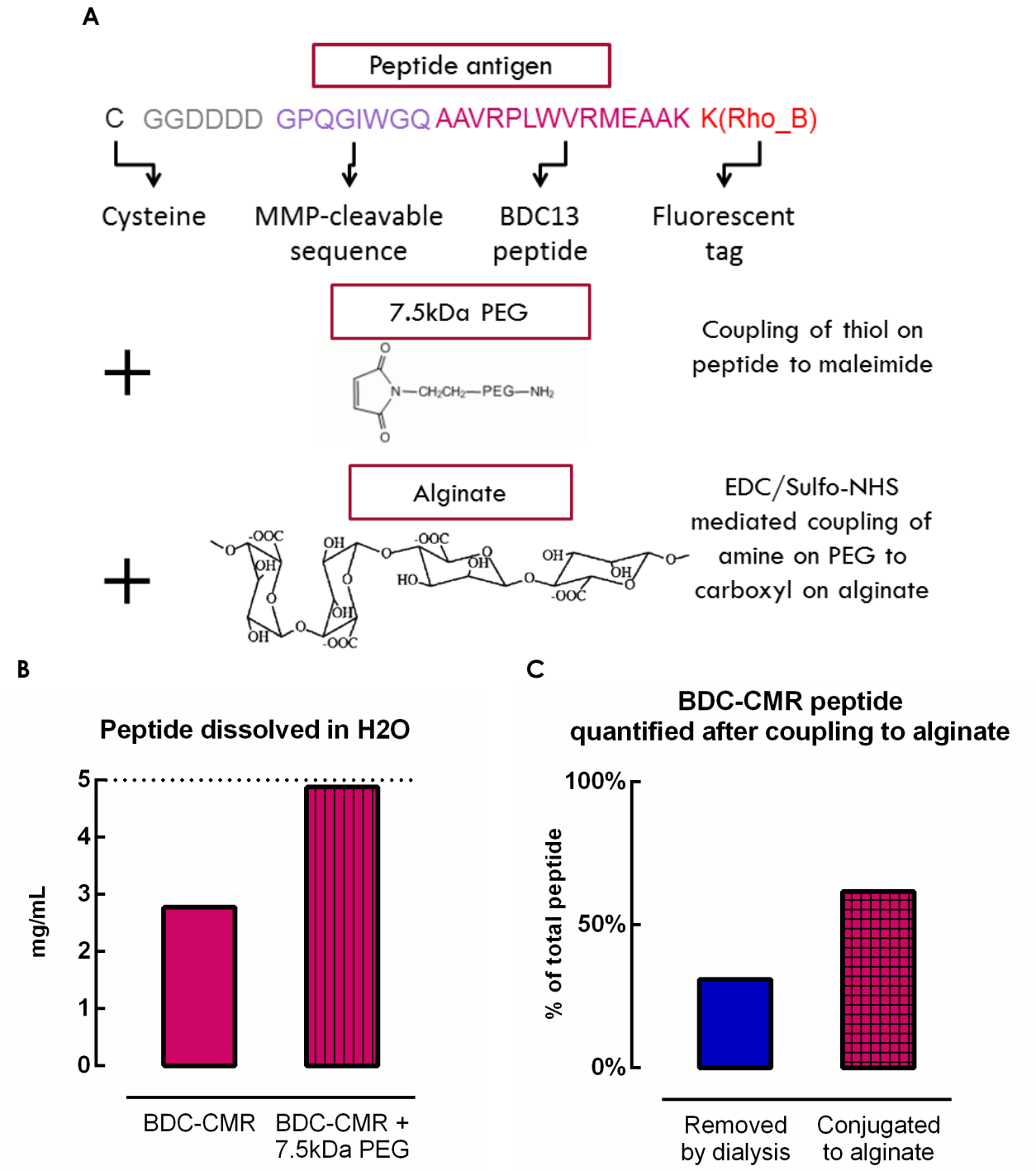

Figure 4.2. A modified, MMP-cleavable BDC peptide was coupled to alginate polymer with an efficiency of 60%. (A) Strategy for the multi-step coupling of the BDC-CMR peptide to alginate. (B) Dissolution of the BDC-CMR peptide in water before and after conjugation to PEG. Dashed line indicates expected concentration (5mg/mL) assuming complete dissolution of the peptide. (C) A 60% efficiency of peptide coupling to alginate was determined by measuring the amount of peptide removed during dialysis and conjugated to the alginate.

Peptide-conjugated alginate mediated functional antigen presentation by DCs *in vitro* and *in vivo*

The BDC-CMR peptide-modified alginate was tested to determine whether DCs would be able to successfully capture and present the peptide both *in vitro* and *in vivo* (Fig. 4.3). *In vitro*, several doses of polymer were added to a coculture of DCs with BDC2.5 responder T cells. The responder T cells proliferated in response to all the tested doses of peptide-conjugated alginate, demonstrating that the peptide can be functionally presented (Fig. 4.3 A). For two of the doses, the proliferation was statistically significantly lower than for the equivalent dose of free peptide. However, for the doses tested here, increasing doses of peptide yielded fewer cells at the end of the culture. *In vivo*, gels were injected subcutaneously and peptide presentation was assayed in a number of different lymph nodes. At day 5, significant levels of peptide presentation were detected in the gels, but not in the other LNs assayed (Fig. 4.3 B).

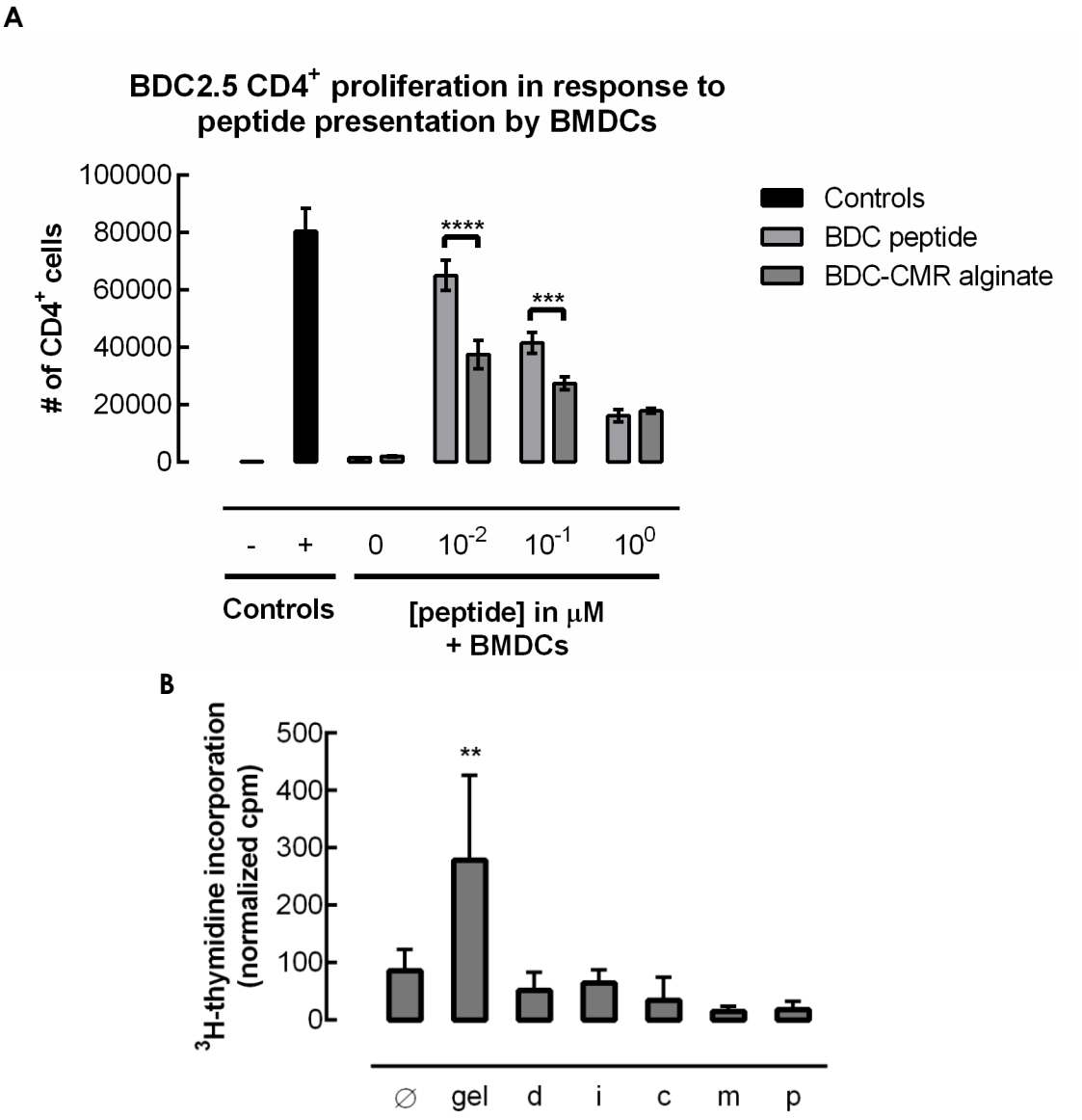

Figure 4.3. Peptide-conjugated alginate resulted in functional peptide presentation both *in vitro* and *in vivo*. (A) *In vitro* proliferation of BDC2.5 T cells in response to soluble BDC peptide or BDC-CMR conjugated alginate, after 3 days of coculture with BMDCs from NOD/ShiLtJ mice. Controls consisted of T cells alone (- control) or T cells cultured with activation beads (+ control for proliferation). (n = 3; mean ± s.d. shown; *** $p < 0.001$; **** $p < 0.0001$.) (B) Proliferation of BDC2.5 T cells in response to peptide presentation by irradiated APCs isolated 5 days after injection of gels delivering BDC-CMR in NOD/ShiLtJ mice. (n = 3 - 4; mean ± s.d. shown; ** $p < 0.01$.)

Delivery of peptide-coupled gels *in vivo* resulted in antigen-specific T cell responses

Next, the effect of delivering peptide-conjugated alginate on T cells *in vivo* was examined. Upon delivery of 0.1nmol of BDC-CMR peptide conjugated to alginate gels, the percentage of endogenous tetramer$^+$ CD4$^+$ T cells increased significantly in the draining LNs at day 5, reaching ~1.2% of the total CD4$^+$ T cells (Fig. 4.4). While the expansion of tetramer$^+$ cells was clearly seen in the draining LNs, the frequency of these cells did not increase in the irrelevant or pancreatic lymph nodes. At day 7, the frequency of tetramer$^+$ cells was reduced, but still appeared higher than baseline (n.s.). By day 14, the frequency of these tetramer$^+$ decreased even further, returning to levels similar to the baseline in naïve mice for all the LNs. The frequency of tetramer$^+$ cells in the irrelevant and pancreatic LNs did not vary significantly over the timecourse examined.

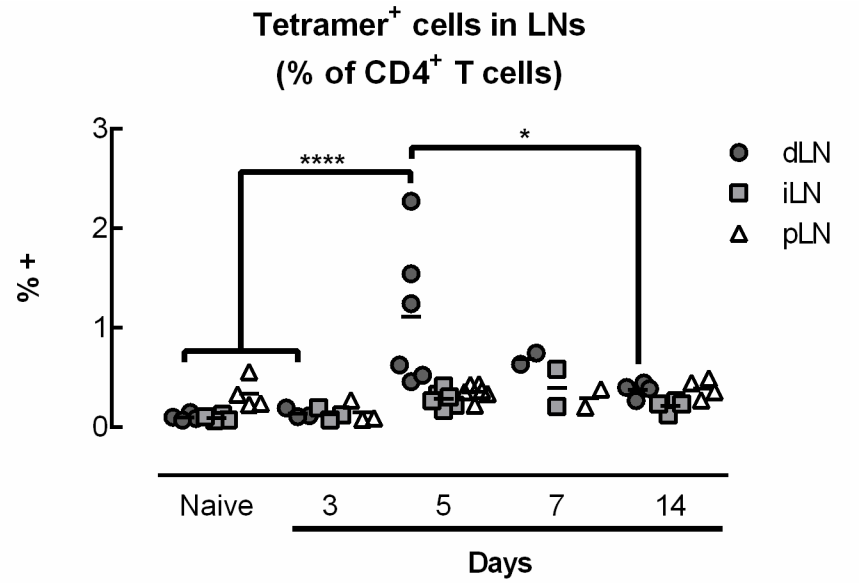

Figure 4.4. Delivery of BDC-CMR peptide in vivo led to the expansion of tetramer$^+$ CD4$^+$ T cells. Gels were injected subcutaneously into the flanks of NOD/ShiLtJ mice; at specified timepoints, gels were isolated and dissociated to analyze infiltrating cells by flow cytometry. (n = 2 - 6; individual data points and mean shown; * $p < 0.05$; **** $p < 0.0001$; for each condition, the different timepoints were compared to each other; statistical tests were only performed for the conditions where n >= 3.)

Gels delivering peptide antigen locally contained a high percentage and number of antigen-specific FoxP3$^+$ cells

The frequency of tetramer$^+$ cells and FoxP3$^+$ cells was examined in the gels delivering peptide and in the LNs (Fig. 4.5). The frequency of T cells in the gels was very low, around ~3% at days 3, 5, and 7 (Fig. 4.5 A). At day 14, the frequency of T cells increased to ~7.2%, but this difference was only statistically significant compared to day 5. Although the frequency of T cells was low, the fraction of these T cells that were tetramer$^+$ increased steadily over time. At days 3, 5, 7, and 14, the frequency of tetramer$^+$ cells were 0.7%, 2.7%, 9.3%, and 27.6%, respectively (Fig. 4.5 B). The frequency of these cells at day 14 was statistically significantly higher than at days 3 and 5. At day

14, the T cells were analyzed for their expression of FoxP3 (Fig. 4.5 C-E). In the gels, the percentage of FoxP3$^+$ cells was significantly higher than in LNs from either naïve mice or mice that received gel injections. This observation held true when FoxP3$^+$ cells were analyzed either as a fraction of CD4$^+$ cells or as a fraction of tetramer$^+$ cells. Approximately 10-fold more CD4$^+$ T cells were FoxP3$^+$ in the gels (~64%) as compared to the LNs (~6%) (Fig. 4.5 C). When analyzed as a fraction of tetramer$^+$ cells, ~62% of the tetramer$^+$ cells in the gels were found to express FoxP3, compared to ~5-14% in the LNs (Fig. 4.5 D). No differences were noted in the frequency of FoxP3$^+$ in the LNs of naïve mice and mice that received injections of the material delivery system. The overall number of tetramer$^+$ FoxP3$^+$ cells was calculated by adjusting for total cell number. The gels contained on average ~7,000 antigen-specific FoxP3$^+$ cells, which was 1 to 2 orders of magnitude greater than the number of these cells found in the lymph nodes, which only contained ~90-500 of these cells (Fig. 4.5 E).

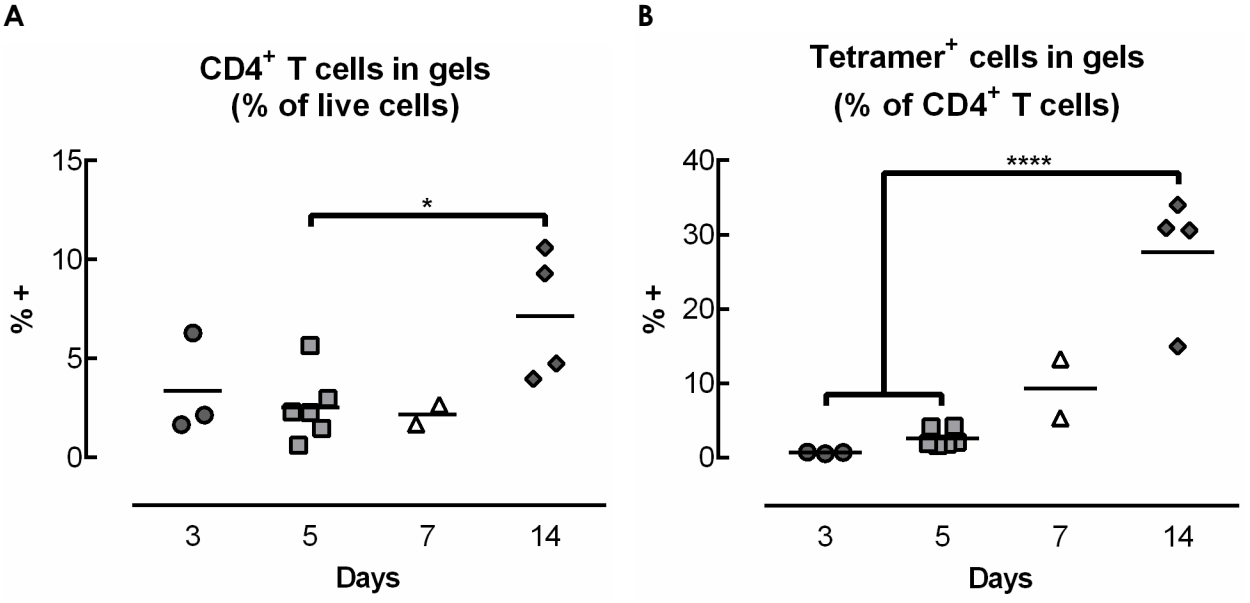

Figure 4.5.

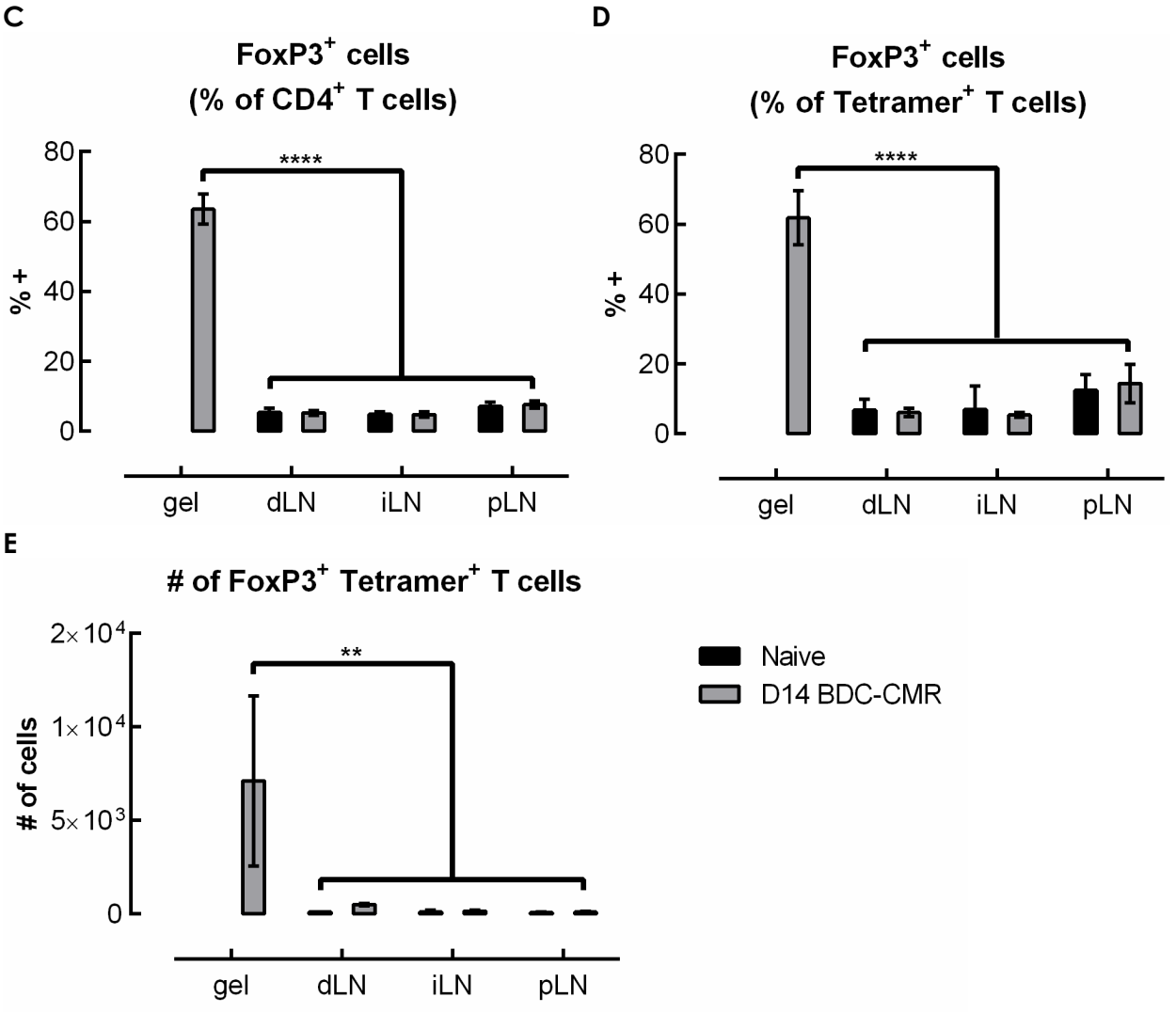

Figure 4.5 (continued). Tetramer+ FoxP3+ CD4+ T cells accumulated in gels delivering BDC-CMR conjugated to alginate. Gels were injected subcutaneously in the flanks of NOD/ShiLtJ mice; at specified timepoints, gels were isolated and dissociated to analyze infiltrating cells by flow cytometry. The percentage of CD4+ cells (A) and tetramer+ CD4+ cells (B) were analyzed. (n = 2 - 6; individual data points and mean shown; * $p < 0.05$; **** $p < 0.0001$; all conditions were compared to each other; statistical tests were only performed for the conditions where n >= 3.) (C-E) Analysis of the CD4+ cells in the gels at day 14, showing the fraction of CD4+ cells that were FoxP3+ (C), the fraction of tetramer+ cells that were FoxP3+ (D), and the number of FoxP3+ tetramer+ CD4+ T cells in the gels (E), as calculated by adjusting for total cell number. (n = 3; mean ± s.d. shown; ** $p < 0.01$; **** $p < 0.0001$; all conditions were compared to each other.)

4.4 Discussion

In this chapter, a new strategy for delivering a peptide antigen in a localized and cell-triggered manner was described. To validate the use of an MMP cleavable sequence for triggered release of the peptide, MMP activity in the gels was first assessed. *In vivo* imaging using a fluorogenic MMP substrate demonstrated that gels delivering GM-CSF exhibit significantly higher MMP activity than control gels. The apparent increase in MMP activity in control gels relative to the surrounding skin was attributed to the higher concentration of substrate in the gels compared to the rest of the skin, since the poor vascularization of the gels necessitated injection of the substrate directly into the gels rather than i.v. Next, the BDC-CMR peptide, which consisted of the BDC peptide antigen with an appended MMP-cleavable sequence, was conjugated to PEG to increase its solubility in water. The peptide-PEG conjugate was then coupled to alginate, and a high coupling efficiency was achieved.

The ability of the BDC-CMR peptide-modified alginate to elicit functional T cell responses was evaluated, first *in vitro*. At all doses of peptide assayed, the peptide modified alginate was successful at inducing the proliferation of BDC2.5 responder T cells in a coculture with BMDCs. When comparing equivalent doses of peptide-modified alginate to soluble peptide added directly to the media, the number of T cells enumerated at the end of the coculture was slightly lower for the peptide-conjugated alginate. This difference may be attributed to the timing of the peptide presentation, since the peptide conjugated to alginate requires cleavage by MMPs to be released, and as a result it may not be immediately available for loading and presentation on

MHCII molecules. In addition, it must be noted that the range of concentrations tested appeared to be higher than the optimal range, since increasing peptide doses resulted in a lower number of T cells at the end of the culture period, both for free peptide as well as for the peptide-modified alginate. Considering this, it is possible that the peptide-conjugated alginate actually resulted in more effective peptide presentation by DCs for the same dose of peptide, which would explain why the final number of T cells was lower than for the equivalent dose of free peptide. *In vivo*, the peptide-modified alginate was also able to be released and presented by DCs. At day 5, peptide was presented in the gels, but not in the other LNs assayed. It should be noted that these data showed a relatively low level of signal, even for the positive controls. Further optimization may have been required to detect signal in the draining LNs.

Overall, these *in vitro* and *in vivo* results show that using an MMP-cleavable sequence to release peptide from a biomaterial allowed functional presentation of the peptideby DCs. This strategy could be used more broadly to deliver different peptide antigens to DCs; however, this technique may require a great deal more optimization for MHCI binding peptides than for MHCII binding peptides, the latter of which were used here. Most MMP-cleavable peptides reported in the literature are ~6-8 amino acids long, and, after cleavage, a few amino acids remain on either side of the cleavage site. For presentation on MHC class II, the peptide length is not tightly restricted, since the MHCII binding pocket is open on both ends, allowing peptides to be bound in a conformation where their ends can extend beyond the edges of the binding pocket. In contrast, MHC I peptides are much more restricted in length (8-9 amino acids) and their terminal amino acids serve as anchor residues for binding, reflecting the fact that the MHC I

peptide binding pocket is closed on both ends. As a result, using a similar strategy to deliver MHC class I peptides would be more challenging, requiring the use of MMP-cleavable sequences that are shorter or share redundant amino acids with the peptide antigen of interest.

In agreement with the peptide presentation that was observed *in vivo*, endogenous antigen-specific T cells expanded in the draining LNs. The frequency of tetramer$^+$ T cells was significantly increased at day 5, but this population then contracted and returned to near baseline levels by day 14. These kinetics were similar to what was seen in Chapter 3, when PLG particles were used to deliver peptide. An analysis of cells isolated from the gels revealed that the fraction of CD4$^+$ cells was very low, but increased to ~7% at day 14. These results were consistent with those seen previously in Chapter 2 when only GM-CSF was delivered, suggesting that the delivery of antigen in addition to GM-CSF here did not have a big impact on T cell recruitment to the gels. Although few CD4$^+$ T cells were found in the gels, the fraction of those cells that were tetramer$^+$ increased markedly over time, reaching a strikingly high level of ~28% at day 14. Interestingly, this increase happened in the same timeframe over which the frequency of tetramer$^+$ cells was seen to decrease in the draining LNs. A more detailed analysis of the T cells in the gels at day 14 revealed that the fraction of FoxP3$^+$ cells was unusually high, constituting 64% of CD4$^+$ T cells and 62% of the more limited tetramer$^+$ subset. The average number of tetramer$^+$ FoxP3$^+$ cells present in the gels was ~7,000, which is on the same order as the number of CD4$^+$ CD25$^+$ BDC2.5 cells that were shown to significantly delay disease in NOD mice[19].

As touched on in Chapter 3, it would be of great interest to determine the fate of the antigen-specific T cells that expanded in the draining LNs at day 5, but subsequently decreased in frequency at later timepoints. Given that the increase in antigen-specific cells in the gels occurs at the same time as their decrease in the draining LNs, it is speculated that some of the antigen-specific T cells that expanded in the draining LNs could have homed to the gels due to the presence of antigen. This phenomenon has been seen in the materials-based cancer vaccine developed by Ali et al., where tumor specific $CD8^+$ T cells are found in the material after 12 days[20]. If the same phenomenon occurred in this system, it raises the distinct possibility that some of the expanded antigen-specific T cells may have migrated into peripheral tissues and homed to the pancreatic islets, where the endogenous antigen is located. However, changes in the frequency of antigen-specific T cells were not seen in the pancreatic LNs, so a direct analysis of the pancreatic islets would be needed to confirm this. Additionally, it would be important to confirm that these $tetramer^+$ cells expressing FoxP3 are functional Tregs, with the ultimate test being the ability of the material system to prevent or reverse disease in NOD mice.

4.5 References

1. Pradeu, T., Jaeger, S. & Vivier, E. The speed of change: towards a discontinuity theory of immunity? *Nat. Rev. Immunol.* **13,** 764–769 (2013).

2. Corse, E., Gottschalk, R. A. & Allison, J. P. Strength of TCR–Peptide/MHC Interactions and In Vivo T Cell Responses. *J. Immunol.* **186,** 5039–5045 (2011).

3. Turner, M. S., Kane, L. P. & Morel, P. A. Dominant role of antigen dose in CD4+Foxp3+ regulatory T cell induction and expansion. *J. Immunol. Baltim. Md 1950* **183,** 4895–4903 (2009).

4. Long, S. A. *et al.* Low-dose antigen promotes induction of FOXP3 in human CD4+ T cells. *J. Immunol. Baltim. Md 1950* **187,** 3511–3520 (2011).

5. Apostolou, I. & Boehmer, H. von. In Vivo Instruction of Suppressor Commitment in Naive T Cells. *J. Exp. Med.* **199,** 1401–1408 (2004).

6. Gottschalk, R. A., Corse, E. & Allison, J. P. TCR ligand density and affinity determine peripheral induction of Foxp3 in vivo. *J. Exp. Med.* **207,** 1701–1711 (2010).

7. Daniel, C., Weigmann, B., Bronson, R. & Boehmer, H. von. Prevention of type 1 diabetes in mice by tolerogenic vaccination with a strong agonist insulin mimetope. *J. Exp. Med.* **208,** 1501–1510 (2011).

8. Murthy, N., Thng, Y. X., Schuck, S., Xu, M. C. & Fréchet, J. M. J. A Novel Strategy for Encapsulation and Release of Proteins: Hydrogels and Microgels with Acid-Labile Acetal Cross-Linkers. *J. Am. Chem. Soc.* **124,** 12398–12399 (2002).

9. Li, C., Madsen, J., Armes, S. P. & Lewis, A. L. A New Class of Biochemically Degradable, Stimulus-Responsive Triblock Copolymer Gelators. *Angew. Chem. Int. Ed.* **45,** 3510–3513 (2006).

10. Page-McCaw, A., Ewald, A. J. & Werb, Z. Matrix metalloproteinases and the regulation of tissue remodelling. *Nat. Rev. Mol. Cell Biol.* **8,** 221–233 (2007).

11. Ratzinger, G. *et al.* Matrix Metalloproteinases 9 and 2 Are Necessary for the Migration of Langerhans Cells and Dermal Dendritic Cells from Human and Murine Skin. *J. Immunol.* **168,** 4361–4371 (2002).

12. Lutolf, M. P. *et al.* Repair of bone defects using synthetic mimetics of collagenous extracellular matrices. *Nat. Biotechnol.* **21,** 513–518 (2003).

13. Lutolf, M. P. *et al.* Synthetic matrix metalloproteinase-sensitive hydrogels for the conduction of tissue regeneration: Engineering cell-invasion characteristics. *Proc. Natl. Acad. Sci.* **100,** 5413–5418 (2003).

14. Seliktar, D., Zisch, A. H., Lutolf, M. P., Wrana, J. L. & Hubbell, J. A. MMP-2 sensitive, VEGF-bearing bioactive hydrogels for promotion of vascular healing. *J. Biomed. Mater. Res. A* **68A,** 704–716 (2004).

15. Kraehenbuehl, T. P. *et al.* Human embryonic stem cell-derived microvascular grafts for cardiac tissue preservation after myocardial infarction. *Biomaterials* **32,** 1102–1109 (2011).

16. Patterson, J. & Hubbell, J. A. Enhanced proteolytic degradation of molecularly engineered PEG hydrogels in response to MMP-1 and MMP-2. *Biomaterials* **31,** 7836–7845 (2010).

17. Turk, B. E., Huang, L. L., Piro, E. T. & Cantley, L. C. Determination of protease cleavage site motifs using mixture-based oriented peptide libraries. *Nat. Biotechnol.* **19,** 661–667 (2001).

18. Huebsch, N. *et al.* Matrix elasticity controls bone formation by transplanted stem cells. *Rev.*

19. Tarbell, K. V., Yamazaki, S., Olson, K., Toy, P. & Steinman, R. M. CD25+ CD4+ T cells, expanded with dendritic cells presenting a single autoantigenic peptide, suppress autoimmune diabetes. *J. Exp. Med.* **199,** 1467–1477 (2004).

20. Ali, O. A., Emerich, D., Dranoff, G. & Mooney, D. J. In situ regulation of DC subsets and T cells mediates tumor regression in mice. *Sci. Transl. Med.* **1,** 8ra19 (2009).

Chapter 5. Conclusions, Implications and Future Directions

5.1 Conclusions

In this thesis, a new material delivery system was developed to recruit DCs in a non-inflammatory context and induce specific responses to defined antigens. Injectable alginate-based hydrogels were designed to release GM-CSF in a sustained manner and form pores that allowed cell infiltration into the material. In addition, these materials were designed to release a peptide antigen in a highly localized manner for uptake by the recruited DCs. This system was tested in the NOD mouse model of type 1 diabetes to examine the ability of the DCs to present the diabetes-related peptide delivered in the material system and induce antigen-specific T cell responses.

In Chapter 2, the development of an injectable hydrogel system for recruiting DCs was described. A strategy was developed for the sustained delivery of GM-CSF, which is not heparin-binding at neutral pH, from alginate. Gradual and sustained release was achieved by conjugating GM-CSF to AuNP carriers and incorporating it into alginate hydrogels in the absence of cystine. The physical structure of the pore-forming gels was also examined to determine the optimal volume fraction and degradation rate for the porogens, which degrade and create a macroporous structure within the bulk hydrogels. This system was able to recruit several million cells into the gels, and closer examination revealed that the vast majority of these cells consisted of $CD11b^+$ $CD11c^+$ DCs, which could attain purities greater than 90% at certain timepoints. Increased

numbers of total cells and frequencies of $CD11c^+$ cells in the lymph nodes draining the gels suggested that the recruited DCs might be migrating to the draining LNs.

Next, in Chapter 3, a defined peptide antigen was incorporated into this system to allow localized delivery and presentation by DCs. PLG microparticles were used to deliver peptide at a slow and sustained rate. Localized biodistribution and peptide presentation were demonstrated. T cells proliferated, expanded, and secreted cytokines in an antigen-specific manner, primarily in the LNs draining the gel. Proliferating T cells were also detected, to a lesser extent, in other LNs, suggesting that they are competent to traffic systemically after interacting with DCs in the draining LNs. The PLG particles were found to significantly alter the phenotype of the cells present in the gels. Whereas gels delivering only GM-CSF experienced a striking enrichment of $CD11c^+$ cells, this enrichment was impaired in gels delivering PLG and peptide. Conversely, the population of $Gr\text{-}1^+$ cells, which decreased in inverse proportion to the $CD11c^+$ population in gels without PLG, remained high with the addition of PLG particles. When gene and protein expression were assayed, the gels containing PLG were found to display higher levels of several inflammatory cytokines compared to gels without PLG. Somewhat surprisingly, at the mRNA level, cells from gels both with and without PLG expressed lower relative levels of many assayed genes compared to control splenic DCs. At the protein level, gels delivering GM-CSF alone were associated with low levels of inflammatory cytokines. In addition, the expression of the negative costimulatory molecules PD-L1 and PD-L2 by DCs recruited to gels delivering GM-CSF was a promising indication that they may have the capacity to induce tolerogenic responses.

The observation that exposure to PLG altered the phenotype of recruited cells motivated the development of a new strategy for delivering peptide in a localized manner, which was described in Chapter 4. The goal was to covalently couple the peptide to the polymer forming the bulk hydrogel, while still allowing release such that the peptide could be loaded and presented on MHCII. After determining that cell infiltration into the gels was associated with increased MMP activity, an MMP-cleavable peptide linker was chosen to allow cell-triggered release upon infiltration of DCs into the material. An MMP-cleavable sequence was added to the N-terminal end of the peptide antigen, which was subsequently conjugated to alginate. This material was shown to trigger antigen-specific T cell responses both *in vitro* and *in vivo*, and an accumulation of tetramer$^+$ FoxP3$^+$ T cells was observed in the gels. A study to evaluate the impact of this material system on disease progression was underway at the time this dissertation was written, and no acceleration in disease progression was observed following the administration of three doses of peptide loaded gels (Appendix D). Approximately 10 weeks after the first gel administration, 70% of the mice that received peptide-loaded gels remained diabetes free, while only 40% of the mice in the control group were diabetes free, but the difference in the disease progression curves were not statistically significantly different at this timepoint.

5.2 Implications

This work has advanced the area of immunomodulatory biomaterials in three important areas.

The material system described here achieved an enrichment of DCs that was unprecedented in terms of the high purity of $CD11b^+$ $CD11c^+$ cells recruited. This property could be useful to develop materials-based vaccines, either for tolerance or immunity, that have the capacity to manipulate a highly enriched population of DCs, potentially allowing more precise and potent control over the downstream responses.

Further, a detailed characterization of this material system revealed that the recruited DCs can be qualified as immature based on cell surface marker expression as well as cytokine expression at the mRNA and protein levels. The goals of effectively recruiting DCs while preventing their maturation are inherently somewhat at odds, but the strategy employed here fulfilled both goals. Immature or semi-mature DCs are present in steady state conditions *in vivo*, but this system presents an opportunity to concentrate a greater number of such DCs in one location.

Finally, this work advanced the methodology for delivering peptide antigens from biomaterials. It was shown that a defined peptide antigen could be covalently coupled to the material system and released in a cell-triggered manner, allowing it to remain highly localized while still retaining the capacity to be functionally presented by DCs to T cells. This advance has important implications for improving the safety of

tolerogenic therapies that involve the administration of disease-related self-antigens, since it provides a strategy to prevent the dissemination of antigens to a site of inflammation and disease, while still making those antigens accessible to the immune system in a non-inflammatory environment.

5.3 Future Directions

In this thesis, significant steps were taken towards the development of a materials-based system that induces antigen-specific tolerogenic responses, but a large parameter space remains to be explored to achieve robust and long-lasting tolerance that is effective in a therapeutic setting. In the process, a great deal stands to be learned about the immunological mechanisms controlling tolerance versus immunity.

The dose, delivery kinetics, and sequences of the delivered peptide antigens may have profound effects on the outcome of the immune response. The use of a material system such as the one described here allows these parameters to be tested in greater detail than would be possible otherwise. The effect of peptide delivery on downstream immune responses can be explored not only by modifying the dose of delivered peptide, but also by tuning the sequence of the MMP cleavable linker to achieve different cell-triggered release kinetics. In addition, different peptide antigens will exert different effects on the induction of tolerance. Even among peptide mimetopes that are recognized by the same TCR, some may be more effective at inducing or expanding Tregs, while others may induce anergy or deletion of self-reactive effector T cells. Studies have shown that high-affinity peptide mimetopes may be more

appropriate for inducing tolerance, since they have an increased capacity to induce conversion of FoxP3$^+$ Tregs, thus preventing disease in a mouse model T1D[1]. In light of these findings, the selection of appropriate peptide antigens should be considered and tested in the design of materials-based vaccines, and it may be of great interest to incorporate more than one peptide into the system. For instance, delivering several peptides with different binding affinities for the same cognate TCR could induce tolerance through multiple mechanisms, i.e. induction of anergy, deletion, as well as expansion and activation of Tregs. Alternatively, it may be useful to incorporate several peptides derived from different antigens to induce Tregs with multiple antigen specificities, which may afford more potent disease suppression. The material system described here could provide a useful platform to test such hypotheses.

The localized delivery of peptide also represents a great opportunity to control the context in which DCs encounter an antigen by creating a microenvironment that is not only non-inflammatory, but also provides tolerogenic signals. The delivery of different types and doses of soluble tolerogenic factors may be explored to induce a more robust tolerogenic DC phenotype. In addition, since this system mediates infiltration of cells within the material, it could provide an ideal platform for incorporating insoluble immunomodulatory cues in the form of tethered antibodies or binding motifs derived from receptors or ECM components. For instance, the material could be modified to provide negative costimulatory signaling to cells by conjugating it to activating antibodies or extracellular domains of receptors, such as CTLA4-Ig or PD-L1/2-Ig. Another interesting line of research has shown that certain ECM proteins can act as tissue integrity signals, as in the case of hyaluronic acid (HA), which was shown to

enhance the function of Tregs[3,4] and induce Tr1 cells[5] in its high molecular weight form, while its low molecular weight form is an indicator of tissue damage and does not exert tolerogenic effects. These findings may be readily applied to enhance this alginate-based material system by decorating the polymer with multivalent signaling motifs to mimic the effects of HMW HA, such as activating anti-CD44 or HA binding sites, in such a way that they cannot be degraded into LMW forms by endogenous enzymes. Finally, modulating physical properties such as the stiffness or viscoelasticity of the material may also have an impact on DC maturation or antigen uptake, as well as on the recruitment and function of other immune cells.

Finally, this platform may be used more broadly to recruit and manipulate different immune cell types, other than DCs. It is speculated that this material acts as a privileged site for the infiltration of immune cells, partly due to the intentional lack of cell adhesion ligands on the alginate polymer. This property could be used to recruit one or more different immune cell populations by delivering different cytokines or chemokines. In the area of immune tolerance, several different bioactive factors have been shown to act on both DCs and T cells, such as IL-10, TGF-b1, or the small molecule AHR ligand ITE[6]. It may be possible to take full advantage of these tolerogenic factors and achieve enhanced priming of tolerogenic responses at the site of the material by recruiting DCs together with naïve T cells, which migrate in response to CCL19 or CCL21. This material system could also serve as a useful model to study the interplay between other innate or adaptive immune cell types, such as B cells, macrophages, or NK cells, in an *in vivo* setting.

Future work will evaluate the feasibility of these ideas, which represent exciting avenues for investigating important questions in immunology and for advancing the development of novel immunomodulatory therapies.

5.4 References

1. Daniel, C., Weigmann, B., Bronson, R. & Boehmer, H. von. Prevention of type 1 diabetes in mice by tolerogenic vaccination with a strong agonist insulin mimetope. *J. Exp. Med.* **208,** 1501–1510 (2011).

2. Liu, G. Y. & Wraith, D. C. Affinity for class II MHC determines the extent to which soluble peptides tolerize autoreactive T cells in naive and primed adult mice—implications for autoimmunity. *Int. Immunol.* **7,** 1255–1263 (1995).

3. Bollyky, P. L. *et al.* CD44 Costimulation Promotes FoxP3+ Regulatory T Cell Persistence and Function via Production of IL-2, IL-10, and TGF-β. *J. Immunol.* **183,** 2232–2241 (2009).

4. Bollyky, P. L. *et al.* Cutting Edge: High Molecular Weight Hyaluronan Promotes the Suppressive Effects of CD4+CD25+ Regulatory T Cells. *J. Immunol.* **179,** 744–747 (2007).

5. Bollyky, P. L. *et al.* ECM components guide IL-10 producing regulatory T-cell (TR1) induction from effector memory T-cell precursors. *Proc. Natl. Acad. Sci.* **108,** 7938–7943 (2011).

6. Quintana, F. J. *et al.* An endogenous aryl hydrocarbon receptor ligand acts on dendritic cells and T cells to suppress experimental autoimmune encephalomyelitis. *Proc. Natl. Acad. Sci. U. S. A.* **107,** 20768–20773 (2010).

Appendices. Preliminary Studies for Future Work and Detailed Protocols

Appendix A. Theoretical packing of spherical proteins on AuNPs.

A.1 Method

The amount of GM-CSF to be conjugated to AuNPs was determined by calculating the theoretical packing of GM-CSF molecules on the surface of the AuNPs. The diameter of GM-CSF was estimated based on its molecular weight, with the assumption that GM-CSF is a globular protein. Synthesized AuNPs were analyzed by DLS to measure their diameter, and their concentration was determined based on their absorbance at 518-519nm. AuNPs and GM-CSF were modeled as spheres (Fig. A.1 A), and simple geometry was used to determine the separation angle theta (θ) between two adjacent small spheres (GM-CSF) contacting a larger sphere (AuNP) at one point (Fig. A.1 B). This angle θ can be looked up in tables of spherical codes[1] to determine the most efficient theoretical packing of GM-CSF molecules onto AuNPs. A 50% excess of protein was used to ensure that the AuNPs are fully coated.

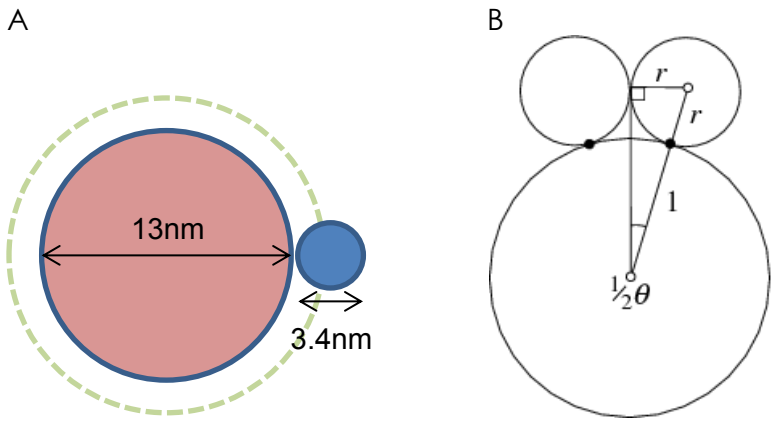

Figure A.1. Protein packing on AuNPs was modeled as packing of spheres. (A) Diagram of GM-CSF and AuNPs modeled as spheres. (B) Geometry used to determine the separation angle theta between two adjacent small spheres sitting on the surface of a larger sphere. (Adapted from Weisstein).

A.2 References

1. Weisstein, E. W. Spherical Code -- from Wolfram MathWorld. at <http://mathworld.wolfram.com/SphericalCode.html>

Appendix B. Flow cytometry reagents.

Table B.1. Staining antibodies, tetramers, and other reagents used for flow cytometry.

Antigen	Clone	Fluorophore	Vendor
CD11b	M1/70	APC-Cy7 or APC-eFluor780	eBioscience or BioLegend
CD11c	N418	Alexa 488 or APC	eBioscience
F4/80	BM8	PE-Cy7	BioLegend
Gr-1	RB6-8C5	Pacific Blue	BioLegend
DX5 (CD49b)	DX5	PE	BioLegend
CD3e	145-2C11	PE-Cy7	BioLegend
CD4	RM4-5 or GK1.5	Pacific Blue or FITC	eBioscience or BioLegend
CD8a	53-6.7	Alexa 488 or PE	eBioscience
CD25	PC61	FITC or APC	BioLegend
MHC II (I-A/I-E)	M5/114.15.2	Pacific Blue	BioLegend
CD86	PO3	APC	BioLegend
CCR7 (CD197)	4B12	PE	BioLegend
PD-L1 (CD274)	10F.9G2	Brilliant Violet 421	BioLegend
PD-L2 (CD273)	TY25	PE	BioLegend
PDCA-1	CD317	PE-Cy7	BioLegend
CD207	4C7	PE	BioLegend
CD205	NLDC-145	PE-Cy7	BioLegend
CD103	2E7	Pacific Blue	BioLegend
FoxP3	FJK-16s	PE	eBioscience
Tetramer (MHCII I-Ag7)		PE or APC	NIH Tetramer Core
7-AAD viability dye			BioLegend
Fc Block (CD16/CD32)	93	-	eBioscience or BioLegend

Appendix C. Representative flow cytometry plots.

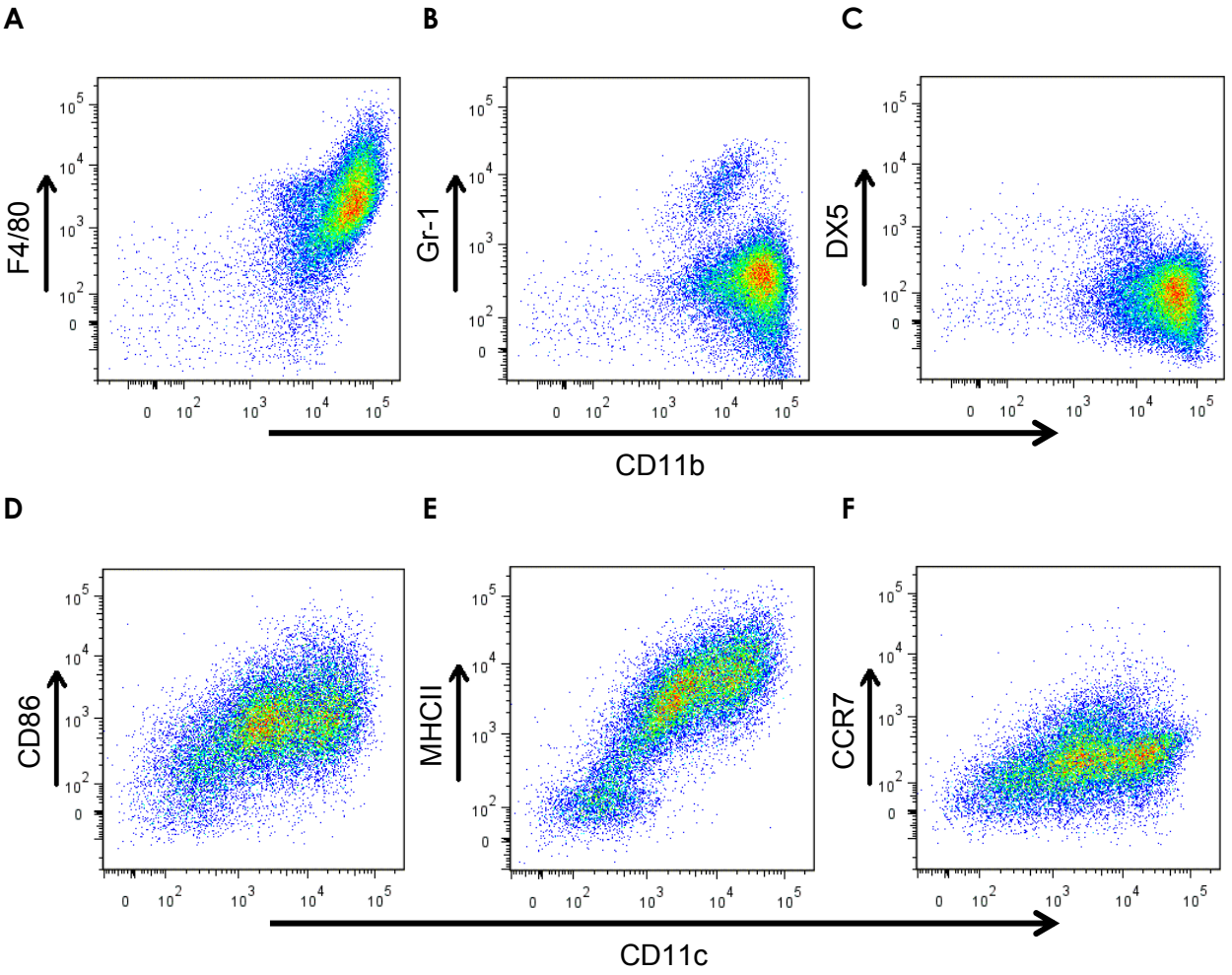

Figure C.1. Flow cytometry plots for cells isolated from gels delivering GM-CSF + AuNP after 5 days. (A-C) CD11b (x-axis) plotted against F4/80 (A), Gr-1 (B), and DX5 (C). (D-F) CD11c (x-axis) plotted against CD86 (D), MHCII (E), and CCR7 (F).

Appendix D. Preliminary disease study in the NOD model of type 1 diabetes.

The safety of the material system described in this thesis, as well as its impact on disease progression, were evaluated in the NOD mouse model of type 1 diabetes. Gels delivering GM-CSF and BDC-CMR peptide-modified alginate were administered at intervals of 25 days. Tolerogenic factors were also included to evaluate whether they could provide any added protection from disease. Three administrations of this material delivery system did not result in any acceleration of disease progression. At the time of writing, 40% of the mice in the control and TGF-β1 groups were diabetes free, while 70% of the mice in the gel and gel + dex groups remained diabetes free. The curves were not statistically significantly different. It will be of great interest to determine whether a protective effect will be seen in the gel or gel + dex conditions.

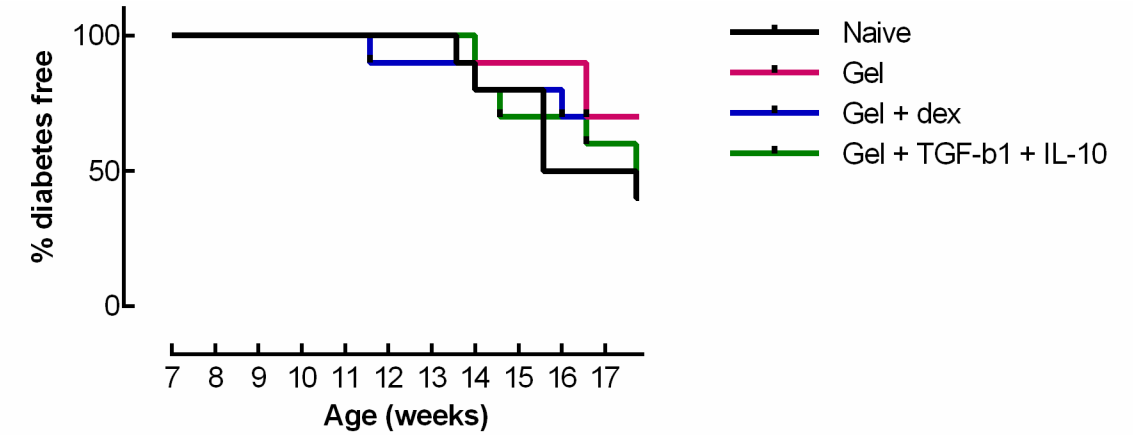

Figure D.1. Effect of the material delivery system on disease progression in NOD mice. Three doses of gels delivering GM-CSF and 0.1nmol of BDC peptide conjugated to alginate were injected subcutaneously into the flanks of female NOD/ShiLtJ mice at intervals between 7 and 13 weeks. For two of the groups, either dexamethasone (dex) or TGF- β1 + IL10 were co-delivered in the gels. Naïve mice did not receive any gel injections. Blood glucose measurements were taken twice weekly, and mice were considered diabetic after two consecutive non-fasting blood glucose readings >250 mg/dL. (n=10).

Appendix E. VEGF abrogates the efficacy of a DC programming materials-based cancer vaccine.

E.1 Introduction

The expression of VEGF by growing tumors and its role in tumor angiogenesis has been extensively characterized. Anti-VEGF therapies are now used in the clinic to limit angiogenesis and normalize the tumor vasculature[1], leading to improved outcomes. More recently, it was found that, in addition to enhancing angiogenesis, VEGF also exerts other effects by acting on tumor cells themselves, as well as on tumor-infiltrating immune cells[1]. There is increasing evidence that VEGF contributes to establishing an immunosuppressive environment in tumors through a number of mechanisms, including inducing myeloid-derived suppressor cells (MDSCs), recruiting immature DCs, suppressing DC maturation[1], and promoting FoxP3$^+$ Treg infiltration[2]. Previously Ali et al. developed a materials-based cancer vaccine that was found to be effective at improving survival in a mouse model of melanoma[3]. This same material system has also been used to deliver VEGF *in vivo* in the setting of ischemia[4]. Here, this implantable material was used as a platform to combine VEGF delivery together with the cancer vaccine and investigate the effects of VEGF on the priming of anti-tumor immunity.

E.2 Materials and Methods

PLG microsphere fabrication

Peptide-loaded PLG microspheres were fabricated following the procedure described in Chapter 2.

Vaccine fabrication and implantation

PLG scaffold based vaccines containing 3ug GM-CSF, 100ug CpG, and lysate from B16 tumors were fabricated and implanted subcutaneously into the flanks of C57BL/6J mice as described previously[3].

Tumor growth assays

10^5 B16-F10 melanoma cells were injected subcutaneously into the back of the necks of C57BL/6J mice. Tumor growth was monitored by measuring the length and width of the tumors using calipers. Mice were euthanized according to humane endpoints.

Cytokine analysis

Cytokine analysis was performed as described in Chapter 3.

E.3 Results

When 3ug of VEGF were added to the fully functional PLG scaffold-based vaccine, vaccine efficacy was completely abrogated in both therapeutic (Fig. E.1 A) and prophylactic (Fig. E.1 B) treatment modalities. In the setting of therapeutic vaccination,

mice that received the standard vaccine exhibited prolonged survival compared to the unvaccinated controls, but the mice that received vaccine + VEGF did not. In the case of prophylactic vaccination, the standard vaccine allowed 90% survival after tumor challenge, whereas the addition of VEGF to the vaccine led to 0% survival. The tumor growth curves from the prophylactic vaccination study were analyzed in greater detail by fitting exponential curves to the experimental data. The tumor growth rate, as indicated by the doubling time, was the same for the unvaccinated controls and the mice that received Vaccine + VEGF. However, the time to tumor initiation was statistically significantly shorter for the vaccine + VEGF condition compared to the control condition. When the scaffolds were analyzed for cytokines, it was found that the scaffolds with added VEGF contained a significantly higher concentration of IL-10 protein than the standard vaccine.

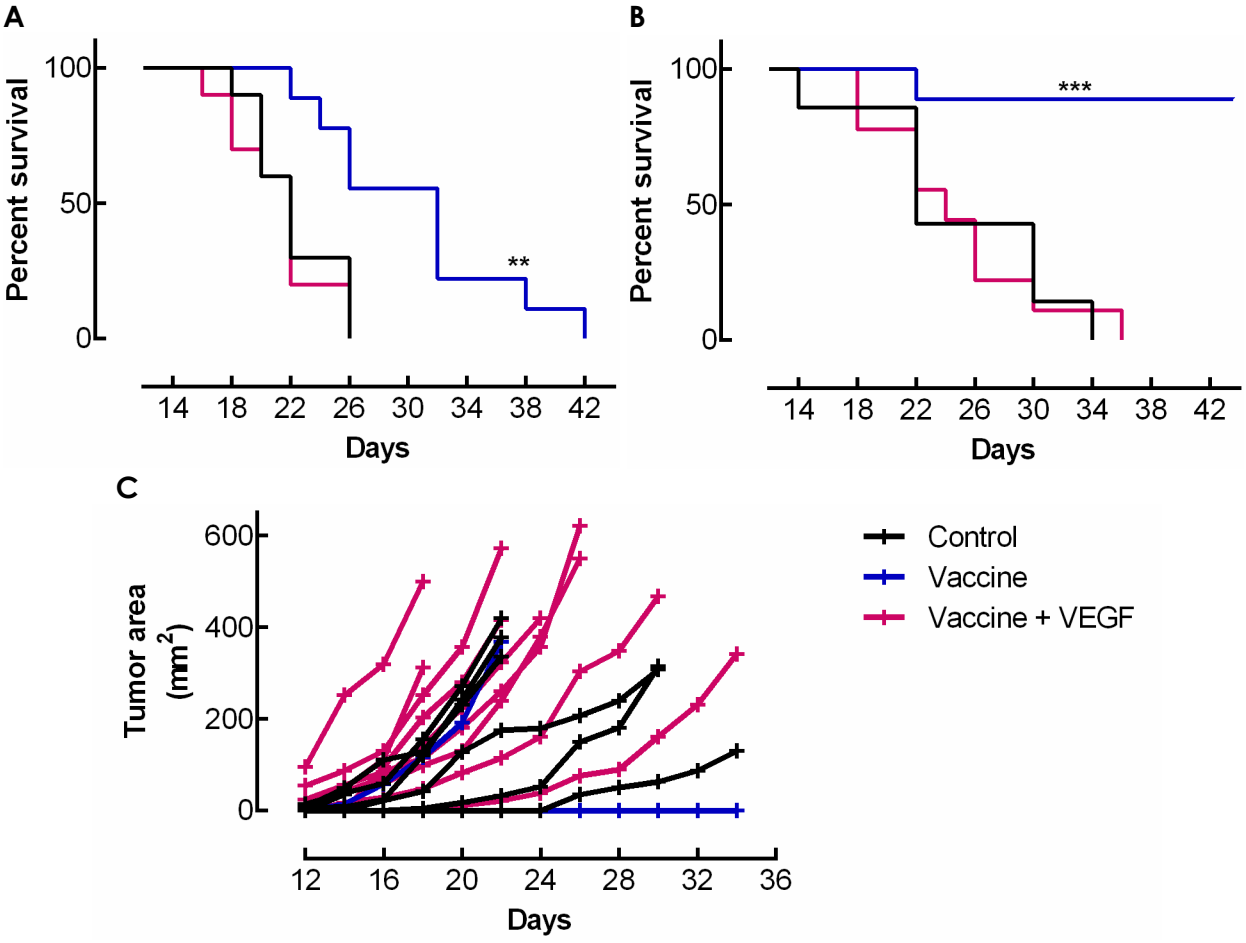
A
Percent survival
100
50
0
**
14 18 22 26 30 34 38 42
Days
B
Percent survival
100
50
0
***
14 18 22 26 30 34 38 42
Days
C
Tumor area (mm²)
600
400
200
0
12 16 20 24 28 32 36
Days
Control
Vaccine
Vaccine + VEGF

Figure E.1.

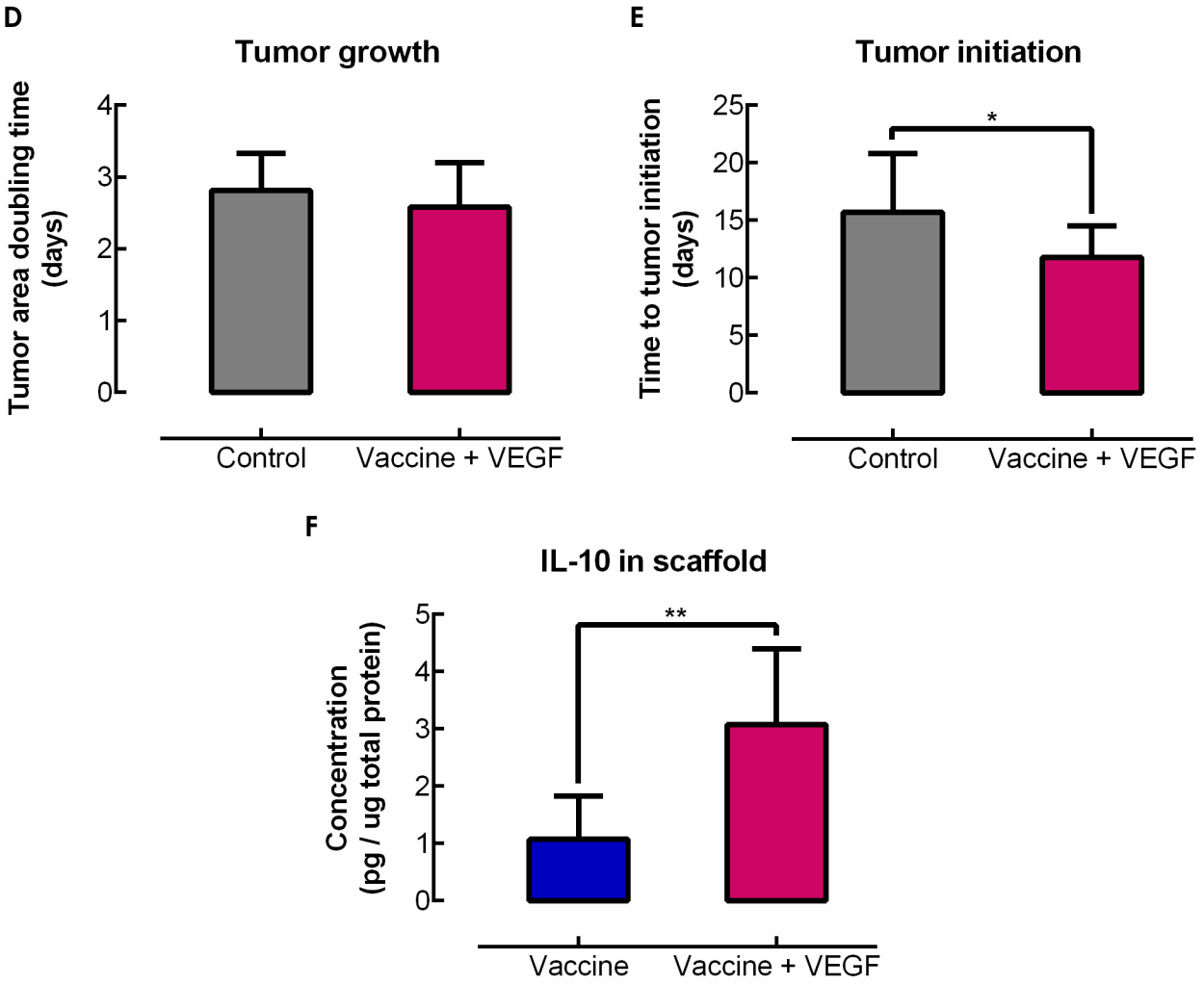

Figure E.1 (continued). Incorporation of VEGF abrogated the efficacy of a materials-based cancer vaccine in a model of melanoma. (A) Survival of mice that were vaccinated 9 days after being inoculated with B16 tumors. (n = 9-10; ** $p < 0.01$). (B) Survival of mice that were prophylactically vaccinated and challenged with B16-F10 tumor cells 14 days later. (n = 7-9; *** $p < 0.001$). (C) Individual tumor growth curves from the prophylactic study shown in (B). (D) Tumor doubling times for unvaccinated controls or mice that were vaccinated with scaffolds containing VEGF in the prophylactic study. (n = 7-9; mean ± s.d. shown). (E) Time until formation of a macroscopic tumor in controls or mice that received vaccines containing VEGF. (n = 7-9; mean ± s.d. shown; * $p < 0.05$). (F) IL-10 concentration in scaffolds 10 days after implantation. (n = 5; mean ± s.d. shown; ** $p < 0.01$).

E.4 Discussion

The addition of VEGF to a functional materials-based cancer vaccine had the striking effect of completely abrogating vaccine efficacy. Based on previous studies analyzing the spatio-temporal presentation of VEGF from PLG scaffolds, the VEGF delivered in the scaffold vaccines was not expected to reach the tumor site. This is consistent with the fact that the presence of VEGF in the vaccines did not affect the growth rate of the tumors. Interestingly, in the setting of prophylactic vaccination, tumors growth initiated earlier in mice that received vaccines containing VEGF compared to controls. This finding suggests that the vaccines containing VEGF may mediate the development of tolerance towards tumor antigens, allowing tumors to emerge sooner. The fact that a higher concentration of IL-10 was detected in vaccines containing VEGF supports the notion that a more tolerogenic environment in those scaffolds may be responsible for impairing the efficacy of the vaccine. These results warrant further investigation and may hold important implications for the design of materials-based cancer vaccines.

E.5 References

1. Ellis, L. M. & Hicklin, D. J. VEGF-targeted therapy: mechanisms of anti-tumour activity. *Nat. Rev. Cancer* **8,** 579–591 (2008).

2. Hansen, W. *et al.* Neuropilin 1 deficiency on CD4+Foxp3+ regulatory T cells impairs mouse melanoma growth. *J. Exp. Med.* **209,** 2001–2016 (2012).

3. Ali, O. A., Huebsch, N., Cao, L., Dranoff, G. & Mooney, D. J. Infection-mimicking materials to program dendritic cells in situ. *Nat. Mater.* **8,** 151–158 (2009).

4. Chen, R. R. *et al.* Integrated approach to designing growth factor delivery systems. *FASEB J* (2007).

Appendix F. Labeling cells to track DC migration *in vivo*

F.1 Introduction

Biomaterials are increasingly being used to recruit and program cells *in vivo* for a variety of applications, such as immune modulation[1] or tissue regeneration[2]. Consequently, it is of great interest to be able to identify and track cells *in vivo* that came into contact with a biomaterial and subsequently migrated to a different location. In the field of immunology, fluorescein isothiocyanate (FITC) has been used to "paint" the skin and identify DCs that migrated from the skin into the lymph nodes. In an analogous manner, FITC was also used by Ali et al. to "paint" PLG scaffolds and track DCs that were recruited into the scaffolds *in vivo* and then redeployed into the draining lymph nodes[1]. While this technique is useful, it may still be improved, since FITC is not as bright or persistent as some other cell tracking dyes. Here, the cell tracking dyes carboxyfluorescein diacetate succinimidyl ester (CFSE) and CellTrace Violet (CTV) were tested for their ability efficiently and specifically labeling of cells that come into contact with a biomaterial without negatively impacting cell viability or function.

F.2 Materials and Methods

PLG microsphere fabrication

Peptide-loaded PLG microspheres were fabricated following the procedure described in Chapter 2. 5 nmol of CFSE (eBioscience) or CTV (Life Technologies) in DMSO were added per 1.5mg of PLG particles.

BMDC labeling assay

Bone marrow was isolated from C57BL/6J mice and BMDCs were differentiated as described in Chapter 3. For C57BL/6J BMDCs, the initial plating density was 2 x 10^6 cells in 10mL of medium. After 6 days of differentiation, BMDCs were collected and plated in 12 well tissue culture treated plates at a density of 10^6 cells / well. 1.5 mg of dye-loaded PLG microspheres were incubated directly with the cells or added to the top compartment of transwell inserts with 1um pores (Greiner). A total of 2mL of medium was added to each well. For wells containing transwell inserts, appropriate volumes of medium were added inside (0.6mL) and outside (1.4mL) the transwell to avoid differences in hydrostatic pressure.

Flow cytometry

Flow cytometry was performed as described in Chapter 2.

F.3 Results

Cells that were incubated directly with dye-loaded PLG particles were efficiently labeled using either CFSE or CTV (Fig. F.1 A-B). On the other hand, when the PLG particles were added to the upper compartment of transwell inserts, little to no cell labeling was observed (Fig. F.1 A-B). This method for labeling DCs did not have a significant impact on their viability or CD11c expression (Fig. F.1 C-D).

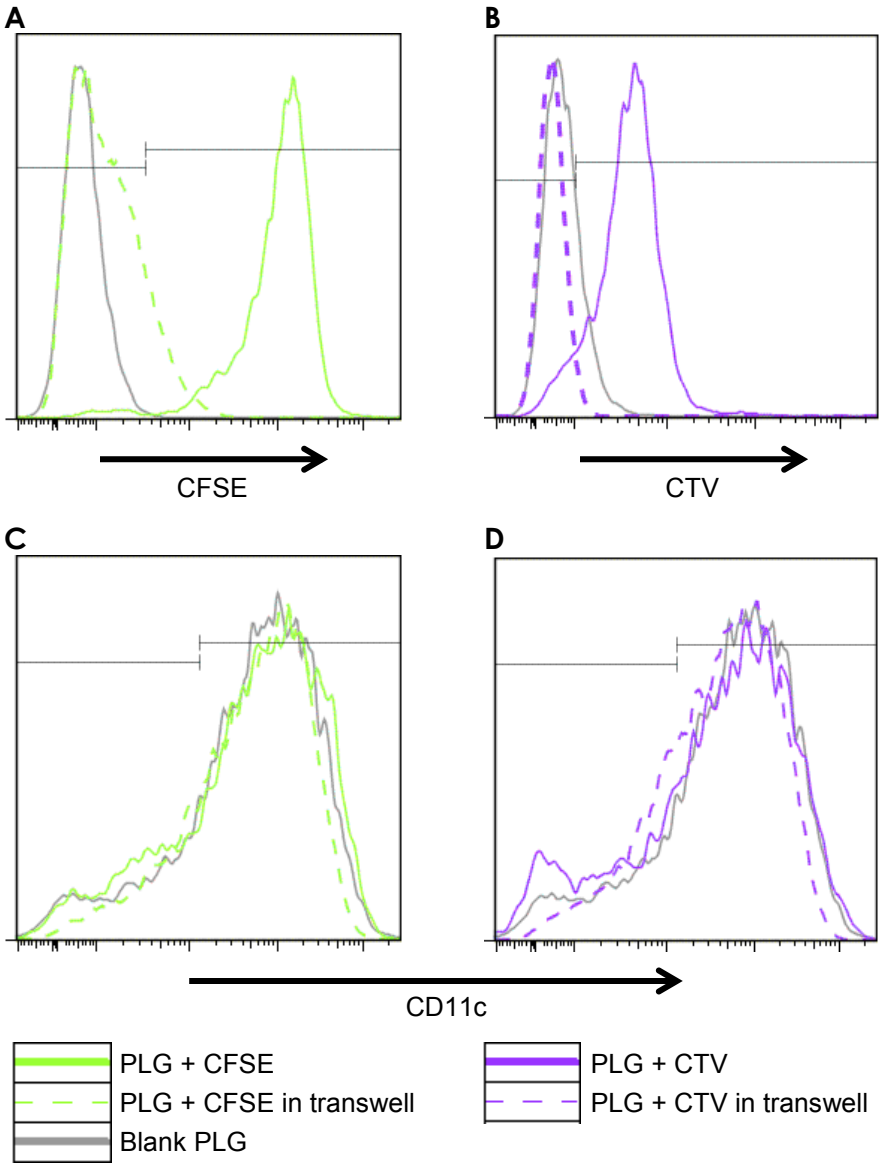

Figure F.1. PLG particles loaded with cell tracking dyes effectively labeled BMDCs. BMDCs were incubated for 6 days either directly with dye-loaded particles, or in wells that contained dye-loaded particles in the top compartment of a transwell insert. (A-B) Labeling of BMDCs with CFSE (A) or CTV (B). (C-D) CD11c expression by DCs labeled with CFSE(C) or CTV (D).

F.4 Conclusion

The cell tracking dyes CFSE and CTV, were shown to effectively label BMDCs when delivered from PLG. The dye-loaded particles did not lead to labeling of cells that they did not contact directly, which may be explained by the fact that they are hydrophobic and do not diffuse significantly out of the PLG. The CFSE and CTV dyes, which are commonly used to label cells *ex vivo* for cell tracking or proliferation experiments, may also prove to be highly useful for achieving direct *in vivo* labeling of cells that come into contact with a biomaterial. Since these dyes are brighter and longer lasting than FITC, it may be possible to achieve more sensitive and accurate tracking of cells that infiltrate a biomaterial and are subsequently redeployed.

F.5 References

1. Ali, O. A., Huebsch, N., Cao, L., Dranoff, G. & Mooney, D. J. Infection-mimicking materials to program dendritic cells in situ. *Nat. Mater.* **8,** 151–158 (2009).
2. Huebsch, N. *et al.* Matrix elasticity controls bone formation by transplanted stem cells. *Rev.*